The analysis of inset dielectric guide by transverse resonance diffraction

Hedges, S. J.

Award date:
1987

Awarding institution:
University of Bath

THE ANALYSIS OF INSET DIELECTRIC GUIDE BY TRANSVERSE RESONANCE DIFFRACTION.

submitted by S.J. Hedges

for the degree of PhD

of the University of Bath

1987

S.J. Hedges

ProQuest LLC
789 East Eisenhower Parkway
P.O. Box 1346
Ann Arbor, MI 48106-1346

SUMMARY

This Thesis is concerned with the analysis of Inset Dielectric Guide (IDG). This is a variation of the image line structure that offers greater ease of manufacture and reduced radiation loss in practical components.

The IDG structure is analysed rigorously by using the Transverse Resonance Diffraction Method. This is an integral equation formulation that operates in the space domain and takes into account the singular boundary conditions to obtain a highly convergent solution. The accuracy of the method is demonstrated by comparison with measured results.

The analysis also enables the field information to be obtained and so enables the conductor loss components to be estimated. The dielectric loss components are also obtained by solving the dispersion equation for a complex value of permittivity. The accuracy of the method is again demonstrated by good correlation with measured loss values.

Inset Dielectric Guide is concluded to be of practical importance for that region of the spectrum where conventional methods such as microstrip and finline are no longer practicable.

ACKNOWLEDGEMENTS

The author would like to thank Professor T. Rozzi for his expert supervision and guidance during the course of this work.

The author also expresses his thanks to fellow Postgraduate students and members of staff of the School of Electrical Engineering for their friendship and many useful contributions to the theoretical and experimental aspects of the work.

This work was funded by a grant from the Science and Engineering Research Council (GR/C/23407) and a C.A.S.E. award with Marconi Research Centre and thanks are due to both of these organisations. Thanks are especially due to Mr S.C. Gratze of Marconi Research Centre for initiating the work and providing the test pieces.

CONTENTS

Publications arising from this work.

[1] S. Hedges and T.E. Rozzi, "The Analysis of Inset Dielectric Guide using Transverse Resonance Diffraction", Proc 15th European Microwave Conference (Paris), Sept 1985, pp.743-749.

[2] T. Rozzi and S. Hedges, "Rigorous Analysis and Network Modelling of the Inset Dielectric Guide", IEEE Trans Microwave Theory Tech. vol. MTT-35, Sept 1987.

[3] S. Hedges and T. Rozzi, "The Loss Analysis of Inset Dielectric Guide including Bending Loss and a Comparison with Image Line", Proc, 17th European Microwave Conference (Rome), Sept 1987,

CHAPTER ONE

INTRODUCTION

1-1 Introduction

The history of radio wave communication has been characterised by a steady increase in operating frequency. Initial problems were those of practicality and ease of construction. However, as more and more users caused spectrum overcrowding, and the need for larger channel capacities required wider signal bandwidths, then the operating frequencies had to increase. The requirements for high definition radar and compact system size have been an additional stimulus for the development of high frequency systems.

The translation to higher system frequencies has conventionally been achieved by the direct scaling of lower frequency circuits. This approach, whilst being still usable over the microwave band becomes less efficient at millimetre wave frequencies. The reasons for this are mostly mechanical. The electrical tolerances, relative to the guided wavelength remain constant, so that as frequencies increase and the wavelength becomes shorter, the mechanical tolerances become increasingly more stringent and difficult to achieve. Production processes thus become more complex and expensive. It is recognized that for operating frequencies in excess of 100 GHz new circuit techniques must be adopted and this in effect was the stimulus for the work presented in this thesis.

This introductory chapter is intended to put this work into context and to give a synopsis of the chapters to follow. The first section defines the millimetre wave region and outlines its importance for modern communication and surveillance systems. It is the practical importance of the millimetre wave region that has prompted much of the research into new waveguiding media. The next section outlines

some of the guide structures that have been considered for use or have been used for millimetre wave systems and briefly discusses their respective merits and shortcomings. Against this backdrop the subject of this thesis, Inset Dielectric Waveguide (IDG) is introduced. This guide has the theoretical advantages of dielectric waveguides but with a structure that is perhaps more amenable to manufacturing techniques. This chapter concludes with an outline of the work presented in the remaining five chapters.

1-2 The Importance of Millimetre Waves

The millimetre waveband is that portion of the electromagnetic frequency spectrum that stretches from 30 GHz to 300 GHz. That is, freespace wavelengths from 1 cm to 1 mm. Interest in millimetre wave research can be traced back to the 1890s. For the history of the development of millimetre waves see for example the review paper by Wiltse [1].

The millimetre wave spectrum has been recognized to have useful properties [2], although many of its uses have been predicted rather than exploited by practical systems. The three main characteristics of millimetre waves that distinguish them from the microwave region are: smaller wavelength, greater bandwidth and greater interaction with gaseous and atmospheric constituents.

The small wavelength provides good target definition which has been used in rangefinding systems, harbour control, and to monitor cloud formation for meterological purposes. It also means that antennas can be made that have a large aperture whilst maintaining a small physical size. Thus systems can be made small enough to fit into confined spaces such as aircraft, and antennas can be used with very narrow beamwidths. This allows high efficiency and covertness in communications systems, and use as a tracking radar. The large band-

width available at these frequencies can support high capacity point to point links. These channels can also be widely separated to prevent cross-channel interference. The highly directive beams are also resistant to jamming and so highly secure communications links can be maintained.

The major disadvantage of the millimetre wave spectrum for radar and communications use is its attenuation by absorption in the atmosphere. Millimetre wave frequencies are comparable to the energy required to shift the energy levels of certain molecules by resonance absorption. When the molecule relaxes it reradiates the energy in a random fashion and causes attenuation of the incident signal. A graph of the average atmospheric absorption across the millimetre wave spectrum for two altitudes is shown in Fig. 1-1. It can be seen that the major resonances are caused by water at 22 and 183 GHz and oxygen at 60 GHz and 119 GHz. The condensed water particles found in clouds, fog and rain are of comparable size to millimetre waves and so cause scattering. In fact the attenuation due to rainfall etc. is the limiting factor in system reliability [4] and the path lengths between repeaters must be kept short (1 - 10 km) in order to combat this. Millimetre waves are however immune to smaller particles such as smoke (which are present in battlefield situations) which limit the use of optical rangefinding equipment. In order to reduce the attenuation by dissipation, radars and communication links have been proposed operating in the absorption spectrum "window " at 94 GHz. To ensure maximum security, it may be required in certain situations to restrict the range of communication. To this end, 60 GHz communication systems have been developed for such applications as battlefield line-on-sight links. In space, atmospheric absorption isn't a problem and millimetre waves have been proposed for satellite to satellite

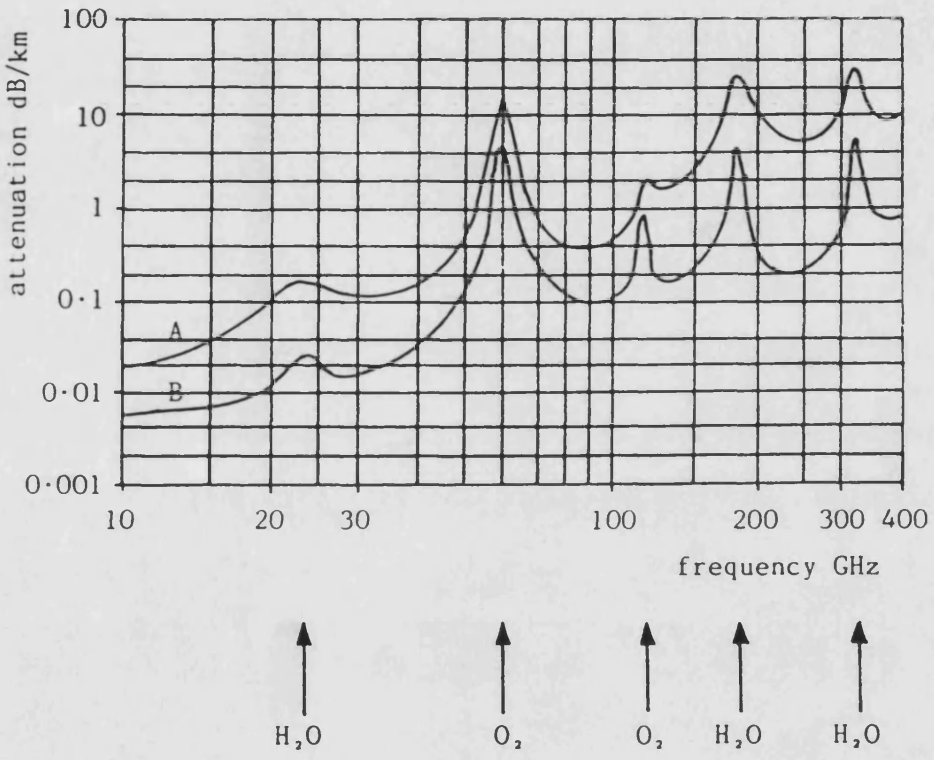

	A	B
altitude	sea level	4 km
temperature	20 °C	0 °C
pressure	760 mm	
density of water vapour	7·5 g/m³	1 g/m³

The average absorption of millimetre waves (taken from [3])

figure 1-1

communications [5]. The extremely wide bandwidth they offer could also be utilized to solve the problem of spectral overcrowding at lower frequencies by utilizing satellite links [6]. The absorption of millimetre waves by gases has led to spectroscopic research and has enabled much information to be obtained about the composition of molecules.

Although there are clearly many advantages to be obtained by using systems at millimetre wave frequencies there at present is a paucity of commercially available systems. This is due, in part to, the poor performance and high cost of solid state devices at these frequencies. Also, there is no preferred medium for designing and building circuits and so development costs can be high. However, with the continuing advances in device fabrication and efficiency and new devices such as HEM transistors [7] it is only a matter of time before the performance of millimetre wave systems allows commercial realization.

1-3 Transmission Lines for Millimetre Wave Use

At the lower microwave frequencies rectangular waveguide has been used both for power transmission and circuit components. Higher frequency applications have often been achieved by scaling down these lower frequency designs. As rectangular waveguide is reduced in size however, the losses increase faster than theory predicts. A typical ratio between the measured and predicted attenuation for rectangular waveguide at 70 GHz is 1.5 [8], increasing with frequency. One way of reducing the loss is to use oversize guide. The TE_{01} mode in circular waveguide has the attractive property that its attenuation decreases with frequency. However it is not the dominant mode and so mode filters must be used which makes component design difficult.

The requirement for a practical transmission line medium for millimetre wave circuits has produced several varied solutions. The choice of which structure to use for a given application is determined by such factors as:-

i) The overall guide loss - the unloaded Q

ii) Radiation loss

iii) Dispersion

iv) Monomode bandwidth

v) Ease of integrating active devices

vi) Realisation of circuit components

vii) Power handling capacity

viii) Ease of transition to other structures

ix) Ease of fabrication

x) Cost.

For many applications i, v and ix are the determining factors for a particular choice.

Many structures have been proposed which have claimed to satisfy the low loss characteristic or the device integration capability. In general no one structure is preferred over the rest due to the wide variety of engineering solutions that are required. Configurations can be broadly separated into the quasi-TEM and E-plane structures, and surface waveguiding structures, and will be discussed under these headings.

1-4 Quasi-TEM and E-plane Structures

The most widely used circuit structure in recent years for microwave integrated circuits has been microstrip [9], shown in Fig. 1-2(a). It consists of a flat low-loss substrate with a conducting ground plane on one side and strip conductors deposited on the other. The structure

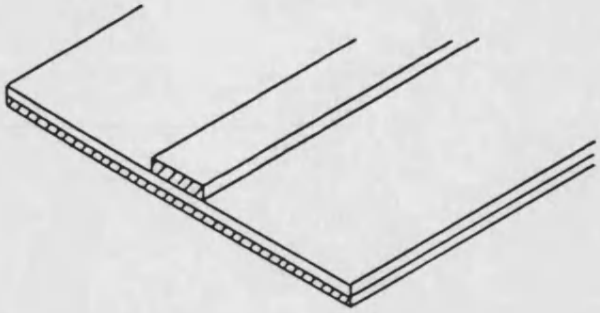

(a) Microstrip

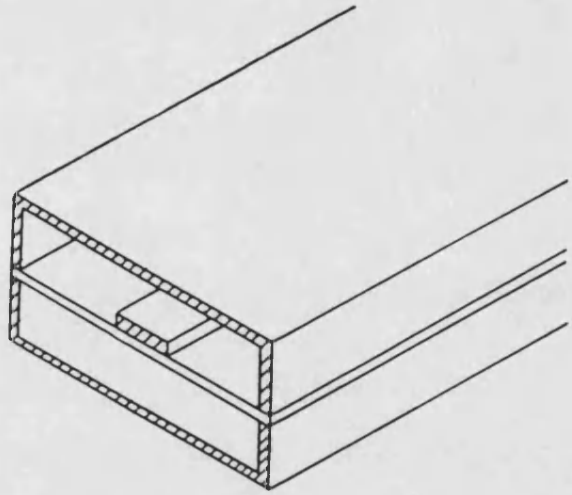

(b) Suspended substrate stripline

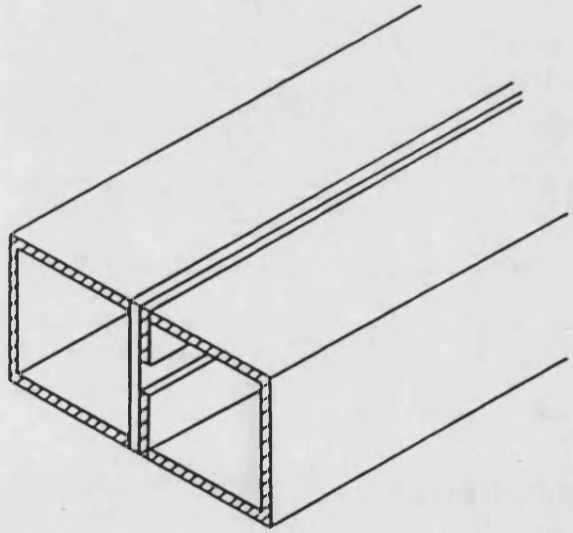

(c) Finline

Some popular quasi-TEM and E-plane structures.

figure 1-2

supports a quasi-TEM field which makes it amenable to device integration and simplifies circuit design. As with most of the planar circuits it can be fabricated using conventional printed circuit techniques. The use of microstrip however is limited at high frequencies by excessive radiation and conduction loss. The grounded dielectric substrate can always support a TM surface wave which can easily be excited by the quasi-TEM field. The coupling from the quasi-TEM field to the surface waves increases with frequency as their phase velocities become similar, and sets the high frequency limit. The conduction loss increases with frequency as the surface roughness of the dielectric upon which the conductors are deposited becomes more significant in relation to the skin depth. The radiation loss can be reduced by using thinner, lower permittivity substrates and the conduction loss can be reduced by using "smoother" substrate materials. The use of special substrate materials such as fused quartz, sapphire and other low loss materials can extend the operating range of microstrip circuits up to 100GHz. The circuit dimensions and tolerances required at these frequencies are at the limit of what can be achieved by the etching process and so it is not likely that the upper frequency limit of microstrip and other such structures can be extended much beyond 100 GHz.

Any practical circuit must be placed in some form of housing. A lower loss variant of microstrip made in this way is suspended substrate stripline (SSS) [10], shown in Fig. 1-2(b). Whilst in microstrip the field is mostly confined in the dielectric beneath the strips, in SSS the substrate is required only to support the strip conductors. The reduced field confinement in the dielectric and the removal of the ground plane from the dielectric surface causes a marked reduction in the loss of SSS when compared with microstrip.

Another popular structure is finline [11], shown in fig. 1-2(c). The planar circuit is placed in the E-plane of a rectangular housing and several variations of conductor orientation are possible. Finline is a widely used medium. The structure is compatible with the integration of beam lead devices, transitions to rectangular waveguide are easily achieved, and the loss, in the order of 0·1 dB/λ measured up to 40 GHz, is almost three times lower than that of a comparable microstrip structure.

In order to avoid higher order mode excitation problems the planar circuits must be housed in closures of similar size to the rectangular waveguide at that frequency. The need to fabricate the planar circuits to increasingly stringent tolerences at higher frequencies is limited by the etching process and so alternative, easier to manufacture structures are sought for frequencies above 100 GHz.

1-5 Surface Wave Structures

Surface waveguides are structures that support guided waves with a phase velocity less than the characteristic velocity for the particular medium. Such guided waves are thus known as "slow" waves. Various types of slow wave structures have been proposed, but they all basically operate by a similar mechanism. The transverse section consists of two or more regions which have different characteristic velocities. These regions may be layers of dielectric with different permitivities, or may be sections of different cross-sectional shape so that the effective dielectric constant (EDC) for each region is different. Either way the interface between the regions can support a wave that has a phase velocity somewhere between the characteristic velocities of both regions. The low loss nature of surface waveguides stems from

the fact that the slow wave propagates in low loss dielectric and can be made to be lossely bound to the structure. However, a loosely bound wave is difficult to efficiently launch and collect, and is significantly affected by even small discontinuities. The loosely bound nature of the field means that any change in the direction of guiding (such as bends) can cause the surface wave to detach itself from the guiding structure and radiate into the surrounding medium.

Some of the surface wave structures that have been proposed for millimetre wave use are shown in fig. 1-3. The simplest structure is that of image line [12], shown in fig 1-3(a). This structure consists of a dielectric rod, which need not be rectangular in cross-section, that is deposited onto a conducting ground plane. The field confinement of image line can be very poor, so whilst straight line loss can be very low (unloaded Q ≈ 2500), the bending loss is high. In order to increase the confinement to the guide a high permittivity dielectric material such as alumina ($\varepsilon_r \approx 9{\cdot}8$) is often used. This however increases the loss due to both dielectric dissipation and conductor loss. The conductor loss can be reduced by the use of insular line [13]. This structure, shown in fig 1-3(b), consists of the high permittivity dielectric line seperated from the ground plane by a thin layer of low permittivity dielectric. Since the majority of the field is confined to the high permittivity material the conduction loss is reduced. However the bend loss is still significant and the thin grounded layer can always support TM surface waves of its own and so leakage can occur [14]. To reduce the bending loss of image line, trapped image line has been proposed [15]. This structure, shown in fig. 1-3(c), consists of a dielectric line recessed into a groove in the ground plane which thus increases the field confinement. This structure has an added complexity

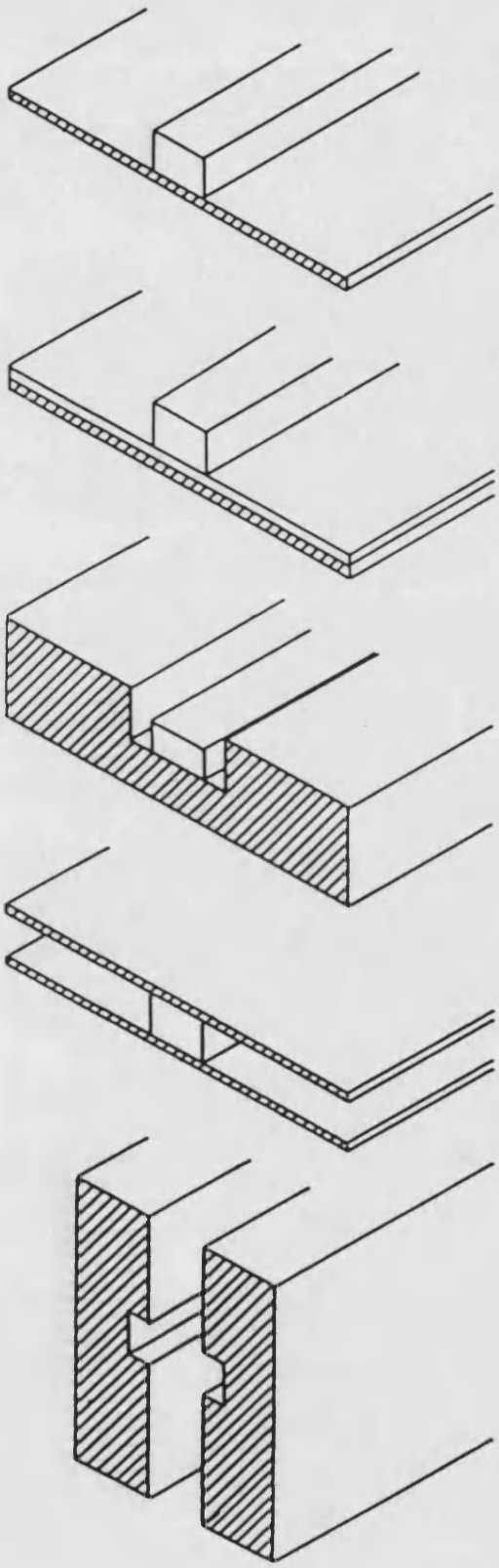

(a) Image line

(b) Insular line

(c) Trapped image line

(d) Non-radiative guide

(e) Groove guide

Some surface wave guiding structures

figure 1-3

of construction however that is a limiting factor for small, high frequency applications.

The radiation from bends can be eliminated by placing a ground plane on top of the image line to form non-radiative guide (NRD)[16] or H-guide shown in fig 1-3(d). It has the advantage that the structure excites a non-radiative mode on a bend. The companion structure to H-guide, groove guide [17], is shown in fig.1-3(e).

It is perhaps apparent that surface wave structures whist capable of achieving lower loss than E-plane structures such as finline are not as amenable to integration with active devices. However, such difficulties are not insurmountable and several active devices incorporated into into image line have been reported [18].

1-6 Inset Dielectric Guide

It is apparent from the cursory survey of waveguiding structures of the previous sections that there is no one preferred choice for millimetre wave applications. Due to the manufacturing complexity of such circuits and the various engineering solutions required, it is possible that there never will. In fact, millimetre wave system designs often incorporate several different waveguiding media. The subject of this thesis is the analysis of inset dielectric guide (IDG) which is shown in fig.1-4. This structure consists of a dielectric filled slot set in a metal ground plane. With so many other structures already available it is worthwhile to consider the motivation for the project.

The IDG structure was mentioned in [19] as a variation of image line that could have a practical use. However, the hybrid field is not

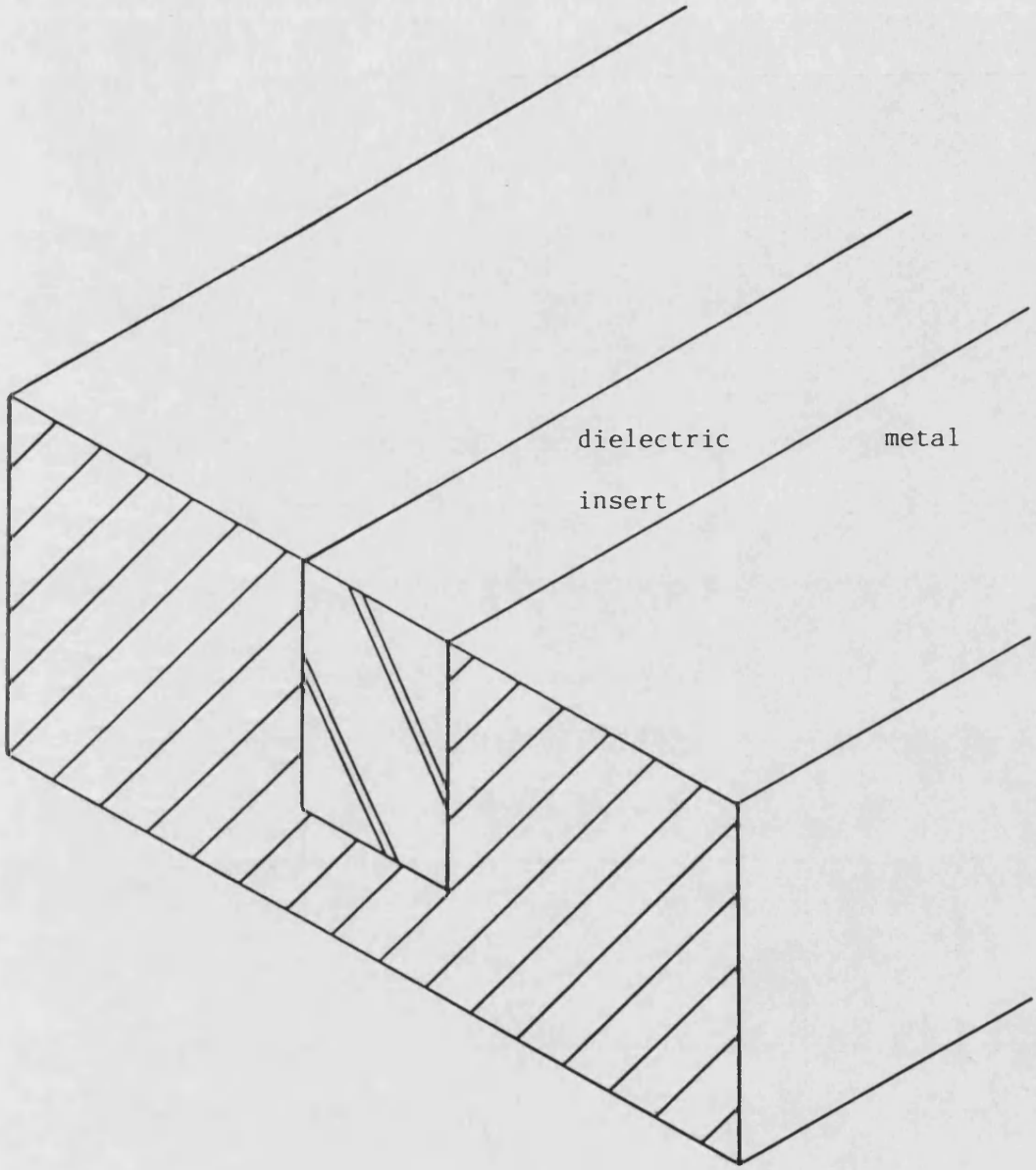

The Inset Dielectric Guide (IDG) structure

figure 1-4

amenable to a closed form expression and so it was not studied in detail. Interest in IDG was rekindled by Marconi Research Laboratories who supported this work, and a patent on the structure has been applied for [20]. This interest arose from a study of image line techniques. It was recognised that for frequencies above 100 GHz a dielectric guide such as image line would be required. However, image line had been found to be difficult to manufacture. The image line structure consists of a dielectric line, normally rectangular in cross-section, that is bonded to a metal ground plane. In order to maximize field confinement to the structure a high permittivity dielectric such as alumina is often used. The material can be prefabricated to the required dimensions and then bonded to the ground plane, although this becomes increasingly difficult for small dimensions and brittle materials. A further problem then is the bonding of the dielectric to the metal so as to provide mechanical strength and a good electrical contact. A manufacturing method more amenable to mass production and intricate circuit designs is screen printing [21]. However problems then become those of maintaining a good guide profile and avoiding air voids in the dielectric. A fundamental problem with image line is that any structural variations in the transverse plane will excite radiation so that the maintenance of a well defined profile is essential. The radiation problem becomes even more acute at bends and although systems have been demonstrated in image line [22] the theoretical predictions of low loss have not been readily achieved in practice. There is also the quite considerable problem of incorporating active devices in image line.

It is easier to machine a precision slot in a metal ground plane and then fill it with dielectric, than it is to manufacture dielectric to

the same dimensions. This was the prime philosophy behind the interest in IDG. The slot can be electroformed, or for mass production purposes, "stamped" into the metal. The dielectric material can be applied using similar techniques to those used in the screen printing of image line. Apart from assisting the manufacturing process, the slot also increases the field confinement in the dielectric and should reduce the radiation loss over image line. This should be especially so at bends and is a significant practical advantage.

For IDG to be of any practical importance it must be able to incorporate circuit components. The similarity between IDG and image line suggests that many of the device configurations demonstrated in image line [22] could be utilised in IDG. The reduction of bending loss could be significant in improving the component performances when incorporated in IDG. It is useful to consider how an active device could be incorporated in IDG since this has been a severe problem with image line. The commonest device to require integration at millimetre wave frequencies is the diode. In its various forms the diode is used for such system applications as power generation, detection, mixing, switching and limiting and so it is an important device. As will be shown in a later chapter the fundamental HE_{01} field in IDG has a constant electric field variation across the slot and a field maximum near the air/dielectric interface. This is a near ideal situation for diode integration since the device can be placed across the slot to couple strongly with the field without needing to modify the IDG structure. Such a situation is shown in fig. 1-5(a). In fig. 1-5(b) a possible method of manufacture of the diode junction is shown which is amenable to complex system design. IDG has also been shown to act as a leaky wave antenna when metal strips are placed across the slot as shown in

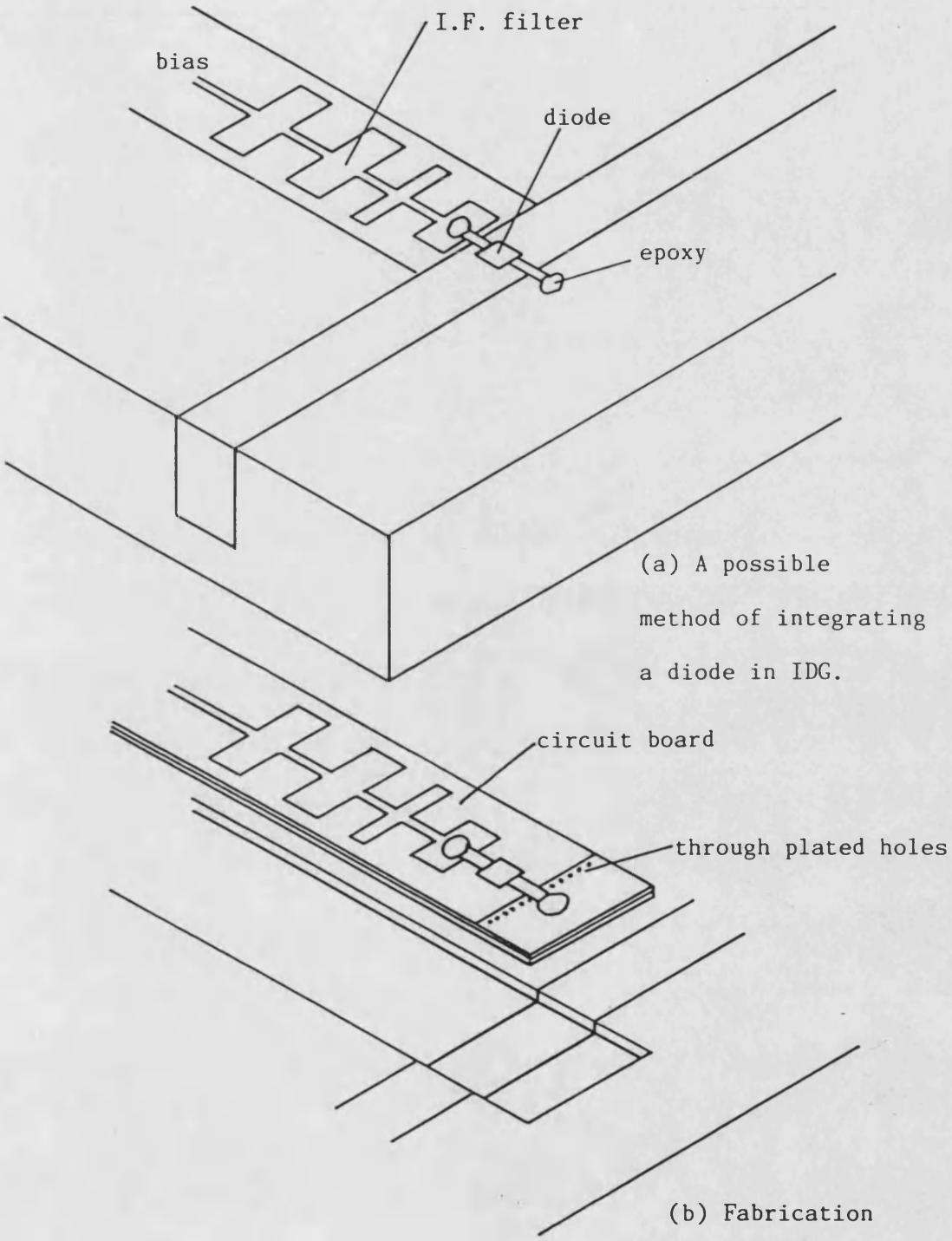

The integration of a diode in IDG

figure 1-5

fig. 1-6 [23]. Thus IDG could find use in phased array applications.

To summarise this section, three distinct advantages can be expected to arise from the use of the IDG structure rather than image line:

i) Simpler manufacture

ii) Lower radiation loss, especially from bends

iii) Easier implementation of active devices.

It was the aim of this work to provide a rigorous analysis of IDG so as to obtain the field and loss information and to assess its practical application and feasibility.

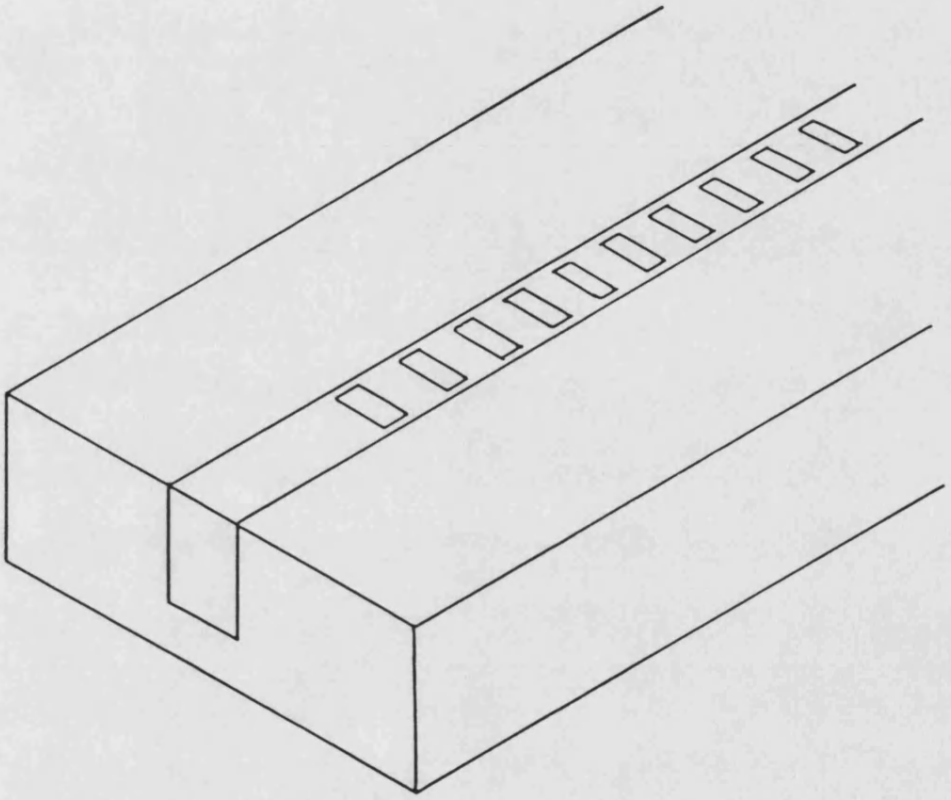

A method of placing metal strips on the IDG structure to form a leaky wave antenna.

figure 1-6

1-7 Outline of The Thesis

This section will briefly outline the content of this work. The remainder of the work is divided into five chapters. Chapter two is used to place the method of analysis adopted for this work, namely Transverse Resonance Diffraction (TRD), into context with the other methods that have been used to analyse other slow wave structures. The TRD method is also outlined in broad detail.

Chapter three is devoted to the full detailed account of the rigorous formulation of the dispersion equation obtained with the TRD method. Chapter four follows with computed solutions of the dispersion equation for various examples. Transverse field plots for various modal solutions are given along with experimental and theoretical comparisons of the propagation constant for several guides.

The loss characteristics of IDG are discussed in chapter five where dielectric and conductor loss for various guide geometries are derived and compared with measured values. The computed loss of a sample of IDG of W-Band (75-110 GHz) dimensions is also compared with published theoretical loss curves for image and insular guides. Some loss measurements of IDG bends are also given.

Finally in chapter six the results of the preceding chapters are brought together to enable observations and conclusions to be made. The need and scope of further work in this area is also discussed.

1-8 References

[1] J.C. Wiltse, "History of Millimetre and Submillimeter Waves", IEE Trans Microwave Theory Tech., Vol. MTT - 32, No 9 September 1984, pp 1118-1127.

[2] M.I. Skolnick, "Millimeter and Submillimeter Wave Applications", Polytechnic Institute of Brooklyn Symp. on Submillimeter Waves, 1970, pp 9-23.

[3] E.S. Rosenblum, "Atmospheric Absorption of 10-400 KMCPS Radiation", Microwave Journal, Vol. 4 March 1961, p 91.

[4] S.J. Dudzinsky, "Atmospheric Effects on Terrestrial MM-Wave Communications", Microwave Journal, Vol. 18 December 1975, pp 39-42.

[5] E.E. Allshuler, "New Applications at Millimetre Wavelenghts", Microwave Journal, Vol. 11, November 1968, pp 38-42

[6] L.C. Tillotson, "Millimetre Waves - Can they provide relief spectrum overcrowding?", Microwave Journal, Vol. 10 November 1967, p 32.

[7] F.A. Benson, "Attenuation of Rectangular Waveguide", Chapter 14, "Millimetre and Submillimetre Waves", Iliffe, London, 1969.

[8] K Joshin et al., "Noise Performance of Microwave HEMT", IEEE MTT-S, 1983, pp 563-565.

[9] D.D. Greig and H.F. Englemann, "Microstrip - A New Transmission Technique for the Kilomegacycle Range", Proc IRE, Vol 40, December 1952, pp 1644-1650.

[10] M.V. Schneider, "Dielectric Loss in Integrated Microwave Circuits", The Bell Syst. Tech. Journal, September 1969, pp 2325-2332.

[11] P.J. Meier, "Integrated Fin-Line Millimeter Components", IEEE Trans. Microwave Theory Tech., Vol. MTT-22, No 12, December 1974, pp 1209-1216.

[12] D.D. King, "Properties of Dielectric Image Lines", IRE Trans. Microwave Theory Tech., Vol MTT-3, March 1955, pp 75-81.

[13] R.M. Knox and P.P. Toulios, "Integrated Circuits for the Millimetre through Optical Frequency Range", Proc. Symp. Submillimetre Waves, New York 1970.

[14] S. Peng and A.A. Oliner, "Guidance and Leakage Properties of a Class of Open Dielectric Waveguides", Part 1 - Mathematical Formulations", IEEE Trans. Microwave Theory Tech., Vol MTT-29, No 9, September 1981, pp 843-854.

[15] T. Itoh and B. Adelseck, "Trapped Image Guide for Millimetre Wave Circuits", IEEE Trans. Microwave Theory Tech., Vol. MTT-28, December 1980, pp 1433-1436.

[16] T Yoneyama and S. Nishida, "Nonradiative Dielectric Waveguide for Millimetre Wave Integrated Circuits", IEEE Trans. Microwave Theory Tech., Vol. MTT-29, November 1981, pp 1188-1192.

[17] F.J. Tisher, "The Groove Guide, a low-loss Waveguide for Millimetre Waves", IEEE Trans. Microwave Theory Tech., September 1963, pp 291-296.

[18] R.M. Knox and N.C. Deo, "Millimetre Wave Dielectic Guide Components and Integrated Sub-Systems", Proc. Military Microwaves Conference, London, England, 1982, pp 455-460.

[19] D.D. King and S.P. Schlesinger, "Dielectric Image Lines", IRE Trans Microwave Theory Tech., Vol MTT-6, July 1958, pp 291-299.

[20] P.H. Wisbey, The Marconi Company Limited, UK Patent, GB 2109640A.

[21] R.V. Gelsthorpe, N. Williams and N.M. Davey, "Dielectric Waveguide; a low-cost technology for Millimetre Wave Integrated Circuits", The Radio and Electronic Engineer, Vol. 52, No 11/12, November/December 1982, pp 522-528.

[22] R.M. Knox, "Dielectric Waveguide Microwave Integrated Circuits - An Overview", IEEE Trans Microwave Theory Tech., Vol MTT-24, No 11, November 1976, pp 806-814.

[23] T. Rozzi and L. Ma, "Scattering of dipoles in Inset Dielectric Guide

and Applications to Millimetric Leaky Wave Applications", Proc 17th European Microwave Conference, September 1987.

CHAPTER TWO

A SURVEY OF NUMERICAL METHODS AND INTRODUCTION TO THE TRANSVERSE RESONANCE DIFFRACTION METHOD

2-1 Introduction

The manufacture of circuits that operate in the millimetre wave region is a very expensive process. The small size and high tolerances required necessitate precision machining operations and can involve special processes such as electroforming and laser cutting. The high unit cost inhibits a trial and error design approach, where many iterations may be necessary. Instead, the design must be optimised as much as possible prior to the initial fabrication stage. This, in turn, requires an accurate knowledge of the electrical properties of the circuit media so that accurate and efficient design and analysis procedures can be developed.

It is the purpose of this chapter to introduce the method of analysis used in this work to compute the field solutions of Inset Dielectric Guide. The full exposition of the method is given in Chapter 3. However, a summary of the major steps involved, provided here, will aid the understanding of this chapter. The method of Transverse Resonance Diffraction (TRD), is an accurate and efficient approach which is easy to formulate and quickly convergent to the solution. In order to put the TRD approach into context a review of some other methodsof analysis is given in the first part of this chapter.

2-2 The Solution of Field Problems

The macroscopic electric and magnetic field vectors are related by Maxwell's equations [1]. A physical field solution must satisfy these equations and must be specified at the boundaries to the region over which the solution is sought. However, the direct solution of Maxwell's equations is only possible for a few simple cases, generally where the boundaries lie on the axes of the co-ordinate system used. Accordingly,

when image line was first proposed [2] a dielectric layer of semi-circular cross-section was chosen since this facilitated a direct field solution in polar co-ordinates, utilizing Bessel functions.

In general two approaches can be made to the solution. On the one hand the approach is a numerical one, where no prior knowledge of the field is assumed and a purely iterative process is used to arrive at a solution. On the other hand, an analytic approach can be adopted, where knowledge of the solution and algebraic manipulation are used to reduce the equations prior to computation. The former approach is very general but can be inefficient, giving slow convergence to a solution and requiring extensive computer resources. The latter approach can give very accurate results with minimal computation. However the formulation is more complex and the various methods tend to be limited to specific types of structures. Several methods of analysis have been developed in recent years [3], [4] and some of these are reviewed in the next sections. This review is not intended to be complete or exhaustive but to highlight some of the main philosophies behind the solution of such problems.

2-3 Numerical Methods

A method that has been much favoured in the past is the finite element method [5]. This method is the least analytical and perhaps the easiest to formulate. However a lot of computing effort is required and solutions are often slow to converge. In its simplest form, the area over which a field solution is sought, say the guide cross-section, is sub-divided into a number of elementary shapes or elements. Each element is defined by the "nodes" that surround it and the field within each element is expressed in terms of the field values at the nodes. Those nodes that lie on the boundaries of the discretised area

are made to satisfy the boundary conditions of the sought after solutions. By imposing continuity between the elements the field values at the other nodes are found. The method, whilst being slow, has the advantage that no prior knowledge of the field variation is required. The accuracy and speed of the method are dependent upon the shape, size and number of the elements, and the function used to derive the elemental field from the node values. This approach can only be used to determine the discrete (bound) modes and care must be taken to avoid the spurious solutions that can occur. Open structures can be analysed although the radiation field cannot be solved for and special steps must be taken at any field singularities.

A more analytical method which still requires extensive computer resources is that of mode matching [6]. Although this approach has classically been used for the solution of discontinuity problems in waveguides, it has been applied to composite guiding structures. For example it was used by Solbach et al to analyse Dielectric Image Lines [7]. In this approach the guide structure is separated into several regions. In each region the fields are written as sets of orthogonal functions (modes) that each satisfy the required boundary conditions. The field solutions are obtained as the superposition of the modes in each region such that the field continuity between the regions is satisfied. That is, by expanding each field component in terms of the modes and equating the field components in each region at any continuous boundary, sets of linear equations in the unknown mode amplitudes can be obtained. These can then be solved using standard matrix techniques.

The mode matching equations are only exact when infinite numbers of modes (i.e. complete sets) are taken in each region. For numerical computation these sets necessarily have to be truncated to finite values. However, to maintain accuracy large matrices may still be required to be handled by the computer, resulting in expensive and slow programs and numerical problems such as "ill-conditioned" matrices. Care also has to be taken when truncating the matrices to ensure that the correct ratio between the number of modes in each region is taken so as to avoid "relative convergence" problems [8].

2-4 Analytical Approaches

A semi-analytical approach often used is the effective dielectric constant (EDC) method, where the structure is approximated to a simpler one for which a direct solution to Maxwell's equations exist. The EDC method was introduced by Knox and Toulios in their analysis of Image Line [9], and has been used by Itoh et al to give useful results for trapped image guide [10].

The approach is to divide the guide into several laterally piecewise uniform regions and to replace each of them by a single homogenous region of "effective" dielectric constant ε_{eff}. The function ε_{eff} is such that a plane wave propagates in this hypothetical medium with the same phase velocity as the guided wave in the composite structure it replaces. In this manner the original problem is transformed into the solution of the propagation of a plane wave along a stack of dielectric slab waveguides. The EDC method is only approximate and its shortcomings are discussed by Oliner et al [11], namely that single mode propagation only is assumed in each region and discontinuities at the boundaries between successive lateral regions are ignored.

As stated previously, a direct solution of Maxwell's equations is only possible in a few cases. Generally, the solution must be found using approximation methods. For this reason it is advantageous to recast Maxwell's equations in their integral form. Since integration is a summation process it is not necessary that the various elements are calculated exactly, only that their overall combination is accurate. Thus in an approximation process as long as the major contributions to an integral are accounted for then a reasonably accurate result can be obtained.

When one set of field components (the excited field) is written in terms of another (the source field), a coupled set of integral equations can be obtained. The integral "operators" that act upon one set to give the other are a form of Green's function [12]. These operators determine the field excitation and so must satisfy the relevant boundary conditions. Hence the field problem is uniquely specified by the Green's functions and the source functions that they act upon. The coupled integral equations obtained in this way must be solved and a variety of approximation techniques have been developed for this purpose such as moment methods [13]. The general objective of these methods is the transformation of the integral equations into sets of algebraic equations that can be solved using matrix techniques. They also have the advantage that many of them are variational in some quantity [14], in this case the propagation constants, β. That is, the sought after quantities are found at a function minimum, so that a first order variation in the excitation function gives a second order variation in the solution. This is a useful property when the excited field is known only approximately. The general moment method proceeds as follows. The excited field, which is an unknown quantity is expanded onto a complete set of known functions. The Green's operators are functions of position of both the source and excited field vectors. Thus the

substitution of the excited field expansion into the integral equation results in a set of inner products which can be evaluated to remove the space dependency of the field unknown. The scalar multiplication of this equation with another set of functions orthogonal in the source space reduces the operator equation into a matrix equation which can be solved using standard techniques. When the same expansion set is used to discretise both the excited and source functions then the method is known as Galerkin's method. From this rather cursory explanation two points can be noted. The ease of formulation and the accuracy of the solution are dependent upon the ability to find the correct Green's operators and the choice of expansion functions.

The solution of Maxwell's equations by the formulation of the appropriate Green's operators and the subsequent application of the method of moments is used by Denlinger [15] to obtain a field solution for microstrip line. An alternative approach to obtaining a set of linear algebraic equations is to manipulate the Fourier transformed field and source quantities into sets of coupled equations prior to discretisation and solution by a moment method. This approach, which involves the formulation of the Green's operators in the Fourier domain is the Spectral Domain approach as introduced by Itoh [16]. The first method involves the transformation of the integral equations in the space domain and the second, the transformation in the spectral (wavenumber) domain. The preference for either approach is dependent upon the relative ease of formulating the problem and the convergence of the solution. For example the coupled integral equations generated in a space domain approach may be unwieldy whilst the operators required in the Fourier domain can be often found "by inspection" [17]. However the major test of any approach is its rate of convergence to a solution and its accuracy. Both the space and Fourier domain approaches

as outlined here use a moment method and expand some unknown function in terms of a complete set of known functions. This unknown may be the current distribution across a metal strip or the electric field at some boundary for example.

The accuracy of the expansions into these basis functions as they are known determines the accuracy of the method. If, for example, a given function required a superposition of thirty basis terms to model it then the resulting matrix inversion would be large resulting in a high computation time. Thus each method can be improved in efficiency if the basis terms are chosen to accurately model the expected solution. This assumes an a priori knowledge of the form of the solution which can generally be ascertained from a consideration of the boundary conditions. More importantly, the basis functions used in a spectral domain analysis must be Fourier transformable. This restriction requires in some cases a non-optimum basis set to be used. Furthermore, the spectral domain approach may not be applicable at all in a situation where the transverse cross-section is non-uniform and there are two or more separate sub-sections, since the Fourier transform in each will be different. In the straight application of the spectral domain method it is essential that one dimension remains the same, namely that with respect to which the Fourier transformation is made. Thus the spectral domain technique could not be applied to the inset dielectric guide structure.

In general the space domain approach can be more difficult to formulate but a specially tailored basis set, chosen to give fast convergence, can always be used. The spectral domain method can be easily formulated but its efficiency and implementation are dependent on the ease of Fourier transforming the variables. Each method is dependent upon the particular structure to be analysed and so each have their merits in certain situations.

2-5 Transverse Resonance Diffraction

Transverse Resonance Diffraction, the method of analysis used in this thesis, is a space domain approach. The coupled integral equations are obtained in terms of a transverse equivalent circuit and are easily formulated. The basis functions are chosen to accurately model the singularities of the unknowns, giving fast convergence to a solution. Whilst this method is used here to analyse IDG, it has been used to efficiently analyse image line [18], finline [19] and microstrip [20]. In order that the TRD formulation, outlined in detail in the next chapter can be followed more easily, it is instructive to give an overview of the method, However, before this is done it is useful to introduce the idea of a transverse equivalent circuit and transverse resonance.

2-6 The Transverse Equivalent Circuit

The correspondance between the solution of the wave equation for an electromagnetic field and the telegraphist's equations for the voltage and current distributions on a uniform transmission line was first introduced by Shelkunoff [21]. The transverse electric and magnetic fields of a TE and TM mode have similar properties to the voltage and current waves of a TEM field on a transmission line. In both cases propagation is of the same $\exp(-j\beta z)$ dependence, and a constant relationship (impedance) can be obtained for the transverse field quantities. Thus it is convenient to define equivalent current and voltage waves for the transverse magnetic and electric fields of a mode, such that the characteristic impedance of the equivalent transmission line is equal to the wave impedance of that mode. The transmission line analogy then enables circuit theory and impedance concepts to be implemented in the solution of discontinuity problems and can simplify the

formulation of certain field problems.

In general any field can be constructed from the superposition of a suitable set of TE and TM modes, each of which can be modelled as a transmission line. Thus if in the direction of propagation considered the structure consists of piecewise uniform and homogeneous regions then an equivalent circuit consisting of uniform TE and TM transmission lines can be found. Thus in a composite structure such as IDG, it is convenient to formulate the field solutions for propagation in a transverse direction (where the structure is piecewise uniform and homogeneous) and obtain a transverse equivalent circuit.

By enforcing the continuity of the electric and magnetic components transverse to the assumed direction of propagation at a suitable plane, then an eigenvalue equation for the propagation constant β can be obtained. In terms of the equivalent circuit this condition requires that the impedance (admittance) seen looking into the circuit each side of the plane be equal and opposite and so it constitutes a condition of resonance [22]. Thus, if the nature of the field is such that an equivalent circuit model can be obtained then the resonant condition of that circuit will give a characteristic equation for β. This approach has been used for example by Dagli et al. to analyse rib dielectric waveguides [23].

An equivalent circuit representation can also simplify the formulation of the Green's operators. In general the TE and TM components of a field will consist of five field components. However, as shown by Itoh [17] a transverse co-ordinate rotation can be defined that decouples the five field components into three, so that a knowledge of the equivalent circuit enables the Green's operators to be formulated almost "by inspection".

2-7 An Overview of the Transverse Resonance Diffraction method as used in this thesis

In the next chapter the formulation of the eigenvalue problem for IDG, as obtained by using the TRD approach is explained in detail. However, as an aid to clarify the essential steps involved it is instructive to include here an overview of the formulation.

An eigenvalue equation is sought for the guided field solutions, or modes of the IDG. That is, a field solution that allows propagation of energy in the axial direction only, with phase velocity β. The co-ordinate system used for the analysis of the IDG structure is given in fig. 2-1. The transverse field distribution of IDG can be conveniently separated into two regions. In the slot region ($y < 0$), the boundary conditions allow a field formulation in terms of a discrete set of waveguide type modes. In the air region ($y > 0$) the semi-infinite region can support a continuum of modes, or partial waves. The transverse field components are of course continuous across the interface between the two regions at $y = 0$.

The field components are derived from y-directed electric and magnetic Hertzian potential functions, defined for each region. This allows the hybrid field to be decoupled into TE and TM components wrt y, allowing an equivalent transmission network to be obtained for the transverse circuit, and simplifying the formulation of the Green's operators. The general deterministic problem can be expressed as:

$$L \cdot f = y \qquad (2\text{-}1)$$

where L is a linear operator, f is an unknown function and y is a source or excitation function. The accuracy and efficiency of the solution of such a problem by a moment method [24] is influenced by the closeness of the expansion functions to the physical solution f.

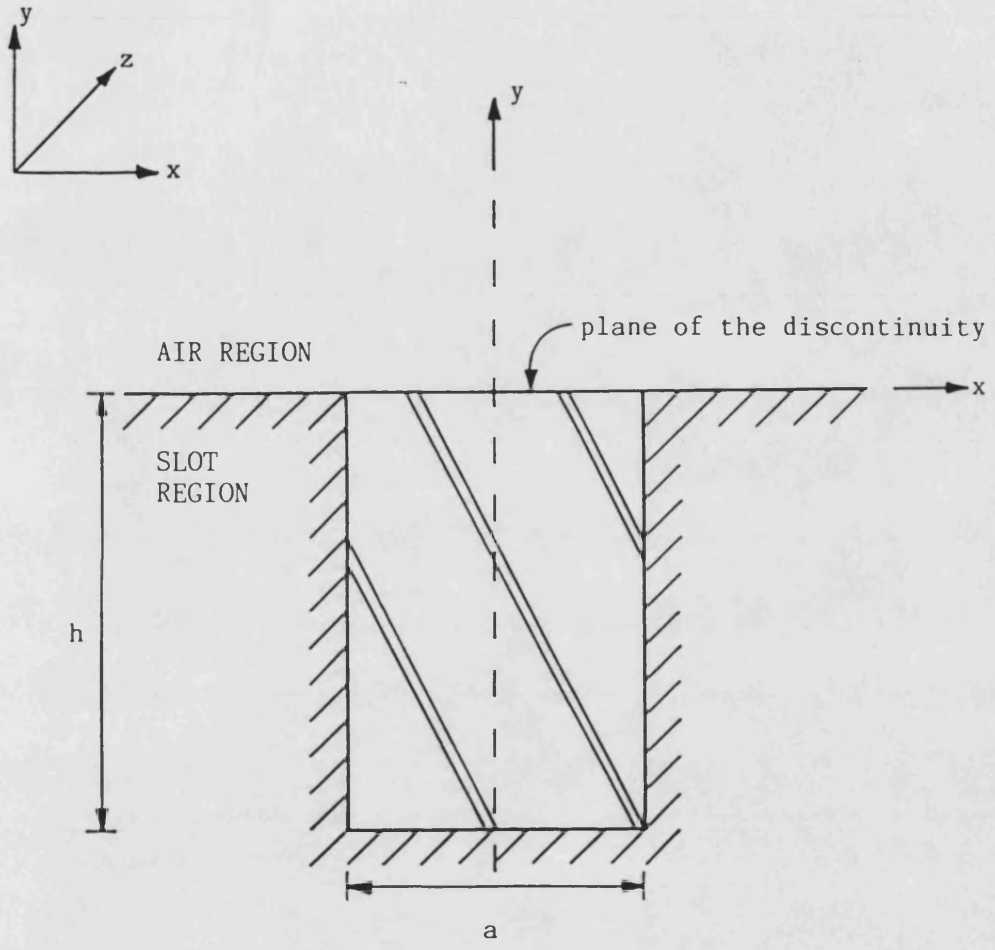

The coordinate system used for the analysis of inset dielectric guide

figure 2-1

In the case of IDG a convenient field to retain as the unknown is the electric field transverse to y at the interface. The field at this plane can be accurately modelled by the modal solutions of parallel plate guide, modified to include the singular effect of the 90^{o} metal edges at $y = 0$, $x = \pm {}^{a}/2$. Thus an efficient set of expansion functions can be used. With the transverse electric field (to y) retained as the unknown and the transverse magnetic field as the source, the Green's operators take the dimensions of an admittance and (2-1) becomes for each region

$$\hat{Y}s \cdot Et = Ht \qquad y \leq 0 \qquad (2\text{-}2(a))$$

$$\hat{Y}a \cdot Et = -Ht \qquad y \geq 0 \qquad (2\text{-}2(b))$$

where s and a refer to the slot and air regions and the minus sign indicates that the operators have been formulated in each case for power flow away from the interface. The operators are linear and so continuity of the transverse field at the interface gives:

$$(\hat{Y}s + \hat{Y}a) \cdot Et = 0 \qquad (2\text{-}3)$$

This is a statement of transverse resonance since the zero source function excites a finite response. Writing $\hat{Y}s + \hat{Y}a = \hat{Y}$, (2-3) can be expanded to:

$$\begin{bmatrix} \hat{Y}_{12} & \hat{Y}_{12} \\ \hat{Y}_{21} & \hat{Y}_{22} \end{bmatrix} \cdot \begin{bmatrix} Ex(x,o) \\ Ez(x,o) \end{bmatrix} = \underline{0} \qquad (2\text{-}4)$$

In this form two sets of expansion functions are required to accurately approximate Ex(x,o) and Ez(x,o), since they each have a different x-dependence. However, it is noted that Ex(x,o) and ${}^{a}/\pi \; dEz(x,o)/dx$ have the same x-dependence and dimensionality and so (2-4) is conveniently

integrated by parts to yield:

$$\begin{bmatrix} \hat{Y}_{11} & \hat{Y}_{12} \\ \hat{Y}_{21} & \hat{Y}_{22} \end{bmatrix} \cdot \begin{bmatrix} Ex(x,o) \\ \frac{a}{\pi} \frac{dEz}{dx}(x,o) \end{bmatrix} = \underline{0} \qquad (2\text{-}5)$$

the same symbols being retained for the changed operators. The same basis set can now be used to accurately expand both field unknowns, namely:

$$Ex(x,o) = W(x) \sum_{m=0,2}^{\infty} Xm\ fm(x) \qquad (2\text{-}6a)$$

$$\left(\frac{a}{\pi}\right) \frac{dEz}{dx}(x,o) = W(x) \sum_{m\ 2,4}^{\infty} Zm\ fm(x) \qquad (2\text{-}6b)$$

where fm(x) are the normalised Gegenbauer polynomials:

$$fm(x) = \frac{1}{Nm} C_m^{1/6} \left(\frac{2x}{a}\right)$$

with the weight function

$$W(x) = \left[1 - \left(\frac{2x}{a} \right)^2 \right]^{-1/3}$$

which is discussed further in the following chapter. By applying Galerkin's method the integral equation is transformed into the matrix equation:

$$\left(\underline{\underline{Y}} \right) \left(\begin{matrix} \underline{X} \\ \underline{Z} \end{matrix} \right) = 0 \qquad (2\text{-}7)$$

This has a non-trivial solution when

$$\det\left(\underline{\underline{Y}}\right) = 0 \qquad (2\text{-}8)$$

which is an equation for β.

However, in order to obtain a scalar transverse equivalent circuit and simplify the computation of the field amplitudes $\underline{X}$ and $\underline{Z}$ it it convenient to recast the problem. The transverse equivalent network consists of a discrete set of short circuited TE and TM transmission lines coupled at the interface into the airspace continuum. For the region of interest, only the fundamental TE slot mode will be above cutoff. By considering the air/dielectric interface to be a discontinuity that excites all the higher order non-propagating slot and air modes the fundamental mode can be removed from (2-5) to give

$$\begin{bmatrix} \hat{Y} \end{bmatrix} \cdot \begin{bmatrix} Ex(x,o) \\ \frac{a}{\pi} \frac{dEz(x,o)}{dx}/dx \end{bmatrix} = \begin{bmatrix} -Hz_o \phi ho(x) \\ 0 \end{bmatrix} \qquad (2-9)$$

where $\phi ho(x)$ is the fundamental TE slot mode function and the operator Y now has the fundamental slot term removed. By defining the inner product:

$$Pmn = \langle W(x)\ fm(x)\ \phi hn(x) \rangle$$

then the discretisation of (2-9) gives:

$$\begin{bmatrix} \underline{\underline{Y}} \end{bmatrix} \begin{bmatrix} \underline{X} \\ \underline{Z} \end{bmatrix} = (-Hzo) \begin{bmatrix} \underline{P}o \\ \underline{0} \end{bmatrix} \qquad (2-10)$$

and the field amplitude are easily found from:

$$\begin{bmatrix} \underline{X} \\ \underline{Z} \end{bmatrix} = (Hzo)\ \underline{\underline{Y}}^{-1} \begin{bmatrix} \underline{P}o \\ \underline{0} \end{bmatrix} \qquad (2-11)$$

By multiplying both sides by $\begin{bmatrix} \underline{P}o \\ \underline{0} \end{bmatrix}^T$ and using the result that

$$\underline{P}_o^T \cdot \underline{X} = Exo$$

gives:

$$\frac{-Hzo}{Exo} = \left((\underline{P_o}^T \; \underline{0}^T) \cdot \underline{\underline{Y}}^{-1} \cdot \begin{bmatrix} \underline{P_o} \\ \underline{0} \end{bmatrix} \right) \qquad (2\text{-}12)$$

The input admittance of the equivalent transmission line for the fundamental mode is:

$$\frac{Hzo}{Exo} = -j \cot kyoh \qquad (2\text{-}13)$$

and so (2-13) represents the admittance of the higher order slot and air modes at resonance

Thus

$$-j \cot kyoh + \left((\underline{P_o}^T \; \underline{0}^T) \cdot \underline{\underline{Y}}^{-1} \cdot \begin{bmatrix} \underline{P_o} \\ \underline{0} \end{bmatrix} \right)^{-1} = 0 \qquad (2\text{-}14)$$

is the condition for transverse resonance of the transverse equivalent circuit and is a scalar dispersion equation for β.

2-8 References

[1] J.A. Stratton, "Electromagnetic Theory", McGraw-Hill, 1941.

[2] D.D. King, "Dielectric Image Line", J. Appl. Physics, vol 23 June 1952, pp. 699-700.

[3] S.M. Saad, "Review of Numerical Methods for the Analysis of Arbitrarily Shaped Microwavw and Optical Dielectric Waveguides", IEEE Trans. Microwave Theory Tech. vol MTT-33, pp. 894-899, Oct 1985.

[4] T. Itoh, "An Overview on Numerical Techniques for Modelling 3-Dimensional Passive Components", Proc 15th European Microwave Conference (Paris) Sept 1985, pp. 1059-1063.

[5] B.M.A. Rahman and J,B, Davies, "Finite-Element Analysis of Optical and Microwave Waveguide Problems", IEEE Trans. Microwave Theory Tech., vol MTT-32, pp. 20-28, Jan 1984.

[6] A. Wexler , "Solution of Waveguide Discontinuities by Modal Analysis", IEEE Trans. Microwave Theory Tech., vol MTT-15, pp 508-517, Sept 1967.

[7] K. Solbach and I. Wolff, "The Electromagnetic Fields and the Phase Constants of Dielectric Image Lines", IEEE Trans. Microwave Theory Tech., vol MTT-26, pp 266-274, April 1978.

[8] R,Mittra, T. Itoh and T. Li, " Analytical and Numerical Studies of the Relative Convergence Phenomenon Arising in the Solution of an Integral Equation by the Moment Method", IEEE Trans. Microwave Theory tech., vol MTT-20, pp 96-104, Feb 1972.

[9] R.M. Knox and P.P. Toulios, "Integrated Circuits for the Millimeter Wave through Optical Frequency Range", Proc. Symp. Submillimeter Waves, Brooklyn, N.Y., Polytechnic Press, April 1970, pp. 497-516.

[10] W. Zhou and T. Itoh, "Analysis of Trapped Image Guides Using Effective Dielectric Constant and Surface Impedances", IEEE Trans. Microwave Theory Tech., vol MTT-30, pp. 2163-2166, Dec 1982.

[11] S. Peng and A.A. Oliner, "Guidance and Leakage Properties of a Class of Open Waveguides", IEEE Trans Microwave Theory Tech. vol MTT-29, pp. 843-869, Sept 1981.

[12] H.M. de Ruiter, "Integral Equation Approach to the Computation of Modes in an Optical Waveguide", J. Opt. Soc. Am., vol 70, pp 1519-1524, Dec 1980.

[13] R.F. Harrington, "Matrix Methods for Field Problems", Proc. IEEE vol-55 No.2, pp. 136-149, Feb 1967.

[14] Waldron, "Theory of Guided Electromagnetic Waves", chapter 8,Van Nostrand, 1970, p. 426.

[15] E. Denlinger, "A Frequency Dependant Solution for Microstrip Transmission Lines", IEEE Trans. Microwave Theory Tech., vol MTT-19, pp. 30-39, July 1980.

[16] T. Itoh and R. Mittra, "A Technique for Computing Dispersion Charactaristics of Shielded Microstrip Lines", IEEE Trans. Microwave Theory Tech., vol MTT-22, pp. 896-898, Oct 1974.

[17] T. Itoh, "Spectral Domain Immitance Approach for Dispersion Charactaristics of Generalised Printed Transmission Lines", IEEE Trans Microwave Theory Tech., vol MTT-28, pp.733-736, July 1980.

[18] J. Kot and T. Rozzi, "Rigorous Modelling of Single and Coupled Rectangular Dielectric Waveguides by Transverse Resonance Diffraction", Proc. 14th European Microwave Conference (Liege), Sept 1984, pp.424-429

[19] C.A. Olley and T. Rozzi, "Characterisation of Unilateral Finline Mode Spectrum Including Loss Analysis", Proc. 16th European Microwave Conference (Dublin), Sept 1986, pp. 551-516.

[20] C.J. Railton, T. Rozzi and J. Kot, " The Efficient Calculation of High Order Shielded Microstrip Modes for use in Discontinuity Problems", Proc 16th European Microwave Conference (Dublin), Sept 1986, pp.529-534.

[21] S. Schelkunoff, "Generalised Telegraphists Equations for Waveguides" The Bell Syst. Tech. J., July 1952, pp.784-801

[22] R.E. Collin, "Field Theory of Guided Waves", McGraw-Hill, 1961, p.115

[23] N. Dagli and C.G. Fonstad, "Analysis of Rib Dielectric Waveguides", IEEE J. Quantum Elec., vol QE-21, No. 4, April 1985, pp. 315-321.

CHAPTER THREE

THE FORMULATION OF THE DISPERSION EQUATION FOR IDG USING THE TRANSVERSE RESONANCE DIFFRACTION METHOD

3-1 Introduction

The purpose of this chapter is to expand fully on the overview of the Transverse Resonance Diffraction method outlined in the previous chapter. The detailed formulation is given for the field solution of the discrete bound modes of Inset Dielectric Guide. Numerical results obtained from the formulation are given in chapter four.

3-2 Field Components and Boundary Conditions

The object of this analysis is the determination of the electromagnetic field distributions of IDG for the bound modes. The functions that can correctly model the electric and magnetic field distributions are limited to those solutions of Maxwell's equations which satisfy the relevant boundary conditions. A direct solution of Maxwell's equations is extremely difficult for all but the simplest boundary conditions and so indirect methods must be used. One method involves the use of "Auxilliary Potential functions". These are mathematical functions that are chosen to have the vector properties of either the electric or magnetic fields, and are thus themselves solutions of Maxwell's equations. Maxwell's equations are assumed here to be linear and homogeneous, so that the superposition of solutions to Maxwell's equations is itself a solution. Thus having chosen a suitable set of potential functions the problem is reduced to that of finding the superposition of the functions that satisfies the boundary conditions.

The cross sectional geometry of IDG along with the coordinate system used in this analysis has already been given in fig. 2-1. It can be supposed from this diagram that the field distribution of IDG would resemble that of a dielectric filled, rectangular waveguide with one of the narrow walls removed. With this analogy the IDG structure can

be split into two regions. The slot region, where discrete waveguide like modes would be expected and the air region which can support a continuum of modes. It is thus apparent that since the nature of the field solutions is different for each region then different sets of potential functions will be required for each region. The two sets will form the overall field solution and so will be continuous across the interface between the two regions.

The field in a parallel plate guide can be conveniently described as TE or TM with respect to the axis of propagation, that is, with a suitable set of three components. The field in IDG can be viewed in the transverse direction as being analogous to that of a short-circuited section of parallel plate guide radiating into freespace. The junction of the parallel plate guide with the ground plane gives rise to a 90^{o} metal edge which introduces a discontinuity into the transverse field components. This discontinuity in the boundary conditiond requires that the field go to infinity at the edge. However the order of this singularity must be such that the energy stored in the vicinity of the edge remains finite. In [1] it is shown that for a 90^{o} metal edge the minimum allowable singularity to satisfy this condition is $r^{-\frac{1}{3}}$, where r is the radial distace from the edge. Such a discontinuity requires a full six field component construction to accurately describe it. However, any arbitrary six component field can be constructed from the superposition of suitably chosen TE and TM fields.

The field in each region will be of a different form although for a guided mode the propagation constant β will be the same and continuity of the transverse fields will apply at the boundary between the two regions. Since the modal field can be derived from a knowledge of the

transverse field components only, and the z-directed variation is common to both regions, it is convenient to analyse the structure for propagation in the transverse y-direction.

A y-directed TE field can be derived from a magnetic hertzian potential [2] defined as:

$$\underline{\Pi}_h = \hat{y}\, \Psi_h(x,y)\, e^{-\gamma z} \tag{3-1}$$

and giving the field components:

$$\underline{H} = \varepsilon \frac{d}{dt}(\nabla \times \underline{\Pi}_h) \qquad \underline{E} = \nabla(\nabla \cdot \underline{\Pi}_h) - \mu\varepsilon \frac{d^2}{dt^2}\underline{\Pi}_h \tag{3-2}$$

The scalar function $\Psi_h(x,y)$ must be chosen so as to have the dimensions of magnetic field and satisfy the boundary conditions relevant to the y-directed magnetic field component. In a completely analogous manner the field components of a y-directed TM field can be derived from a single y-directed electric hertzian potential function defined as:

$$\underline{\Pi}_e = \hat{y}\, \Psi_e(x,y)\, e^{-\gamma z} \tag{3-3}$$

giving:

$$\underline{E} = -\mu \frac{d}{dt}(\nabla \times \underline{\Pi}_e) \qquad \underline{H} = (\nabla \cdot \underline{\Pi}_e) - \mu\varepsilon \frac{d^2}{dt^2}\underline{\Pi}_e \tag{3-4}$$

Assuming a time dependence of $e^{-j\omega t}$ and β complex so that $\gamma = j\beta$ then the field components as derived from the superposition of y-directed TM and TE fields can be written as:

$$\underline{E} = -j\omega\mu_0\, \nabla \times \underline{\Pi}_h + \varepsilon_r Ko^2 \underline{\Pi}_e + \nabla\nabla \cdot \underline{\Pi}_e \tag{3-4a}$$

$$\underline{H} = j\omega\varepsilon_0\varepsilon_r \nabla \times \underline{\Pi}_e + \varepsilon_r Ko^2 \underline{\Pi}_h + \nabla\nabla \cdot \underline{\Pi}_h \tag{3-4b}$$

giving the field components:

$$Ey = (\varepsilon_r Ko^2 + \partial y^2)\, \Psi_e(x,y)\, e^{-j\beta z} \qquad (3\text{-}6a)$$

$$Hy = (\varepsilon_r Ko^2 + \partial y^2)\, \Psi_h(x,y)\, e^{-j\beta z} \qquad (3\text{-}6b)$$

$$Ex = (\partial x\, \partial y\, \Psi_e(x,y) + \omega \mu_0 \beta\, \Psi_h(x,y)) e^{-j\beta z} \qquad (3\text{-}6c)$$

$$Ez = (-j\beta\, \partial y\, \Psi_e(x,y) - j\omega \mu_0\, \partial x\, \Psi_h(x,y))\, e^{-j\beta z} \qquad (3\text{-}6d)$$

$$Hx = (-\omega \varepsilon_0 \varepsilon_r\, \beta\, \Psi_e(x,y) + \partial x\, \partial y\, \Psi_h(x,y))\, e^{-j\beta z} \qquad (3\text{-}6e)$$

$$Hz = (j\omega \varepsilon_0 \varepsilon_r\, \partial x\, \Psi_e(x,y) - j\beta\, \partial y\, \Psi_h(x,y))\, e^{-j\beta z} \qquad (3\text{-}6f)$$

These very general expressions are made to conform to the IDG case by choosing the scalars $\Psi_e(x,y)$ and $\Psi_h(x,y)$ for each region such that they satisfy the relevant boundary conditions.

Assuming perfectly conducting metal surfaces then the boundary conditions in the coordinate system used (see fig.2-1) are given as:

Ez,Hz continuous throughout, with $Ez = \partial Hz/\partial x = 0$ at the metal boundaries.

$Hx = \partial Ex/\partial x = 0$; $x = \pm a/2$, $-h \leq y \leq 0$

$Ex = \partial Hx/\partial y = 0$; on the remaining metal boundaries,

$Ey = \partial Hy/\partial x = 0$; $x = \pm a/2$, $-h \leq y \leq 0$

$Hy = \partial Ey/\partial y = 0$; on the remaining metal boundaries,

Ez, Hz, Ex, Hx are continuous across the air/dielectric interface.

At $x = \pm a/2$, $y = 0$ the transverse components have a weak singularity of the type $r^{-\frac{1}{3}}$.

In order to simplify the equations in the work that follows the time and z-dependence $e^{-j(\beta z - \omega t)}$ will be assumed but not written. Due to the symmetry of the IDG structure the field solutions are initially assumed to be even only, wrt x. For this case the fields need only be formulated over one half of the guide width, with a magnetic wall placed in the y-z plane at x=0.

3-3 The Field Components in the Slot Region

The field components in the slot region are given by equations (3-6) when the scalar functions $\Psi_h(x,y)$ and $\Psi_e(x,y)$ satisfy the boundary conditions of the slot. Since a cartesian coordinate system is used, the x and y directed boundary conditions for the functions can be satisfied independently. The potentials $\Psi_h(x,y)$ and $\Psi_e(x,y)$ must be able to generate every possible field solution that satisfies the boundary conditions. Thus they must be composed from sets of functions that each satisfy the boundary conditions and can be superimposed to give any possible field solution. This requires that the functions form a complete set that are orthogonal over the transverse slot area.

It has been mentioned previously that the slot region has similiar boundary conditions to that of a short-circuited section of parallel plate waveguide. Thus the x-dependent variation of the y-directed electric and magnetic fields can be obtained from a Fourier series expansion in terms of the discrete mode solutions of parallel plate guide. These functions, $\Phi en(x)$ and $\Phi hn(x)$, that satisfy the boundary conditions in x for Ey and Hy respectively, are defined as:

$$\Phi en(x) = \frac{2}{\sqrt{a}} \sin(n\pi/a)x \qquad n = 0,2,4,..... \tag{3-7a}$$

$$\Phi hn(x) = \frac{2\delta n}{\sqrt{a}} \cos(n\pi/a)x \quad \text{where } \delta n = 1/\sqrt{2} \quad n = 0 \tag{3-7b}$$

$$\delta n = 1 \qquad n = 2,4,....$$

These functions give the field variations for even solutions only, i.e. with a magnetic wall placed at x=0. The formulation can easily be extended to include the odd solutions as is shown in a later section. The functions $\Phi hn(x)$ and $\Phi en(x)$ each form a complete series and are orthogonal over the slot half width, since the fields are symmetrical

with x. Hence the amplitudes of the functions are chosen for convenience to give the normalisation:

$$\int_0^{a/2} \Phi h,en(x)\, \Phi h,em(x)\, dx = \delta nm \qquad (3\text{-}8)$$

With these mode functions the conservation of wavenumber equation for the slot region is :

$$\varepsilon_r Ko^2 = (n\pi/a)^2 + Kyn^2 + \beta^2 \qquad (3\text{-}9)$$

As discussed in chapter two, the slot field can be viewed as that arising from a set of transmission lines which model the y-directed TE and TM field components. For a TE wave the voltage distribution across each line will be given by the $\Phi hn(x)$, and for a TM line, the current by the $\Phi en(x)$. From (3-9) for each transmission line mode n there will be an associated y-directed wavenumber Kyn, which will be given by the phase variation of the current or voltage along the associated TM or TE equivalent transmission line. For the case of a dielectric filled slot, the phase variation will be that of a short-circuited length of transmission line. The derivation of the y-dependence terms is given in Appendix I.

In order that a transmission line analogy can be obtained, the potentials $\Psi_e(x,y)$ and $\Psi_h(x,y)$ are given the forms of wave impedance and admittance respectively, to derive the Ey and Hy field components. This ensures that the potential amplitudes then have dimensions of current and voltage respectively, in order to maintain the dimensionality of (3-6). The potential functions for the slot region are thus chosen to be:

$$\Psi_e(x,y) = \sum_{n=0,2}^{\infty} \frac{In'}{j\omega\varepsilon} \frac{1}{((n\pi/a)^2 + \beta^2)^{\frac{1}{2}}} \Phi en(x) \frac{\cos Kyn(y + h)}{\cos Kyn\, h} \qquad (3\text{-}10a)$$

$$\Psi_h(x,y) = \sum_{n=0,2}^{\infty} \frac{Vn''}{j\omega\mu_0} \frac{1}{((n\pi/a)^2 + \beta^2)^{\frac{1}{2}}} \Phi hn(x) \frac{\sin Kyn(y + h)}{\sin Kyn\, h} \quad (3\text{-}10b)$$

$$-h \leq y \leq 0$$

The wavenumber term in the denominators is written in terms of the wavenumbers transverse to y to enable the y-directed TE and TM components to be decoupled at a later stage in the analysis. The y-dependent terms have been fixed to be unity at y = 0 to ensure continuity across the interface.

Upon substituting (3-10) into equations (3-6) the field components for the slot region are found to be:

$$Ex(x,y) = \sum_{n=0,2}^{\infty} Exn \quad \Phi hn(x) \frac{\sin Kyn(y + h)}{\sin Kyn\, h} \quad (3\text{-}11a)$$

where $Exn = \left[\frac{j\,In'}{\omega\varepsilon} Kyn\,(n\pi/a) \tan Kyn\, h - j\beta\, Vn''\right] \frac{1}{((n\pi/a)^2 + \beta^2)^{\frac{1}{2}}}$

$$Ey(x,y) = \sum_{n=2,4}^{\infty} Eyn\ \Phi en(x) \frac{\cos Kyn(y + h)}{\cos Kyn\, h} \quad (3\text{-}11b)$$

where $Eyn = \frac{In'}{j\omega\varepsilon} ((n\pi/a)^2 + \beta^2)^{\frac{1}{2}}$

$$Ez(x,y) = \sum_{n=2,4}^{\infty} Ezn\ \Phi en(x) \frac{\sin Kyn(y + h)}{\sin Kyn\, h} \quad (3\text{-}11c)$$

where $Ezn = \left[\frac{In'}{\omega\varepsilon} \beta\, Kyn \tan Kyn\, h + Vn''\,(n\pi/a)\right] \frac{1}{((n\pi/a)^2 + \beta^2)^{\frac{1}{2}}}$

$$Hx(x,y) = \sum_{n=2,4}^{\infty} Hxn\ \phi en(x) \frac{\cos Kyn(y + h)}{\cos Kyn\, h} \quad (3\text{-}11d)$$

where $Hxn = \left[j\,In'\,\beta + \frac{j\,Vn''}{\omega\mu_0}\,(n\pi/a)\,Kyn \cot Kyn\,h \right] \frac{1}{\left((n\pi/a)^2 + \beta^2\right)^{\frac{1}{2}}}$

$$Hy(x,y) = \sum_{n=0,2}^{\infty} Hyn\ \Phi hn(x)\ \frac{\sin Kyn(y+h)}{\sin Kyn\,h} \qquad (3\text{-}11e)$$

where $Hyn = \frac{Vn''}{j\omega\mu_0}\left((n\pi/a)^2 + \beta^2\right)^{\frac{1}{2}}$

$$Hz(x,y) = \sum_{n=0,2}^{\infty} Hzn\ \Phi hn(x)\ \frac{\cos Kyn(y+h)}{\cos Kyn\,h} \qquad (3\text{-}11f)$$

where $Hzn = \left[In'\,(n\pi/a) - \frac{Vn''\,\beta\,Kyn \cot Kyn\,h}{\omega\mu_0} \right] \frac{1}{\left((n\pi/a)^2 + \beta^2\right)^{\frac{1}{2}}}$

The amplitudes of the field components in the slot are given by the Exn, Ezn etc. By rearranging (3-11a) and (3-11c) the mode amplitudes for the electric field transverse to y can be written:

$$\begin{bmatrix} Exn \\ Ezn \end{bmatrix} = \left((n\pi/a)^2 + \beta^2\right)^{-\frac{1}{2}} \begin{bmatrix} (n\pi/a) & -j\beta \\ -j\beta & (n\pi/a) \end{bmatrix} \begin{bmatrix} j\frac{Kyn}{\omega\varepsilon}\tan Kyn\,h & 0 \\ 0 & 1 \end{bmatrix} \begin{bmatrix} In' \\ Vn'' \end{bmatrix} \qquad (3\text{-}12)$$

If an angle θ is defined such that :

$$\cos\theta = \frac{(n\pi/a)}{\left((n\pi/a)^2 + \beta^2\right)^{\frac{1}{2}}} \qquad \sin\theta = \frac{\beta}{\left((n\pi/a)^2 + \beta^2\right)^{\frac{1}{2}}} \qquad (3\text{-}13)$$

then equation (3-12) may be rewritten :

$$\begin{bmatrix} Exn \\ Ezn \end{bmatrix} = \begin{bmatrix} \cos\theta & -j\sin\theta \\ -j\sin\theta & \cos\theta \end{bmatrix} \begin{bmatrix} j\frac{Kyn}{\omega\varepsilon}\tan Kyn\,h & 0 \\ 0 & 1 \end{bmatrix} \begin{bmatrix} In' \\ Vn'' \end{bmatrix} \qquad (3\text{-}14)$$

In general, the field components Ex and Ez are composed of terms in both

In' and Vn". That is, they are derived from a combination of y-directed TM and TE fields respectively, and are hybrid. However, when $\cos\theta = 0$ in (3-14) Ex and Ez are respectively derived from y-directed TE and TM modes only. Similiarly when $\sin\theta = 0$, Ex and Ez are expressed in terms of TM and TE fields only. Thus (3-14) can be considered to consist of a rotation of θ followed by a matrix multiplication by $\begin{pmatrix} 0 & j \\ j & 0 \end{pmatrix}$ which decouples the TE and TM fields. The four transverse components for each y-directed field are reduced to two by this rotation. This is illustrated in fig. 3-1 where a y-directed five component TM field, defined by x,y,z, is reduced to a three component definition by an axis rotation about y to the new position x',y,z'. Thus by finding the TE and TM transmission line analogies for the transverse section of a structure then the hybrid field can be found by their superposition through the transformation Tn, defined in equation (3-16).

The input impedance of a short-circuited length of transmission line which supports an n^{th} order TM mode is given as:

$$Zn' = j\frac{Kyn}{\omega\varepsilon}\tan Kyn\, h = j\, Zon'\tan Kyn\, h \qquad (3\text{-}15)$$

where Zon' is the characteristic impedance of the n^{th} TM mode. If the coordinate transformation is written as:

$$Tn = \begin{pmatrix} \cos\theta & -j\sin\theta \\ -j\sin\theta & \cos\theta \end{pmatrix} \qquad (3\text{-}16)$$

then (3-14) can be simplified to

$$\begin{pmatrix} Exn \\ Ezn \end{pmatrix} = Tn \begin{pmatrix} Zn' & 0 \\ 0 & 1 \end{pmatrix} \begin{pmatrix} In' \\ Vn" \end{pmatrix} \qquad (3\text{-}17)$$

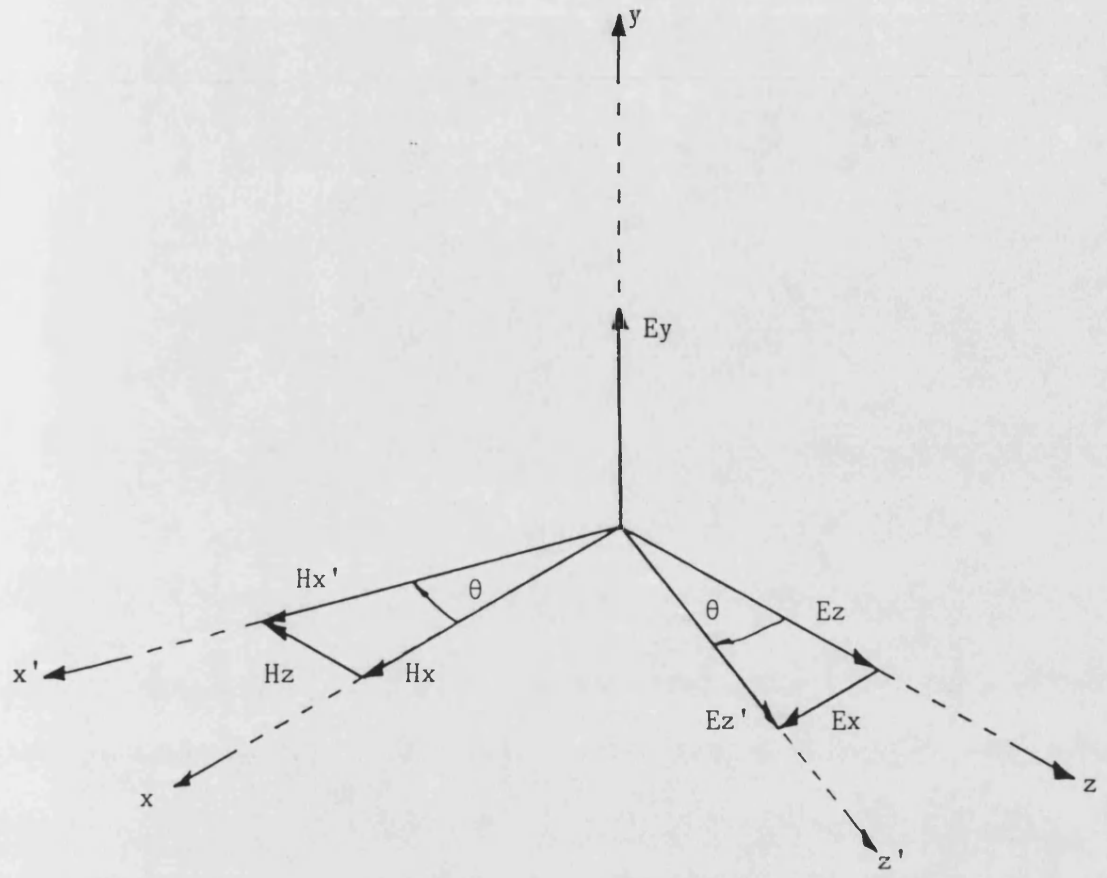

A diagram to illustrate how a coordinate rotation θ can reduce the number of field components required to define a mode

figure 3-1

A similiar expression for the transverse magnetic field amplitudes is found to be:

$$\begin{bmatrix} Hzn \\ \\ -Hxn \end{bmatrix} \quad Tn \begin{bmatrix} 1 & 0 \\ \\ 0 & Yn'' \end{bmatrix} \begin{bmatrix} In' \\ \\ Vn'' \end{bmatrix} \tag{3-18}$$

where

$$Yn'' = -j \frac{Kyn}{\omega\mu_0} \cot Kyn\, h = -j\, Yon'' \cot Kyn\, h \tag{3-19}$$

is the input admittance of the slot as seen by an n^{th} order TE mode at y=0. By eliminating the amplitude coefficients Vn" and In' from (3-17) and (3-18) the field amplitudes can be related to each other as:

$$\begin{bmatrix} Hzn \\ \\ -Hxn \end{bmatrix} = Tn \begin{bmatrix} Yn' & 0 \\ \\ 0 & Yn'' \end{bmatrix} Tn^{-1} \begin{bmatrix} Exn \\ \\ Ezn \end{bmatrix} \tag{3-20}$$

Thus the transverse field components can be obtained directly from the y-directed equivalent circuits for the TE and TM modes. This allows a transverse equivalent network for the hybrid field to be obtained directly. The operator Tn acts to couple the TE and TM components into the hybrid field and so can be considered terms to be an ideal transformer of unit turns ratio. The transverse equivalent circuit for the slot field can thus be represented as shown in fig.3-2.

The decoupling of the field into it's TE and TM components not only simplifies the initial formulation but enables it to be easily modified to variations in the guide structure. For example if the dielectric is lowered in the slot then the transverse equivalent circuits become lengths of transmission line of characteristic impedance of the mode in freespace, cascaded with a short-circuited length of transmission line with the characteristic impedance of the mode in the dielectric medium.

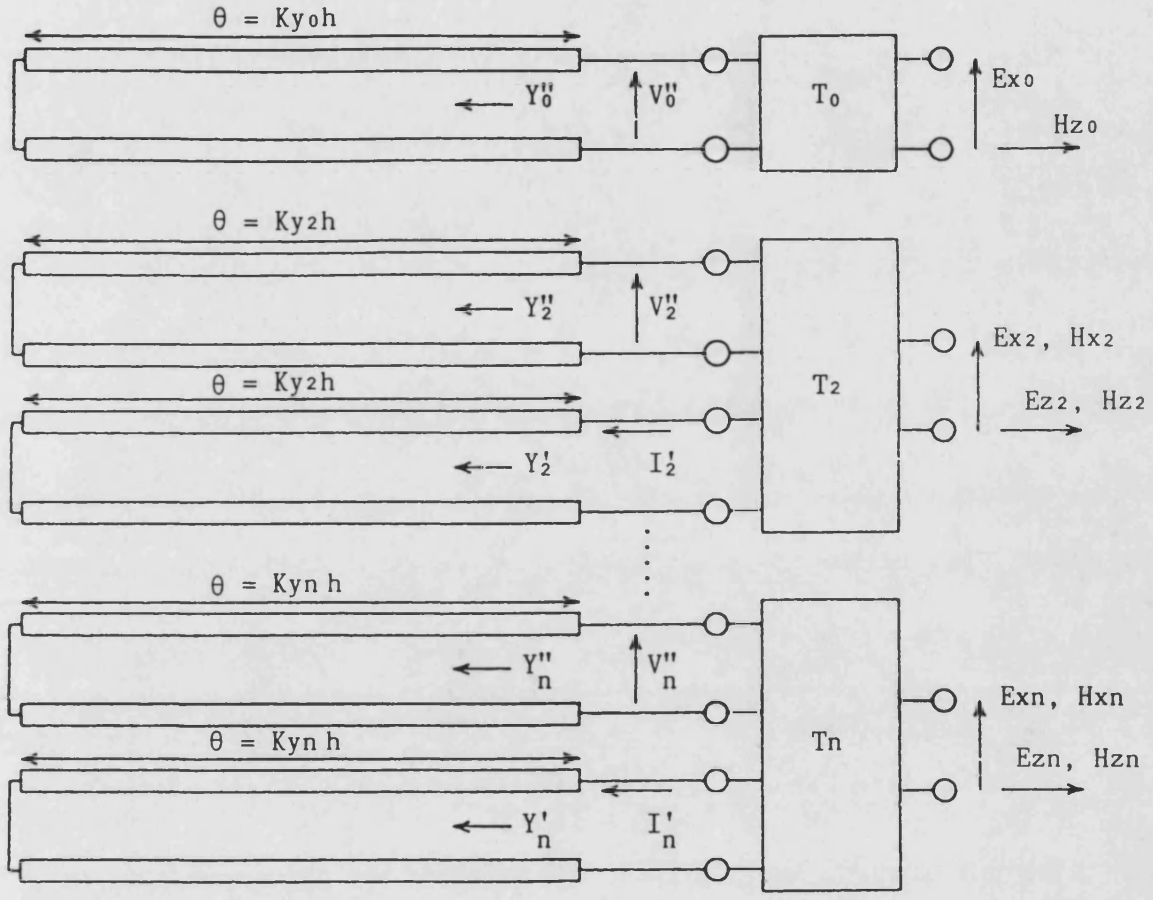

The Transverse Equivalent Network for the slot field

figure 3-2

The input admittance of these circuits can easily be found from transmission theory and placed directly in (3-20). The idea of simplifying the formulation of the Green's operators by decoupling the hybrid field into its TE and TM components was introduced by Itoh [3].

3-4 The Air Region

The air region (y>0) is an open unbounded region, apart from the guide surface in the plane y=0. By analogy with the formulation for the slot field, the x-dependence of the air field potentials can be written as a Fourier series expansion in the x-directed wavenumber Kx = ρ. However, since the region is unbounded in x, ρ can lie anywhere in the range $0 \leq \rho \leq \infty$, and the discete summation of the slot functions becomes a continuous integral in ρ. The x-dependent functions for the air potentials are thus chosen to be:

$$\Phi h(\rho,x) = \sqrt{\frac{2}{\pi}} \cos \rho x \qquad \Phi e(\rho,x) = \sqrt{\frac{2}{\pi}} \sin \rho x \tag{3-21}$$

where the normalisation is such that:

$$\int_0^\infty \Phi h,e(\rho,x) \;\; \Phi h,e(\rho',x)\, dx = \delta(\rho - \rho') \tag{3-22}$$

where $\delta(\rho - \rho')$ is the Dirac delta function which is infinite when $\rho = \rho'$ but zero when $\rho \neq \rho'$. In the slot potentials (3-10) the discrete components are orthogonal over the transverse cross-section for $y \leq 0$, and normalisable. That is, each "mode" carries a finite amount of power, independently of the others. Since the total power carried by the guide must be finite for a physically realisable system then the summation of the terms in (3-21) over ρ must converge to a finite value. The integral (3-22) suggests that the integral over x may not converge. However the field in the air region will consist of a continuous spectrum and not of discrete modes. The functions Φe(ρ,x) and Φh(ρ,x) cannot be

considered for discrete values of ρ in isolation, since they only occur as part of the continuous spectrum, and so it is the total field and not the individual partial waves that must be square integrable, i.e.

$$\int_0^\infty E^2(x)\, dx < \infty \tag{3-23}$$

For a given value of ρ and β , Ky is fixed by the requirement:

$$Ko^2 = \rho^2 + Ky^2 + \beta^2 \tag{3-24}$$

In order to satisfy the radiation condition that energy decays away from the guide and flows in a positive y-direction, Ky must satisfy:

$$\text{Re } Ky > 0 \qquad \text{Im } Ky < 0$$

For a bound mode solution the air field must decay exponentially away from the guide surface so that there is no real power flow in the transverse direction. Thus, with the unknown amplitudes $I'(\rho)$ and $V''(\rho)$ the potential functions for the air region analogous to (3-10) are chosen to be:

$$\Psi_e(x,y) = \int_0^\infty d\rho\, \frac{I'(\rho)}{j\omega\varepsilon_0} \frac{1}{(\beta^2 + \rho^2)^{\frac{1}{2}}} \Phi e(\rho,x)\, e^{-j\,Ky(\rho)\,y} \tag{3-25a}$$

$$\Psi_h(x,y) = \int_0^\infty d\rho\, \frac{V''(\rho)}{j\omega\mu_0} \frac{1}{(\beta^2 + \rho^2)^{\frac{1}{2}}} \Phi h(\rho,x)\, e^{-j\,Ky(\rho)\,y} \tag{3-25b}$$

valid for $y \geq 0$

It is evident from (3-10) and (3-25) that the potential functions are continuous across $y = 0$.

The field components in the air region are found by substituting the expressions for the potentials (3-25) into (3-6) to give:

$$Ex(x,y) = \int_0^\infty d\rho\ ex(\rho)\ \Phi h(\rho,x)\ e^{-j\,Ky(\rho)\,y} \qquad (3\text{-}26a)$$

where $ex(\rho) = \left[\frac{-I'(\rho)\,\rho\,Ky(\rho) - j\,\beta\,V''(\rho)}{\omega\varepsilon_0}\right] \frac{1}{(\beta^2 + \rho^2)^{\frac{1}{2}}}$

$$Ey(x,y) = \int_0^\infty d\rho\ ey(\rho)\ \Phi e(\rho,x)\ e^{-j\,Ky(\rho)\,y} \qquad (3\text{-}26b)$$

where $ey(\rho) = \frac{I'(\rho)}{j\omega\varepsilon_0}\ (\beta^2 + \rho^2)^{\frac{1}{2}}$

$$Ez(x,y) = \int_0^\infty d\rho\ ez(\rho)\ \Phi e(\rho,x)\ e^{-j\,Ky(\rho)\,y} \qquad (3\text{-}26c)$$

where $ez(\rho) = \left[\frac{j\,I'(\rho)\,\beta\,Ky(\rho) + V''(\rho)\,\rho}{\omega\varepsilon_0}\right] \frac{1}{(\beta^2 + \rho^2)^{\frac{1}{2}}}$

$$Hx(x,y) = \int_0^\infty d\rho\ hx(\rho)\ \Phi e(\rho,x)\ e^{-j\,Ky(\rho)\,y} \qquad (3\text{-}26d)$$

where $hx(\rho) = \left[j\,\beta\,I'(\rho) + \frac{V''(\rho)\,\rho\,Ky(\rho)}{\omega\mu_0}\right] \frac{1}{(\beta^2 + \rho^2)^{\frac{1}{2}}}$

$$Hy(x,y) = \int_0^\infty d\rho\ hy(\rho)\ \Phi h(\rho,x)\ e^{-j\,Ky(\rho)\,y} \qquad (3\text{-}26e)$$

where $hy(\rho) = \frac{V''(\rho)}{j\omega\mu_0}\ (\beta^2 + \rho^2)^{\frac{1}{2}}$

$$Hz(x,y) = \int_0^\infty d\rho\ hz(\rho)\ \Phi h(\rho,x)\ e^{-j\,Ky(\rho)\,y} \qquad (3\text{-}26f)$$

where $hz(\rho) = \left[\rho\,I'(\rho) + j\,\beta\,Ky(\rho)\,\frac{V''(\rho)}{\omega\mu_0}\right] \frac{1}{(\beta^2 + \rho^2)^{\frac{1}{2}}}$

In an analogous way to the slot components, the Fourier amplitudes for the fields transverse to y can be written in terms of the potential amplitudes as:

$$\begin{bmatrix} ex(\rho) \\ ez(\rho) \end{bmatrix} = (\beta^2 + \rho^2)^{-\frac{1}{2}} \begin{bmatrix} \rho & -j\beta \\ -j\beta & \rho \end{bmatrix} \begin{bmatrix} \frac{Ky(\rho)}{\omega\varepsilon_0} & 0 \\ 0 & 1 \end{bmatrix} \begin{bmatrix} -I'(\rho) \\ V''(\rho) \end{bmatrix} \tag{3-27a}$$

$$\begin{bmatrix} -hz(\rho) \\ hx(\rho) \end{bmatrix} = (\beta^2 + \rho^2)^{-\frac{1}{2}} \begin{bmatrix} \rho & -j\beta \\ -j\beta & \rho \end{bmatrix} \begin{bmatrix} 1 & 0 \\ 0 & \frac{Ky(\rho)}{\omega\mu_0} \end{bmatrix} \begin{bmatrix} I'(\rho) \\ V''(\rho) \end{bmatrix} \tag{3-27b}$$

where the signs are consistant with power flow into the air region from the interface. In a similiar manner to the slot region, the coordinate transformation $T(\rho)$ can be defined as:

$$T(\rho) = (\beta^2 + \rho^2)^{-\frac{1}{2}} \begin{bmatrix} \rho & -j\beta \\ -j\beta & \rho \end{bmatrix} \tag{3-28}$$

The charactaristic impedance of a TM plane wave of wavenumber $Kx = \rho$ is given by:

$$Z(\rho)' = \frac{Ky(\rho)}{\omega\varepsilon_0} \tag{3-29}$$

and the charactaristic admittance of a TE plane wave:

$$Y(\rho)'' = \frac{Ky(\rho)}{\omega\mu_0} \tag{3-30}$$

Thus from (3-27a) and (3-27b):

$$\begin{bmatrix} -hz(\rho) \\ hx(\rho) \end{bmatrix} = T(\rho) \begin{bmatrix} Y(\rho)' & 0 \\ 0 & Y(\rho)'' \end{bmatrix} T(\rho)^{-1} \begin{bmatrix} ex(\rho) \\ ez(\rho) \end{bmatrix} \tag{3-31}$$

The air admittance can be thought of as being the sum of all the TE and TM plane waves that are excited by the slot field at the interface giving the transverse equivalent circuit for the IDG field of fig.3-3.

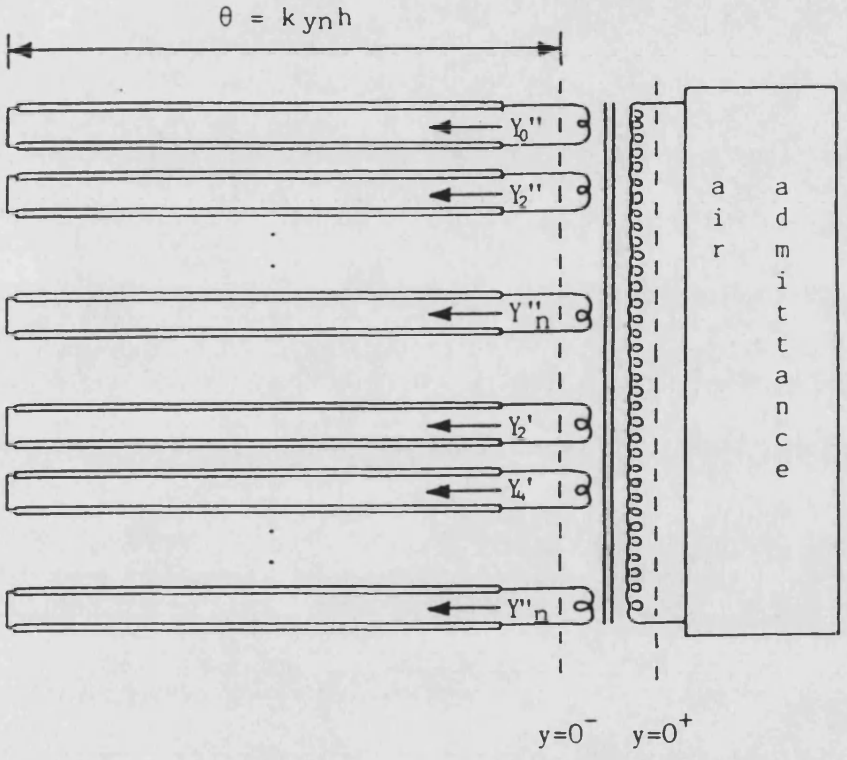

The Transverse Equivalent Circuit for Inset Dielectric Guide

figure 3-3

3-5 The Formulation of the Admittance Operators

In the previous two sections expressions for the field components in each region have been obtained. By enforcing the continuity of field components transverse to y at the interface between the two regions, equations are obtained that can be solved for β. However this approach would require extensive computation and would be very inefficient. In order to reduce the required computer time some further analytical manipulation is needed.

The continuity of the transverse field components at the interface can be stated as the resonance of the transverse equivalent circuit. In order that the required admittance or impedance operators can be determined, then two of the transverse field components must be written in terms of the other. By analogy with rectangular waveguide the fundamental IDG field can be expected to be dominantly TE wrt. y and so the transverse electric field components are retained as the unknown quantities.

The value of the magnetic field at a point (x,y) due to the electric field at a point (x',y') will be given by an equation of the form

$$H(x,y) = Y(x,x',y,y')\, E(x',y') \qquad (3\text{-}32)$$

where Y is a function that satisfies the required boundary conditions and has the dimensions of an admittance. This function gives the field (H) due to a point source (E) and so is a form of Green's function [4]. The transverse resonance condition is to be applied at the interface (y=0) and so the admittance terms must be defined at this plane. The magnetic field at the interface will due to the net effect of all the point electric sources across the interface and so the required

admittance operators are defined by equations of the type:

$$H(x,o) = \int_{o}^{a/2} Y(x,x',y=y'=o)\, E(x',o)\, dx' \qquad (3\text{-}33)$$

Thus expressions are sought of the type:

$$\begin{bmatrix} Hz(x,o) \\ -Hx(x,o) \end{bmatrix} = \begin{bmatrix} \hat{Y}^s_{11} & \hat{Y}^s_{12} \\ \hat{Y}^s_{21} & \hat{Y}^s_{22} \end{bmatrix} \cdot \begin{bmatrix} Ex(x,o) \\ Ez(x,o) \end{bmatrix} \qquad (3\text{-}34a)$$

$$\begin{bmatrix} -Hz(x,o) \\ Hx(x,o) \end{bmatrix} = \begin{bmatrix} \hat{Y}^a_{11} & \hat{Y}^a_{12} \\ \hat{Y}^a_{21} & \hat{Y}^a_{22} \end{bmatrix} \cdot \begin{bmatrix} Ex(x,o) \\ Ez(x,o) \end{bmatrix} \qquad (3\text{-}34b)$$

where the "·" signifies the process of convolution over the slot half aperture. The signs are consistent with the admittances being defined for positive power flow into each region from the interface. The superscripts s and a refer to the slot and air regions respectively.

It is constructive at this stage to consider the interpretation of the admittance terms. Consider the case of a plane wave along the guide, confined to the guide by successive reflections between the sidewalls in the x-direction, and by reflections between the bottom of the slot and the dielectric/air boundary in the y-direction. Relative to the y and z directions the field will be TE if the plane wave is orientated with the electric field vector aligned with the x-axis, giving the components Ex,Hy,Hz. Similarly a TM field will have components Hx,Ey, Ez. When propagation is viewed in the positive y-direction then the TE admittance is -Hz/Ex and the TM admittance Hx/Ez. Thus the operator $\hat{Y}_{11}$ can be viewed as a TE admittance and the $\hat{Y}_{22}$ operator as a TM admittance.

In general the hybrid field will consist of both TE and TM components so that the Hz component for example will be due to both the Ex and Ez components. Thus the $\hat{Y}_{12}$ and $\hat{Y}_{21}$ operators can be viewed as the

coupling between the TE and TM mode families. Since the coupling process is reciprocal, with the choice of signs as in (3-34) the condition

$$\hat{Y}_{12} = -\hat{Y}_{21} \tag{3-35}$$

must be satisfied.

To illustrate the formulation of the operators consider the derivation of $\hat{Y}_{11}$ in (3-24a) defined as:

$$Hz(x,o) = \int_{o}^{a/2} Y^{s}_{11}(x,x',y=y'=o)\, Ex(x',o)\, dx' \Big|_{Ez(x',o)} \tag{3-35}$$

From equation (3-17) with Ezn set to zero:

$$Hzn = Exn(Yn' \cos\theta^2 + Yn'' \sin\theta^2) \tag{3-36}$$

However from equation (3-11a)

$$Exn = \int_{o}^{a/2} Ex(x',o)\, \Phi hn(x')\, dx' \tag{3-37}$$

and so from (3-11f)

$$Hz(x,o) = \sum_{n=0,2}^{\infty} (Yn' \cos\theta^2 + Yn'' \sin\theta^2)\, \Phi hn(x) \int_{o}^{a/2} Ex(x',o)\, \Phi hn(x')\, dx' \tag{3-38}$$

giving:

$$Y^{s}_{11}(x,x') = \sum_{n=0,2}^{\infty} (Yn' \cos\theta^2 + Yn'' \sin\theta^2)\, \Phi hn(x)\, \Phi hn(x') \tag{3-39a}$$

The other slot admittances are found in a similar manner to be:

$$Y^{s}_{12}(x,x') = \sum_{n=2,4}^{\infty} j(Yn' - Yn'') \sin\theta \cos\theta\, \Phi hn(x)\, \Phi en(x') \tag{3-39b}$$

$$Y^{s}_{21}(x,x') = -Y^{s}_{12}(x',x) \tag{3-39c}$$

$$Y^{s}_{22}(x,x') = \sum_{n=2,4}^{\infty} (Yn' \sin\theta^2 + Yn'' \cos\theta^2)\, \Phi en(x)\, \Phi en(x') \tag{3-39d}$$

A constant magnetic field cannot be supported between two electric walls and so it is noted that the summations in the Y_{12},Y_{21}, and Y_{22} operators commence from n=2. It is also noted that when sinθ or cosθ=0 then the TE and TM fields are completely decoupled, i.e. $Y_{12}= Y_{21} = 0$.

The admittance operators are formulated for propagation in the transverse y-direction and in the dispersion equation eventually derived from them, β is found directly by solving for Ky in both regions. In the slot region

$$Kyn^2 = \varepsilon_r Ko^2 - \beta^2 - (n\pi/a)^2 \qquad (3\text{-}40)$$

The fundamental field in IDG can be expected to be dominated by the n=0 term in the slot and so it is useful to define a normalised frequency variable U as:

$$U = (a/\pi)\sqrt{\varepsilon_r Ko^2 - \beta^2} \qquad (3\text{-}41)$$

so that

$$Kyn = (a/\pi)\sqrt{U^2 - n^2} \qquad (3\text{-}42)$$

It is also useful to normalise all admittances to the characteristic admittance of the fundamental TE mode:

$$Yoo'' = \frac{Kyo}{\omega\mu_0} = \frac{\pi U}{a\omega\mu_0} \qquad (3\text{-}43)$$

By inserting the terms for Yn' and Yn'' ((3-15) and (3-19)) in (3-39) and normalising to Yoo'', the slot dyadic admittances simplify to:

$$Y^s_{11}(x,x') = -jU \sum_{n=0,2}^{\infty} \frac{\cot\sqrt{U^2 - n^2}(\pi h/a)}{\sqrt{U^2 - n^2}} \Phi hn(x)\, \Phi hn(x') \qquad (3\text{-}44a)$$

$$Y^s_{12}(x,x') = -Y^s_{21}(x',x) = \frac{(a/\pi)\beta}{U} \sum_{n=2,4}^{\infty} \frac{n \cot \sqrt{U^2 - n^2}(\pi h/a)}{\sqrt{U^2 - n^2}} \Phi hn(x)\, \Phi en(x') \qquad (3\text{-}44b)$$

$$Y^s_{22}(x,x') = \frac{1}{jU} \sum_{n=2,4}^{\infty} (\varepsilon_r Ko^2 - n^2) \frac{\cot \sqrt{U^2 - n^2}(\pi h/a)}{\sqrt{U^2 - n^2}} \Phi en(x)\, \Phi en(x') \qquad (3\text{-}44c)$$

In a similar manner the normalised admittance operators for the air region are found to be:

$$Y^a_{11}(x,x') = \frac{(a/\pi)(Ko^2 - \beta^2)}{U} \int_0^{\infty} \frac{\Phi h(\rho,x)\, \Phi h(\rho,x')}{Ky(\rho)}\, d\rho \qquad (3\text{-}44d)$$

$$Y^a_{12}(x,x') = -Y^a_{21}(x',x) = \frac{j\beta}{U} \int_0^{\infty} \frac{\rho\, \Phi h(\rho,x)\, \Phi e(\rho,x')}{Ky(\rho)}\, d\rho \qquad (3\text{-}44e)$$

$$Y^a_{22}(x,x') = \frac{(\pi/a)}{U} \int_0^{\infty} (Ko^2 - \rho^2) \frac{\Phi e(\rho,x)\, \Phi e(\rho,x')}{Ky(\rho)}\, d\rho \qquad (3\text{-}44f)$$

The electric and magnetic field components transverse to y are continuous at y = 0 and so from (3-34a) and (3-34b):

$$\begin{bmatrix} \hat{Y}^s_{11} + \hat{Y}^a_{11} & \hat{Y}^s_{12} + \hat{Y}^a_{12} \\ \hat{Y}^s_{21} + \hat{Y}^a_{21} & \hat{Y}^s_{22} + \hat{Y}^a_{22} \end{bmatrix} \cdot \begin{bmatrix} Ex(x,o) \\ Ez(x,o) \end{bmatrix} = 0 \qquad (3\text{-}45)$$

This is a set of integral equations in the unknowns β, Ex(x,o) and Ez(x,o). These equations are to be solved by transformation into the space spanned by the field unknowns so that they are reduced to a matrix equation. This is carried out by writing Ex(x,o) and Ez(x,o), the field unknowns, in terms of complete sets of known functions, each of which satisfy the required boundary conditions. Ex(x,o) and Ez(x,o) satisfy different boundary conditions in x and so would require different sets of functions to accurately expand them both. For convenience in the computation it is required that both the field unknowns are expanded by the same set

of functions. To this end, it is noted that Ex(x,o) and $(a/\pi)dEz(x,o)/dx$ have the same x-dependence, satisfy the same boundary conditions, have the same dimensions and so can be discretised by a single set of functions.

In order to introduce $(a/\pi)dEz(x,o)/dx$ as an unknown in equations (3-34), the integrals containing $Y_{12}(x,x')$ and $Y_{22}(x,x')$ are integrated by parts wrt x', and those containing $Y_{21}(x,x')$ and $Y_{22}(x,x')$ integrated wrt x. After integration the admittance relations become:

$$\begin{bmatrix} Hz(x,o) \\ (\pi/a)\int Hx(x,o)\,dx \end{bmatrix} = \begin{bmatrix} \hat{Y}^s_{11} & \hat{Y}^s_{12} \\ \hat{Y}^s_{21} & \hat{Y}^s_{22} \end{bmatrix} \cdot \begin{bmatrix} Ex(x,o) \\ (a/\pi)dEz(x,o)/dx \end{bmatrix} \quad (3\text{-}46a)$$

$$\begin{bmatrix} -Hz(x,o) \\ -(\pi/a)\int Hx(x,o)\,dx \end{bmatrix} = \begin{bmatrix} \hat{Y}^a_{11} & \hat{Y}^a_{12} \\ \hat{Y}^a_{21} & \hat{Y}^a_{22} \end{bmatrix} \cdot \begin{bmatrix} Ex(x,o) \\ (a/\pi)dEz(x,o)/dx \end{bmatrix} \quad (3\text{-}46b)$$

where for convenience the same symbols have been retained for the modified admittance operators. The (π/a) and (a/π) terms have been inserted so as to maintain the dimensional uniformity of the equations. The integration has the added bonus of improving the convergence properties of the operators. After integration the admittances are now:

$$Y^s_{11}(x,x') = -jU \sum_{n=0,2}^{\infty} \frac{\cot\sqrt{U^2 - n^2}(\pi h/a)}{\sqrt{U^2 - n^2}} \Phi hn(x)\, \Phi hn(x') \quad (3\text{-}47a)$$

$$Y^s_{12}(x,x') = -Y^s_{21}(x',x) = \frac{(a/\pi)\beta}{U} \sum_{n=2,4}^{\infty} \frac{\cot\sqrt{U^2 - n^2}(\pi h/a)}{\sqrt{U^2 - n^2}} \Phi hn(x)\, \Phi hn(x') \quad (3\text{-}47b)$$

$$Y^s_{22}(x,x') = \frac{1}{jU} \sum_{n=2,4}^{\infty} \left[\frac{\varepsilon_r Ko^2 - (n\pi/a)^2}{(n\pi/a)^2}\right] \frac{\cot\sqrt{U^2 - n^2}(\pi h/a)}{\sqrt{U^2 - n^2}} \Phi hn(x)\, \Phi hn(x') \quad (3\text{-}47c)$$

$$Y^a_{11}(x,x') = \frac{(a/\pi)(Ko^2 - \beta^2)}{U} \int_0^\infty \frac{\Phi h(\rho,x)\, \Phi h(\rho,x')}{Ky(\rho)}\, d\rho \qquad (3\text{-}47d)$$

$$Y^a_{12}(x,x') = -Y^a_{21}(x',x) = \frac{j\beta}{U} \int_0^\infty \frac{\Phi h(\rho,x)\, \Phi h(\rho,x')}{Ky(\rho)}\, d\rho \qquad (3\text{-}47e)$$

$$Y^a_{22}(x,x') = \frac{(\pi/a)}{U} \int_{0^+}^\infty \left[\frac{Ko^2 - \rho^2}{\rho^2}\right] \Phi h(\rho,x)\, \Phi h(\rho,x')\, d\rho \qquad (3\text{-}47f)$$

It is noted that the principal value of the integral in (3-47f) is taken since $dEz/dx \neq$ constant, and so the pole at $\rho = 0$ cannot be included.

3-6 The Application of Galerkin's Method

After integration, the continuity equation (3-45) becomes:

$$\begin{bmatrix} \hat{Y}^s_{11} + \hat{Y}^a_{11} & \hat{Y}^s_{12} + \hat{Y}^a_{12} \\ \hat{Y}^s_{21} + \hat{Y}^a_{21} & \hat{Y}^s_{22} + \hat{Y}^a_{22} \end{bmatrix} \cdot \begin{bmatrix} Ex(x,o) \\ (a/\pi)dEz(x,o)/dx \end{bmatrix} = 0 \qquad (3\text{-}48)$$

with the operators as defined in (3-47). In order that this equation can be solved, it needs to be transformed into a matrix form. This can be done by applying Galerkin's method as follows;
The field unknowns Ex and $(a/\pi)dEz/dx$, chosen for their similar boundary conditions, are both expanded in terms of the functions fm(x) so that:

$$Ex(x,o) = \sum_{m=0,2}^{\infty} Xm\, fm(x) \;,\; (a/\pi)dEz(x,o)/dx = \sum_{m=2,4}^{\infty} Zm\, fm(x) \qquad (3\text{-}49)$$

The functions fm(x) form a complete set, are orthogonal over the slot and satisfy the slot boundary conditions at y=0. The choice of the fm(x) is discussed in the next section. The basis functions fm(x) inner products over the slot half-aperture with the slot and air mode functions defined as:

$$Pnm = \int_0^{a/2} fm(x)\, \Phi hm(x)\, dx \qquad Pn(\rho) = \int_0^{a/2} fn(x)\, \Phi h(\rho,x)\, dx \qquad (3\text{-}50)$$

By substuting the series expressions (3-49) into (3-48) and integrating over the slot half aperture wrt x', and then scalar multiplying with fm(x) and integrating over the half aperture wrt x, then, providing that the inner products can be evaluated, the result is obtained:

$$\left(\underline{\underline{Y}} \right) \begin{bmatrix} \underline{X} \\ \underline{Z} \end{bmatrix} = 0 \qquad (3\text{-}51)$$

This matrix equation has a non-trivial solution when

$$\det\left(\underline{\underline{Y}} \right) = 0 \qquad (3\text{-}52)$$

This equation is sufficient to solve for β although the field amplitudes Xn and Zn cannot be found directly. In order to recover a scalar transverse equivalent circuit, and obtain the field amplitudes it is convenient to reformulate the continuity equation prior to discretisation. Consider the fundamental transverse propagating mode in the slot, seen as a parallel plate waveguide terminated with a short-circuit at y = -h. The higher order slot and air modes can be considered to be excited by the fundamental mode as it is incident on the air/dielectric interface in the classic discontinuity manner. With this analogy it is convenient to isolate the fundamental mode term from (3-48) and lump together all the other terms to give:

$$\left(\hat{Y} \right) \cdot \begin{bmatrix} Ex(x,o) \\ (a/\pi)dEz(x,o)/dx \end{bmatrix} = \begin{bmatrix} -Hzo\ \Phi ho(x) \\ \underline{o} \end{bmatrix} \qquad (3\text{-}53)$$

where $\hat{Y} = \hat{Y}'^{,s} + \hat{Y}^{a}$, $\hat{Y}'^{,s}$ =slot admittance operator with fundamental term (n=0) removed. Also, the quantity $\hat{Y}$ denotes from now on the total admittance with the fundamental slot term removed.

Upon discretisation (3-63) becomes :

$$\begin{bmatrix} & \underline{Y} & \end{bmatrix}\begin{bmatrix} \underline{X} \\ \underline{Z} \end{bmatrix} = (-Hzo)\begin{bmatrix} \underline{Po} \\ \underline{o} \end{bmatrix} \qquad (3\text{-}54)$$

which can be rearranged to give :

$$\begin{bmatrix} \underline{X} \\ \underline{Z} \end{bmatrix} = (-Hzo)\begin{bmatrix} & \underline{Y} & \end{bmatrix}^{-1}\begin{bmatrix} \underline{Po} \\ \underline{o} \end{bmatrix} \qquad (3\text{-}55)$$

Once β and hence the admittance elements have been determined this equation can be solved for the basis amplitude coefficients. Upon multiplying both sides by $\begin{bmatrix} \underline{Po} \\ \underline{o} \end{bmatrix}^T$:

$$(\underline{Po}^T \quad \underline{o}^T)\begin{bmatrix} \underline{X} \\ \underline{Z} \end{bmatrix} = (-Hzo)(\underline{Po}^T \quad \underline{o}^T)\begin{bmatrix} & \underline{Y} & \end{bmatrix}^{-1}\begin{bmatrix} \underline{Po} \\ \underline{o} \end{bmatrix} \qquad (3\text{-}56)$$

However from (3-11a) and (3-49)

$$\underline{Po}^T \cdot \underline{X} = Exo$$

and so (3-56) can be written :

$$\frac{-Hzo}{Exo} = \left[(\underline{Po}^T \quad \underline{o}^T)\begin{bmatrix} & \underline{Y} & \end{bmatrix}^{-1}\begin{bmatrix} \underline{Po} \\ \underline{o} \end{bmatrix}\right]^{-1} \qquad (3\text{-}57)$$

The normalised admittance of the fundamental slot mode looking from y=0 into the slot is :

$$\frac{Hzo}{Exo} = -j \cot Kyo\, h \qquad (3\text{-}58)$$

At resonance the total admittance must vanish and so (3-57) must represent the normalised admittance of all the higher order slot modes and air waves as seen from the interface. The equation for resonance is thus:

$$-j \cot Kyo\, h + \left[\begin{pmatrix} \underline{Po}^T & \underline{o}^T \end{pmatrix} \begin{bmatrix} & \\ & \underline{Y} \end{bmatrix}^{-1} \begin{bmatrix} \underline{Po} \\ \underline{o} \end{bmatrix} \right]^{-1} \qquad (3\text{-}59)$$

The basis expansion for $(a/\pi)dEz(x,o)/dx$ starts from the second term so that when N basis terms are used, Y_{11} is of order N × N, Y_{12} is of order N × N-1, Y_{21} is of order N-1 × N, and Y_{22} is of order N-1 × N-1. The overall admittance matrix becomes a square matrix of order (2N-1). The array elements are thus given by:

$$(Y^s_{11})km = -jU \sum_{n=2,4}^{\infty} \frac{\cot\sqrt{U^2 - n^2}(\pi h/a)}{\sqrt{U^2 - n^2}} Pkn\, Pmn \qquad (3\text{-}60a)$$

$$(Y^s_{12})km = -(Y^s_{21})mk = \frac{(a/\pi)\beta}{U} \sum_{n=2,4}^{\infty} \frac{\cot\sqrt{U^2 - n^2}(\pi h/a)}{\sqrt{U^2 - n^2}} Pkn\, Pmn \qquad (3\text{-}60b)$$

$$(Y^s_{22})km = \frac{1}{jU} \sum_{n=0,4}^{\infty} \left[\frac{\varepsilon_r Ko^2 - (n\pi/a)^2}{(n\pi/a)^2} \right] \frac{\cot\sqrt{U^2 - n^2}(\pi h/a)}{\sqrt{U^2 - n^2}} Pkn\, Pmn \qquad (3\text{-}60c)$$

$$(Y^a_{11})km = \frac{(a/\pi)(Ko^2 - \beta^2)}{U} \int_0^{\infty} \frac{Pk(\rho)\, Pm(\rho)}{Ky(\rho)}\, d\rho \qquad (3\text{-}60d)$$

$$(Y^a_{12})km = -(Y^a_{21})mk = \frac{j\beta}{U} \int_0^{\infty} \frac{Pk(\rho)\, Pm(\rho)}{Ky(\rho)}\, d\rho \qquad (3\text{-}60e)$$

$$(Y^a_{22})km = \frac{(\pi/a)}{U} \int_0^{\infty} \left[\frac{Ko^2 - \rho^2}{\rho^2} \right] \frac{Pk(\rho)\, Pm(\rho)}{Ky(\rho)}\, d\rho \qquad (3\text{-}60f)$$

where $k = 0,2,4,\ldots$ $m = 0,2,4,\ldots$ for Y_{11}

$k = 0,2,4,\ldots$ $m = 2,4,6,\ldots$ for Y_{12}

$k = 2,4,6,\ldots$ $m = 0,2,4,\ldots$ for Y_{21}

$k = 2,4,6,\ldots$ $m = 2,4,6,\ldots$ for Y_{22}

3-7 The Choice of the Basis Functions

The success of the discretisation process is dependent upon the choice of a suitable set of the orthogonal functions fm(x). The functions fm(x) are said to "span" the space occupied by the field unknowns. That is, a particular value of say Ex(x,y) is given as a point in n-dimensional space where the distances along each of the n-axes, which defines that point, are given by the coefficients Xn. Thus the integral equation (3-48) by its reduction into a matrix form is said to have been transformed into the function space used to span the unknown functions.

In order that the matrix equation (3-59) can be solved it must be of a finite order, which requires that the expansion series (3-49) must be truncated at some point. For the truncation to introduce an acceptable error the series in fm(x) must converge rapidly to a solution, which in turn requires that the fm(x) closely approximate the expected field distribution across the slot. The choice of the fm(x) is thus crucial for the accuracy and efficiency of the method.

In the present formulation only even field solutions are allowed for and so the basis functions must themselves be even. For $y < 0^-$ the slot can support a constant x-directed field variation across it and so fo(x) must be a constant term so that Ex(x,o) can be modelled accurately. However, $(a/\pi)dEz(x,o)/dx$ cannot have a constant component since this would give rise to a ramp function in x for Ez(x,o) which does not satisfy the boundary conditions. Thus the series for $(a/\pi)dEz(x,o)/dx$ in (3-49) is taken to start from the m=2 term, i.e. Zo = 0. The functions fm(x) are normalised to unity over the slot half aperture so that the relative amplitudes of Xm and Zm can easily be determined.

The electric field distribution between two infinite parallel plates can be found by using the mode functions $\Phi hn(x)$ for the even TM fields [5]. However, in this analysis the field is sought at the end of the parallel plates where the 90^{o} degree edges will peturb the solution from the infinite parallel plate case. The effect of the 90^{o} conducting wedge will be to concentrate the field to it and introduce a singularity into the field distribution there. Although the field is concentrated by a conducting wedge, the energy stored in the vicinity of the edge cannot be infinite for a physically realisable system. Collin [1] has calculated the maximum order of the singularity that is permissible at an edge to give a finite energy storage. In particular for a 90^{o} edge the maximum allowed order of the singularity is $\frac{1}{3}$. That is, the field variation in the vicinity of the edge tends to $r^{-\frac{1}{3}}$ where r is the radial distance from the edge. The field across the slot at y=0 will be influenced by both of the metal edges at $x = \pm a/2$. Thus a function that describes the singularity behaviour at a point in the guide is

$$W(x,y) = r_1^{-\frac{1}{3}} r_2^{-\frac{1}{3}} \tag{3-61}$$

where r_1 and r_2 are the radial distances from each edge. For the field at $y = 0$, $|x| \geq a/2$ this can be written in terms of x as

$$\begin{aligned} W(x,y) &= ((a/2) + x)^{-\frac{1}{3}} ((a/2) - x)^{-\frac{1}{3}} \\ &= (a/2)^{2}(1 - (2x/a)^{2})^{-\frac{1}{3}} \end{aligned} \tag{3-62}$$

This function shows the correct singularity behaviour and has a continuous derivative, and so in order to accurately model the expected field solution the first term of the expansion set fm(x) is chosen to be :

$$fo(x) = A\,(1 - (2x/a)^{2})^{-\frac{1}{3}} \tag{3-63}$$

where A is an amplitude term.

The set $\Phi hn(x)$ is known to give the field solutions for parallel plate guide and so it is reasonable to assume that an orthogonal series constructed from the $\Phi hn(x)$'s modified by $W(x)$ would closely approximate the field across the slot at $y = 0$. This would certainly satisfy (3-63) and the remaining terms can easily be obtained by using the Gram-Schmidt orthogonalisation process. However, a further criterion must also be satisfied. In order that the principal value of the Y_{22}^{a} integral is taken, the inner product $Pm(\rho)$ must satisfy:

$$Pm(\rho) = \langle fm(x)\, \Phi h(\rho,x) \rangle = 0 \quad \text{for } m \geq 2,\ \rho = 0 \tag{3-64}$$

in order that the second order pole at the origin can be removed. It has been found that the modified $\Phi hn(x)$'s do not satisfy (3-64) and so another set of functions must be found. Dropping the amplitude term, the function $W(x)$ is found to be the weight function for the orthogonalisation of the Gegenbauer polynomials [6]. These have a constant first term and have the orthogonality relationship :

$$\int_0^1 (1 - x^2)^{\nu-\frac{1}{2}}\, C_n^{\nu}(x)\, C_m^{\nu}(x)\, dx = 0, \quad m \neq n \tag{3-65}$$

Thus in order to model the correct singularity behaviour the expansion functions are chosen as

$$fm(x) = \frac{1}{Nm} (1 - (2x/a)^2)^{-\frac{1}{3}}\, C_m^{\frac{1}{6}}(2x/a) \qquad m = 0,2,4,\ldots \tag{3-66}$$

where Nm is a normalisation factor. The inner products :

$$Pm(\rho) = \frac{1}{Nm} \langle (1 - (2x/a)^2)^{-\frac{1}{3}}\, C_m^{\frac{1}{6}}(2x/a), \Phi h(\rho,x) \rangle \tag{3-67}$$

are found to satisfy (3-64). The normalisation of the Gegenbauer polynomials and the evaluation of the inner products is given in Appendix II. Plots of the first four expansion terms for the even and odd cases across the slot are given in fig.3-4.

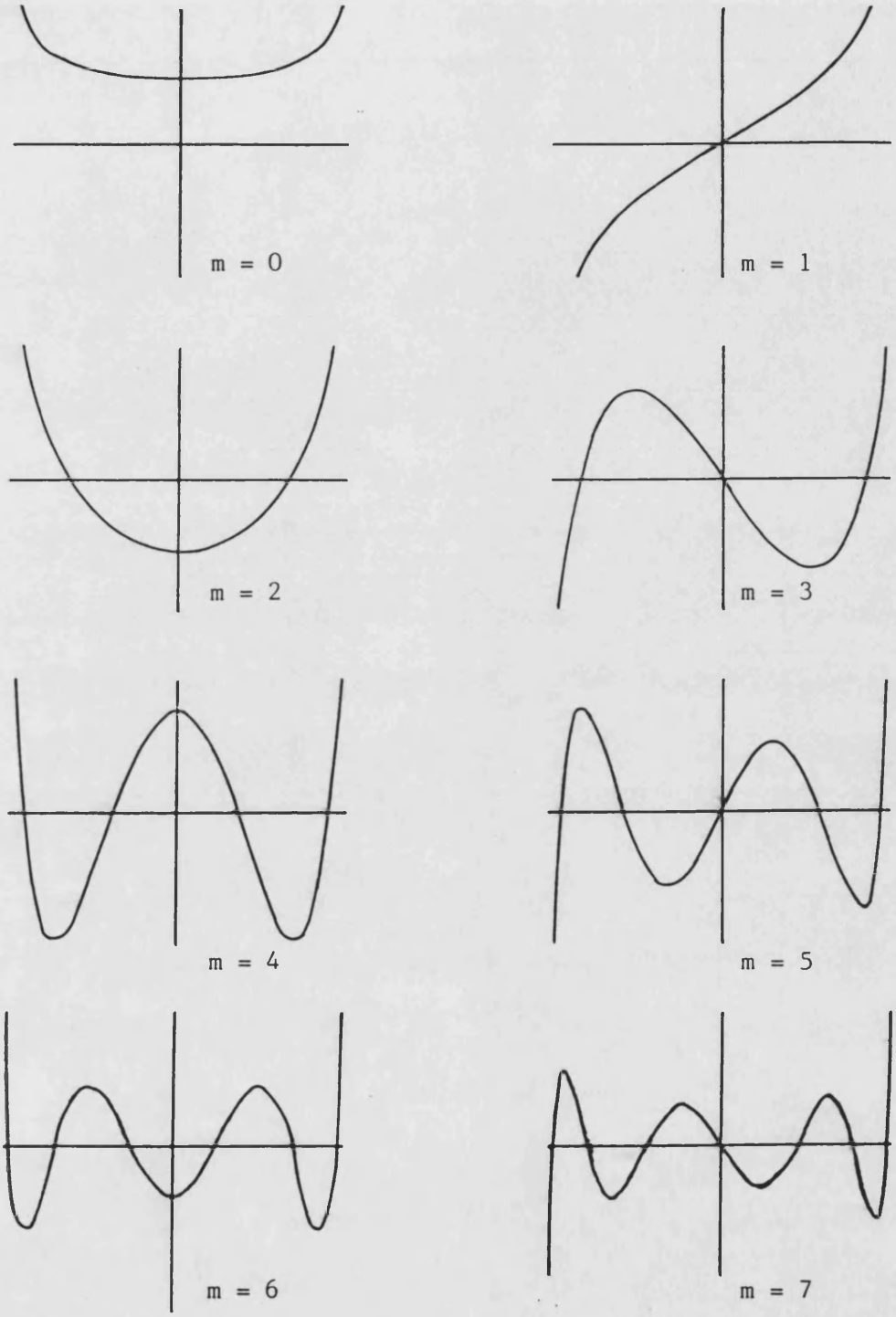

Amplitude plots of the weighted Gegenbauer polynomials $w(x)\,C_m^{\frac{1}{6}}(x)$ plotted across the slot aperture.

figure 3-4

3-8 The Formulation for Odd Solutions

The formulation previously described has been for the field solutions that are even wrt x. Due to the symmetry of the IDG structure these will be the general solutions. However any asymmetric changes in the guide's axial geometry will excite and support odd modes. The most obvious example of this is the bend. In a bend, odd modes will be excited in order that the field can satisfy the asymmetric boundary conditions. However, if the propagation characteristics of the odd modes are known, then the guide dimensions can be chosen so that the odd modes are below cutoff when excited. Thus the dispersive losses of the bend can be reduced.

The solutions for odd modes can be found easily by modifying the even mode formulation. However, whilst in the even case the fundamental slot mode (n=0) is purely TE and so can be removed from the higher order terms, the fundamental odd (n=1) mode will consist of both TE and TM contributions. Hence a two port network interpretation is not applicable in this case. Once the operators have been formulated the eigenvalues and eigenvectors (β and trial fields) can be found in the usual way by solving the determinantal equation (3-52). For an odd solution, the slot mode functions analogous to (3-7) will be :

$$\left.\begin{aligned} \Phi hn(x) &= \frac{2}{\sqrt{a}} \sin(n\pi/a)x \\ \Phi en(x) &= \frac{2}{\sqrt{a}} \cos(n\pi/a)x \end{aligned}\right\} \quad n = 1,3,5,... \qquad (3\text{-}63)$$

In all other respects the formulation of the admittance operators is identical. The expansion of the fields Ex(x,o) and $(a/\pi)dEz(x,o)/dx$ at y = 0 is now in terms of the odd Gegenbauer polynomials, with the same weight function as for the even case and so the inner products will be

of the form

$$Qmn = \langle fm(x), \sqrt{\frac{2}{a}} \sin(n\pi/a)x \rangle \qquad (3\text{-}69a)$$

$$n,m = 1,3,5,\ldots$$

$$Qm(\rho) = \langle fm(x), \sqrt{\frac{2}{\pi}} \sin\rho x \rangle \qquad (3\text{-}69b)$$

The analytic forms for these products are given in Appendix II, and plots of the first four odd basis terms have already been given in fig.3-5.

To summarise; the solutions for the odd modes are found by solving (3-52) with the matrix elements as given in (3-60) modified in that the inner products Pnm are replaced with the Qnm given in (3-69), and the summations and array elements are over odd integer values. If N basis terms are used in the odd formulation then the resulting admittance matrix will be of order 2N.

3-9 The Extension to Other Guide Geometries

The TRD approach can be used to analyse other guiding structures if suitable potential functions and expansion sets can be found. For example the method has been used to analyse image line [7] and finline [8]. Its advantage of high convergence over frequency domain methods occurs when the transverse fields contain a discontinuity that cannot be easily be expanded by fourier transformable functions. The method thus requires an a priori knowledge of the form of the guide field so that an accurate basis set can be found.

For guide structures that are simple modifications of IDG a complete reformulation is unnecessary. Examples include the case of the lowering of the dielectric in the slot or even the use of several dielectric layers in the slot. A desirable feature of the TRD approach (but not

unique to it) is that the TE and TM equivalent circuit contributions are decoupled in the formulation of the admittance operators. Thus they can be written as :

$$(Y^s_{11})km = \sum_{n=2,4}^{\infty} (Yn' \cos\theta^2 + Yn'' \sin\theta^2)\, Pkn\, Pmn \qquad (3\text{-}70a)$$

$$(Y^s_{12})km = -(Y^s_{21})mk = \sum_{n=2,4}^{\infty} (j/n)(Yn' - Yn'') \sin\theta \cos\theta\, Pkn\, Pmn \qquad (3\text{-}70b)$$

$$(Y^s_{22})km = \sum_{n=2,4}^{\infty} (1/n)^2 (Yn' \sin\theta^2 + Yn'' \cos\theta^2)\, Pkn\, Pmn \qquad (3\text{-}70c)$$

$$(Y^a_{11})km = \int_0^{\infty} (Y'(\rho) \cos\theta^2 + Y''(\rho) \sin\theta^2)\, Pk(\rho)\, Pm(\rho)\, d\rho \qquad (3\text{-}70d)$$

$$(Y^a_{12})km = -(Y^a_{21})mk = \int_0^{\infty} (\pi/a\rho)(Y'(\rho) - Y''(\rho)) \sin\theta \cos\theta\, Pk(\rho)\, Pm(\rho)\, d\rho \qquad (3\text{-}70e)$$

$$(Y^a_{22})km = \int_{0^+}^{\infty} (\pi/a\rho)^2 (Y'(\rho) \sin\theta^2 + Y''(\rho) \cos\theta^2)\, Pk(\rho)\, Pm(\rho)\, d\rho \qquad (3\text{-}70f)$$

where the angle θ is defined by equations (3-13) and (3-28) for each region. The admittances Yn' etc are defined at the plane of resonance of the transverse equivalent circuit. If this plane is unchanged then the same expansion sets and inner products can be used for other similiar structures. In the case of IDG the slot input admittances are those of short-circuited lengths of transmission line. If the dielectric is lowered in the slot then the admittances become those of a cascade of transmission line sections of different characteristic admittance terminated with a short-circuit, and so on. Thus, provided that the TE and TM admittances can be found in this manner then the admittance operators can be formulated by inspection by substitution into (3-69) leading directly to a dispersion equation equation.

3-10 Concluding Remarks

In this chapter a detailed explanation of the transverse resonance diffraction method as applied to IDG has been given. Whilst no one analytical approach can claim to be superior in all respects to any others, the TRD method for guide geometries with boundary conditions that include singularities such as IDG, finline and ridged waveguide can promise very accurate results with a minimum of computational effort. The formulation of the problem in terms of transverse equivalent circuits enables the admittance operators for other compatible structures to be found almost by inspection.

The choice of basis set for the discretisation of the unknown fields governs both the rate of convergence and the final accuracy of the solution of this type of approach. The expansion of the integral equations into the space domain rather than the frequency domain (as with spectral analysis) has enabled an accurate approximation to be made for the trial fields. Hence the the convergence rate and subsequently the required computational time can be expected to be reduced in comparison with the spectral domain approach in this instance.

3-11 References

[1] R.E. Collin, "Field Theory of Guided Waves", McGraw-Hill, 1960, p.18

[2] J.A. Stratton, "Electromagnetic THeory", McGraw-Hill, 1941

[3]T. Itoh, "Spectral Domain Immittance Approach for Dispersion Charactaristics of Generalised Printed Transmission lines", IEEE Trans Microwave Theory Tech., vol. MTT-28, pp. 733-736, July 1980.

[4] R.F. Harrington, "Time-Harmonic Electromagnetic Waves", McGraw-Hill, 1961, p. 120.

[5] S. Ramo, J.R. Whinnery and T. Van Duzer,"Fields and Waves in Communication Electronics",John Wiley & Sons, 1965, p.383.

[6] Abramowitz and Stegun, "Handbook of mathematical functions",Dover, 1965, p.887.

[7] J. Kot and T. Rozzi," Rigorous Modelling of Single and Coupled Rectangular Dielectric Waveguides by Transverse Resonance Diffraction", in Proc. 14th European Microwave Conf.(Liege), Sept, 1984, pp.424-429.

[8] C. Olley and T. Rozzi,"Characterisation of Unilateral Finline Mode Spectrum Including Loss Analysis", Proc. 16th European Microwave Conf.(Dublin), 1986, pp. 551-556.

CHAPTER FOUR

THE RESULTS OBTAINED FROM THE SOLUTION OF THE DISPERSION EQUATION

4-1 Introduction

In this chapter the results obtained from the solution of the dispersion equation are presented. The computational methods for the determination of both real and complex solutions for β are outlined, and the rapid convergence of the solutions is demonstrated. The hybrid mode solutions are classified and their cutoff frequencies are determined as functions of the guide geometry. The solutions for β enable the fields to be determined, and these are presented for several modes.

The experimental work is discussed and the measured dispersion curves for several guide geometries are presented. These results are in excellent agreement with the computed values and demonstrate the accuracy of the method of analysis.

4-2 The Solution of the Dispersion Equation

The dispersion equation for IDG has been derived in the previous chapter and can be written as:

$$-j \cot ky_0 h + jb = 0 \qquad (4\text{-}1)$$

where

$$jb = \left[\left(\underline{P}_0^T \; \underline{0}^T \right) \cdot \underline{\underline{Y}}^{-1} \cdot \begin{pmatrix} \underline{P}_0 \\ \underline{0} \end{pmatrix} \right]^{-1}$$

The admittance terms have been derived by using transverse resonance and equation (4-1) itself is a statement of the resonance of the transverse equivalent circuit discussed previously and shown in Fig. 3-4. The resonance condition is imposed at the interface ($y = 0$) where the unknown fields $Ex(x,0)$ and $Ez'(x,0)$ are expressed by means of weighted basis functions. For each combination of the basis functions that satisfies the boundary conditions, a value of β can be found that

brings the equivalent circuit to resonance. Thus, for a given frequency, equation (4-1) has several solutions for β. Each solution corresponds to a different mode of propagation. Series of basis functions with amplitude coefficients Xn and Zn obtained for a given value of β will give the field components Ex(x,0) and $E_z'(x,0)$ that correspond to that particular mode.

It is immediately obvious that in order to obtain an accurate value of β for a particular mode then the basis functions must be able to model the transverse fields for that mode. Any complete set of functions could thus be used as the basis set. However, the number of terms required to give the fields also determines the order of the matrix inversion that has to be carried out in (4-1). In fact, if n basis terms are used then the order of the matrix for inversion will be 2n - 1. To reduce the numerical complexity of the problem, the field expansion must converge rapidly, requiring that each basis function itself must model the expected field variation across the slot. This condition has indeed been enforced, as discussed in section 3-7 of the previous chapter.

When a solution is sought for a mode which has a constant Ex variation across the slot (modified by the edge condition), then a solution obtained from (4-1) by using only the first basis term can be expected to be accurate. However, when a mode solution with a higher order variation is sought, then sufficient basis terms must be taken so that this variation can be modelled.

4-3 The Fundamental Approximation

When only one basis term is used in the field expansion, the dispersion equation is reduced to the scalar equation:

$$-j \cot\left[\frac{\pi u h}{a}\right] + jC - jL = 0 \qquad (4\text{-}2)$$

where $$jC = ju \sum_{n=2}^{\infty} \frac{\coth\sqrt{n^2 - u^2}\,[\pi h/a]}{\sqrt{n^2 - u^2}} \left[\frac{P_0}{P_{00}}\right]^2$$

$$-jL = \frac{w^2}{ju} \int_0^{\infty} d\rho \frac{1}{\sqrt{w^2 + \bar{\rho}^2}} \left[\frac{P_0(\rho)}{P_{00}}\right]^2$$

and $u = (a/\pi)\sqrt{\varepsilon_r Ko^2 - \beta^2}$, $w = (a/\pi)\sqrt{\beta^2 - Ko^2}$, $\bar{\rho} = (a/\pi)\rho$

Apart from the reduction in computational time, this equation is useful in that it provides a simple transverse equivalent circuit model which gives an insight into the essential nature of the IDG field. In this case (n = 0), then dEz(x,0)/dx = 0 and so to a first order approximation the field is TE wrt y. In terms of the normalised y-directed wavenumber for the fundamental mode, u, equation (4-2) can be related to the TE equivalent circuit parameters as follows. The first term in (4-2) is the admittance of a short-circuited length of transmission line for the fundamental slot mode. The second term has the dimensions of a capacitive admittance and models the energy storage in the slot due to the higher order non-propagating slot modes. When the guide is above cutoff, no energy can flow into the air region from the slot. The third term in (4-2) is inductive in u, and models the energy stored near the interface by the non-propagating air field.

The three admittance terms of (4-2) identified in this way give the simple transverse equivalent circuit representation given in Fig.4-1.

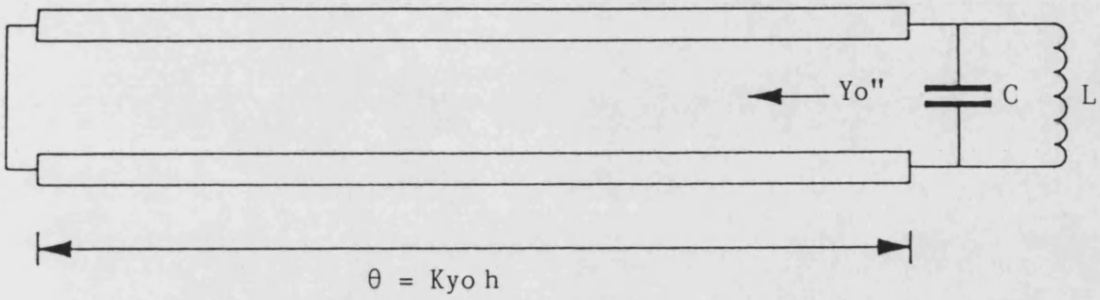

The simplified transverse equivalent circuit obtained from the first order expansion for monomode propagation.

figure 4-1

4-4 The Computational Method

The dispersion equation (4-1) was solved using a mainframe computer with programs written in Fortran 77. The computational method involved evaluating the left hand side of (4-1) for varying values of β, and finding those values of β that reduced this function to zero. When all losses are neglected, the function zeros lie on the real β axis. When losses are included the zeros can lie anywhere in the $\beta' - j\beta''$ quadrant. Thus these two different conditions required different computation techniques.

The Solution for Real β

When β is restricted to be purely real and losses are neglected, then the function value (4-1) is also a purely real quantity. This is a useful approximation for many design applications which greatly improves the speed of computation. The function zero on the real β axis was determined by an interval halving technique. This can be briefly explained as follows: For a given frequency the function value is calculated for real β as β is stepped over the range of interest ($k_0 < \beta \leq \sqrt{\epsilon r}\ k_0$). The function value will either be positive or negative. When a change of sign of the function value occurs between successive steps then that interval in β must either contain a function zero or a pole. By then successively halving this interval and choosing the half-interval that contains the zero (or pole), the zero can be converged upon until the required accuracy is obtained. Since the dispersion equation is transcendental, this method has to be repeated to cover all possible solutions.

The determination of the function involves the computation of the series:

$$S = \sum_{n=2,4}^{N} \frac{\coth \sqrt{n^2 - u^2}\,(\pi h/a)}{\sqrt{n^2 - u^2}} \, Pmn \, Pkn \qquad (4\text{-}3)$$

For the slot terms, and the integral

$$I = \int_0^{\infty} \frac{1}{\sqrt{w^2 + \bar{\rho}^2}} \, Pm(\bar{\rho}) \, Pk(\bar{\rho}) \, \frac{\pi}{a} \, d\bar{\rho} \qquad (4\text{-}4)$$

for the air terms. The values of the inner products Pmn and $Pm(\rho)$ are easily evaluated from the expressions given in Appendix II. For a given m, the inner product Pmn converges as $J_{m+\frac{1}{6}}(n) / n^{\frac{1}{6}}$, and so the series and intergrand converge as $n^{-7/3}$ and $\rho^{-7/3}$ respectively. The integral has to be evaluated numerically and the method of Gaussian Quadrature was used [1]. The evaluation of the integral for each m, k and w would have vastly lengthened the computation. Therefore, for each value of m and n, the integral was evaluated for several values of w. A polynomial curve approximation was then fitted to these points to provide values of the integrals for any w. This enabled the program to be quick and simple. The speed of the program is dependent upon the number of terms taken in the field expansion. In tables 4-1(a), (b) and (c), the computed values of β for three different IDG samples are given for the first four orders of the expansion. It can be seen that the convergence is very rapid and that one or two terms are all that are needed for most calculations.

The Solution for Complex β

When losses are accounted for both β and the function value can take on complex values. For the function to vanish, both the real and imaginary parts must go to zero. That is, the function value must

Completely Filled Slot : a = 1.016 cm $h/a = 1.5$ $\varepsilon_r = 2.08$

FREQ (GHz)	1st ORDER	2nd ORDER	3rd ORDER	4th ORDER
7	1.71413	1.70957	1.70943	1.70941
8	2.03039	2.02561	2.02546	2.02544
9	2.34639	3.34156	2.34141	2.34139
10	2.66174	2.65702	2.65686	2.65683
11	2.97649	2.97197	2.97181	2.97178
12	3.29119	3.28689	3.28674	3.28671
13	3.60578	3.60177	3.60161	3.60158

Table 4-1(a)

Partially Filled Slot : a = 1.016 cm $h/a = 1.5$ $h_d = a$ $\varepsilon_r = 2.08$

FREQ (GHz)	1st ORDER	2nd ORDER	3rd ORDER	4th ORDER
7	1.46192	1.46190	1.46190	1.46190
8	1.73550	1.73555	1.73555	1.73555
9	2.02434	2.02449	2.02449	2.02449
10	2.32308	2.32331	2.32331	2.32331
11	2.63038	2.63068	2.63068	2.63068
12	2.94392	2.94428	2.94428	2.94428
13	3.26159	3.26194	3.26194	3.26194

Table 4-1(b)

The Computed Values of β for two X-Band IDG Samples for the first Four Orders of Expansion

FREQ (GHz)	1st ORDER	2nd ORDER	3rd ORDER	4th ORDER
26	6.79378	6.78010	6.77961	6.77961
28	7.42453	7.41103	7.41062	7.41056
30	8.05432	8.04118	8.04074	8.04067
32	8.68362	8.67095	8.67048	8.67041
34	9.31307	9.30081	9.30038	9.30031
36	9.94245	9.93076	9.93031	9.93023
38	10.57111	10.56004	10.55956	10.55948
40	11.19782	11.18751	11.18700	11.18692

Guide Dimensions
$a = 0.3556$ cm, $h/a = 1.5$ $\varepsilon r = 2.08$

The Computed Values of β for the Q-Band

IDG Sample for The First Four Orders of Expansion

Table 4-1(c)

be at the origin on the complex function value plane. The real and imaginary parts of the function value can each take on positive or negative values so that the complex value can take one of four signs, corresponding to each quadrant of the complex plane. A function zero (or pole) must be surrounded by values from each quadrant since by definition it lies at the origin. The location of a zero (or pole) is thus found as follows: The complex β plane over which a solution is sought is discretised into a rectangular grid. An array is set up so that each element corresponds to a node on this grid. For each value of β correspondingly to a node, the function value is computed and the associated array element is given a value 1, 2, 3 or 4 according to which quadrant the function value lies in. For example, if Re (function)>0, Im (function)>0 then the element = 1, and if Re (function) <0, Im(function)>0 then the element = 2, and so on. In this manner a grid of numbers is set up which follows the variation of the function value over the range of β. The zeros are then found by searching the array for groups of $\begin{matrix}1 & 2\\ 4 & 3\end{matrix}$ etc. Having located the approximate position of the zero, three of the four surrounding node values were passed to a Muller quadratic interpolation routine [2] to determine the accurate value for β. A sample output from this program is shown in Fig. 4-2. Care must be taken to ensure that the grid size is fine enough to allow sufficient definition for the location of the zeros. This is especially true when the function varies rapidly with β, which occurs for some higher mode solutions.

With complex β, the variable w in the integrals (4-4) are complex so that a curve fitting routine as used for the real case would now be required in two dimensions. This would be unwieldy and so the integrals were evaluated using Gaussian Quadrature and a "look-up" table for the values of $Pn(\rho)$, for each value of β. This increased the computing time

```
order of expansion 3

real beta area from beta=    .44011638E+01
                  to beta=    .58682184E+01
imag beta area from beta=    .00000000E+00
                  to beta=   -.50000000E-02

11111111111144444444433333332
22222221111144444444443333332
22222222222233333333444444441
22222222222233333333344444441
22222222222233333333344444441
22222222222233333333344444441
22222222222233333333344444441
22222222222233333333344444441
22222222222233333333344444441
22222222222233333333344444441
22222222222233333333344444441
frequency=    .20000000E+02
     beta= (    .49752942E+01,    -.63433193E-03)
      Zero at beta/Ko=  0.1186972E+01
Function value=    0.135519E-04    0.155847E-04
no. of iteraticns= 6

frequency=    .20000000E+02
     beta= (    .57893999E+01,    -.61238452E-03)
      Zero at beta/Ko=  0.1381196E+01
Function value=    0.196498E-03    0.790397E-05
no. of iteraticns= 4
```

A sample output from the complex quadratic interpolation program used to solve the dispersion equation.

Figure 4-2

required for each function value and so limited the number of basis terms that could be practically used to two or three.

The computed results for a given sample of IDG at two frequencies are given in table 4-2 for the first four orders of expansion in order to show the convergence of the solution. It must be noted that the absolute accuracy of the computed results is dependent upon the accuracy of the numerical evaluation of the air integrals and truncation errors in the machine itself. Hence variations in the fifth decimal place in the tabulated results are included only for the sake of comparison and not as an indication of the accuracy actually achieved.

The speed of both programs, solving for real or complex β, is dependent upon the number of terms taken in the field expansions, which determine the number of matrix elements to be evaluated and the order of the matrix inversion. The computed results given in tables 4-1 and 4-2 demonstrate the convergence of the solutions with increasing order and show that one or two terms are generally all that are required.

The speed of computation of the matrix elements was determined by the evaluation of the integrals in ρ. For real β the integrals were approximated from curve fits and so the program was very fast, only taking several seconds per frequency point. The solution for complex β took a lot longer since the integrals were numerically evaluated for each new value of β. The process was also slowed down by the need to evaluate the function many times to establish the search grid for the solutions in the complex β plane.

The "real" program was thus more suited for "real time" computation and was compact enough to be implemented on a desk top computer. The "complex" program was more amenable to "batch" computation on a main-frame computer.

Frequency = 8·0 GHz

order	β	β'/Ko
1	2·030669 - j0·000220	1·21116
2	2·025831 - j0·000219	1·20827
3	2·025668 - j0·000219	1·20817
4	2·025647 - j0·000219	1·20816

Frequency = 12·0 GHz

order	β	β'/Ko
1	3·291453 - j0·000357	1·30875
2	3·387114 - j0·000356	1·30703
3	3·286933 - j0·000356	1·30696
4	3·286910 - j0·000356	1·30695

The complex values of β computed for the first four orders of expansion of the dispersion equation.

IDG parameters : a = 1·016cm h/a = 1·5 $\varepsilon_r = 2{\cdot}08 - j4{\cdot}16\times10^{-4}$

Table 4-2

4-5 The Classification of Mode Types

The modal solutions for IDG cannot be characterised as TE or TM. The 90^{o} edge discontinuity requires a full six field description. However it can be shown that any field distribution can be constructed from an appropriate superposition of TE and TM modes [3]. The field then, as a combination of the two mode families is known as a "hybrid mode".

Field solutions that have no Ey component, ie are TM wrt y or LSE wrt z, can be derived from a y-directed magnetic Hertzian potential. Similarly, the TE wrt y solutions can be derived from a y-directed electric Hertzian potential. The two hybrid components can thus be classed as E or H-modes wrt y (LSM and LSE respectively) and the resultant hybrid mode can be classed as HE or EH depending on which component is dominant. For example an HE designation indicates that the field is dominantly H-type wrt y.

In a full multiport transverse equivalent circuit representation of the guide, the H-type components correspond to voltages of parallel TE transmission lines and E-modes to currents in parallel TM lines. Therefore the relative magnitudes of the current and voltage components on the TM and TE lines respectively will determine the mode type. From equation (3-12) the current and voltage amplitudes on each equivalent transmission line are given as:

$$I_n' = \frac{Y_n'}{[(\frac{n\pi}{a})^2 + \beta^2]^{\frac{1}{2}}} [(\frac{n\pi}{a})Exn + j\,\beta Ezn] \qquad (4\text{-}5a)$$

$$V_n'' = \frac{1}{[(\frac{n\pi}{a})^2 + \beta^2]^{\frac{1}{2}}} [j\,\beta Exn + (\frac{n\pi}{a})\,Ezn] \qquad (4\text{-}5b)$$

where Y_n' is the input admittance of the n^{th} order TM transmission line. By writing the above coefficients in terms of the amplitudes of the field expansion these equations can be further simplified to:

$$I_n' = \frac{Y_n'}{[(\frac{n\pi}{a})^2 + \beta^2]^{\frac{1}{2}}} [(\frac{n\pi}{a})^2 \underline{X}^T \cdot \underline{P}_0 + j (\frac{\beta}{n}) \underline{Z}^T \cdot \underline{P}_0] \qquad (4\text{-}6a)$$

$$V_n'' = \frac{1}{[(\frac{n\pi}{a})^2 + \beta^2]^{\frac{1}{2}}} [j\beta \underline{X}^T \cdot \underline{P}_0 + (\frac{\pi}{a}) \underline{Z}^T \cdot \underline{P}_0] \qquad (4\text{-}6b)$$

Thus by summing the magnitudes of the I_n' over n and comparing it with the corresponding sum for Vn", the mode type can be determined.

The order of a given mode is determined in the usual fashion by noting the number of phase changes in the transverse field components. Thus the hybrid mode will be classified either EHnm or HEnm where n gives the number of $\pi/2$ phase changes occurring in the x-direction (across the slot) and the integer m gives the relative phase change in the y-direction (throughout the slot). Using this notation, the fundamental IDG mode solution was found to be of the type HE_{01}. This is to be expected since, for the geometry analysed the slot field is very similar to that of rectangular waveguide. As the slot width is made narrower the field can be expected to become increasingly TE dominated as the perturbation from the rectangular waveguide geometry is lessened. Inversely, as the slot width is increased the TM component can be expected to increase as the structure approaches the grounded slab case for which a TM surface wave is the fundamental mode.

The dispersion equation was solved for the guide dimensions of one of the X-Band test pieces (a = 1·016cm, h/a = 1·5, ε_r = 2·08) for frequencies up to 40 GHz. The resulting dispersion curves are plotted in fig. 4-3 against the normalised dispersion parameter $((\beta/Ko)^2 - 1)/(\varepsilon_r - 1)$. The modes have been classified in accordance with the notation outlined above.

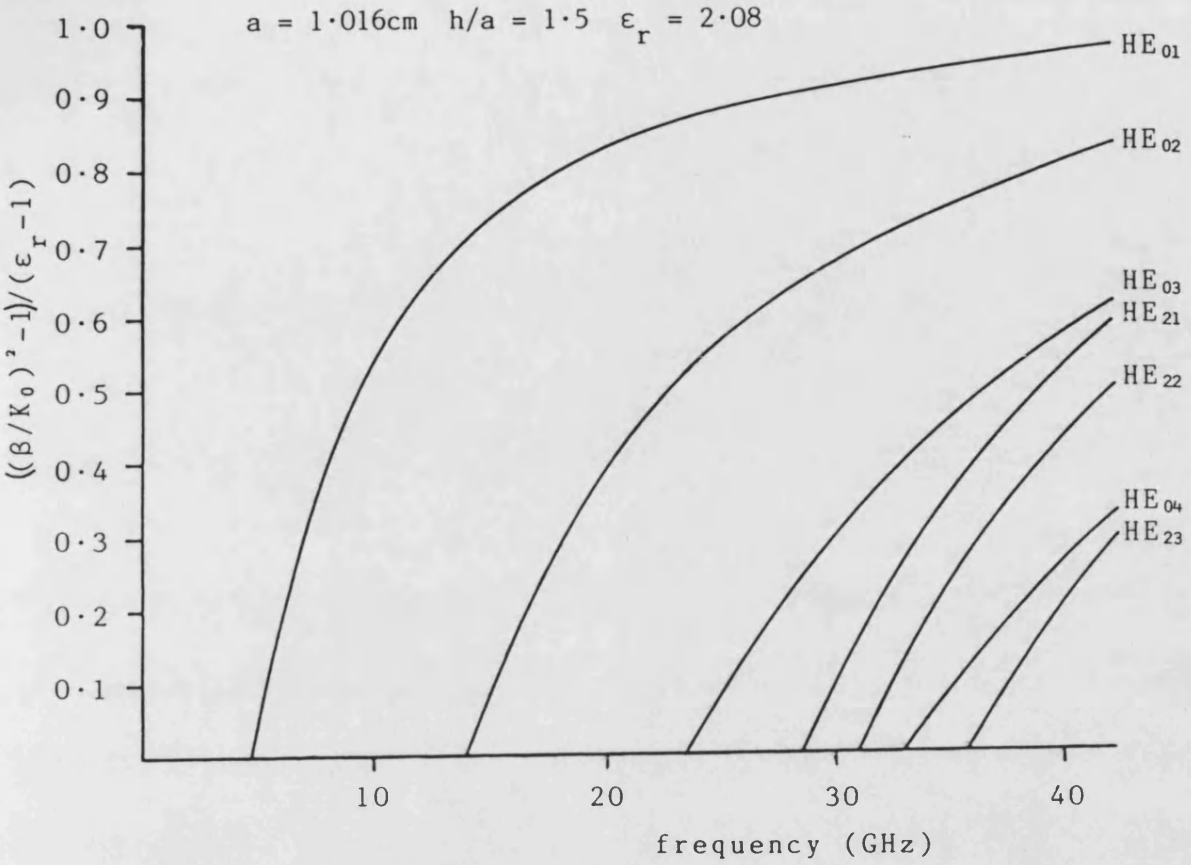

The computed dispersion curves for the even modes of an X-band sample of IDG up to 40GHz.

Figure 4-3

4-6 IDG Cutoff Frequencies

The guiding property of a dielectric guide is basically due to the confinement of the propagating energy within the dielectric by total internal reflection. The propagation constant of a fully bound mode satisfies the condition $k_1 \leq \beta \leq k_2$ where k_1 and k_2 are the free space wavenumbers in the medium surrounding the guide and the guiding medium respectively. As long as this condition is satisfied, real energy flow can only take place along the guide. If $\beta \leq k_1$, then energy can flow away from the guide and radiation losses occur. This point is discussed further in the next chapter. The limiting frequency below which low loss propagation cannot take place is that frequency for which $\beta = k_1$. This is the cutoff condition for dielectric waveguides.

A knowledge of the cutoff frequencies of the various possible modes is important for the characterization of any guiding structure. Generally, propagation is required in the fundamental mode only and so its cutoff frequency is an important parameter. In order to preserve monomode operation the cutoff frequencies of any higher order modes must be determined so that the useful operating range of the guide can be ascertained. A knowledge of the influence of changes of cross-sectional geometry upon the cutoff frequencies can enable discontinuities such as impedance transformers to be designed that only excite non-propagating modes.

The cutoff frequencies for IDG were found by solving the dispersion equation for the case $\beta = k_0$, or, more specifically for the case $\beta \to k_0$. This is because, for the lossless case, there is a branch point at $\beta = k_0$ in the air admittance operators. The cutoff frequency for the fundamental mode is not influenced by the slot width (a) although the h/a ratio will determine the useful monomode range. The cutoff

frequencies for the first two odd and even modes were computed for various guide dimensions and are shown plotted in Figs. 4-4 to 4-6, for variations in $^{h}/a$ ratio, dielectric depth and relative dielectric constant. It is noted that for a deep slot (relative to width) the monomode bandwidth is limited by the onset of the HE_{02} mode, whilst for a shallow slot the HE_{11} mode is the next to propagate. From Fig. 4-4 it appears that the largest monomode operating range is achieved when $^{h}/a \simeq 1.45$, giving approximately double that of rectangular waveguide of the same width (for $\varepsilon_r = 2.0$). For the sake of low dispersion and monomode bandwidth, a low value of dielectric constant is preferred. However, for the sake of economy of fabrication and increased field confinement to the slot, a higher value may be required such as that afforded by a casting resin for example.

The simplest way to change the IDG characteristics may be to change the depth of the slot. Figure 4.7 gives the dispersion curves for two guides, identical apart from a difference in slot depth.

It is noted that although for practical purposes $\beta = k_0$ is the condition for cutoff, the rigorous condition, i.e. when no propagation at all is possible along the guide, is given by $\beta = o$. For this condition $Y_{12} = Y_{21} = o$ indicating that the TE and TM components are completely decoupled. This is to be expected since for $\beta = o$, propagation can only take place in the y-direction, and independent TE and TM solutions are possible for parallel plate waveguide.

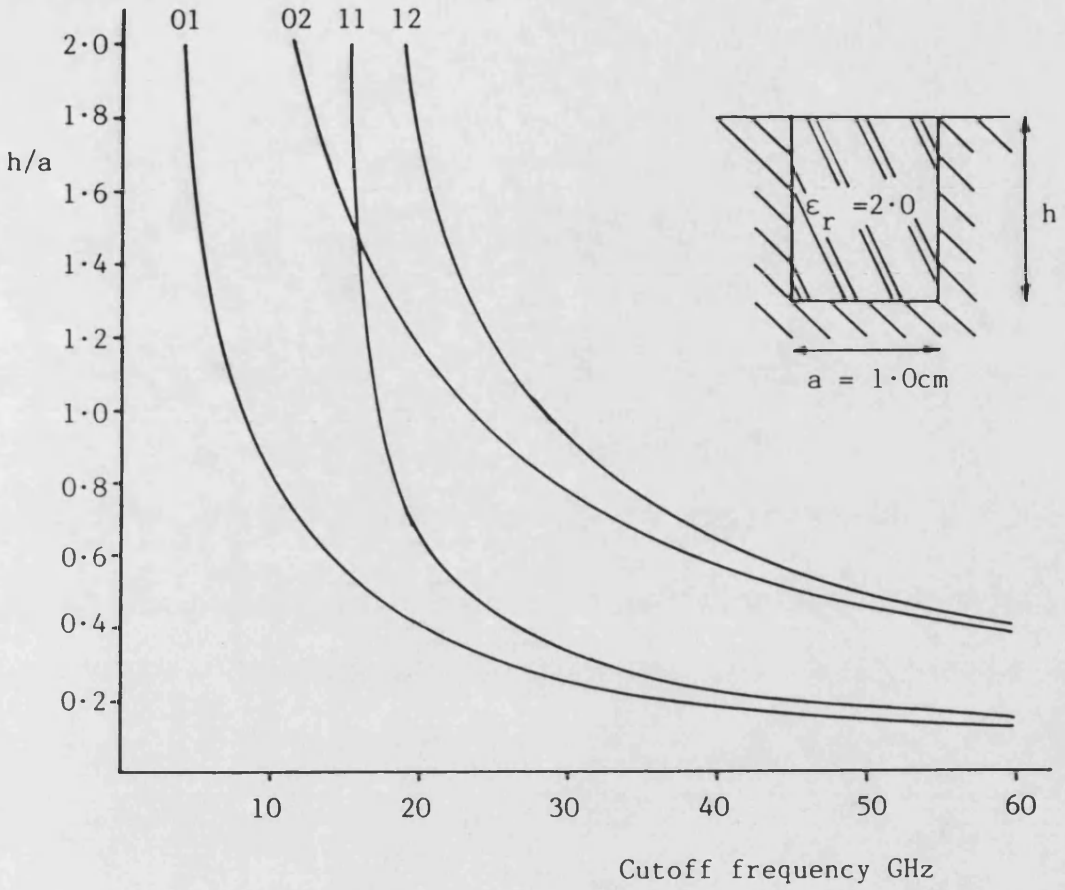

The computed cutoff frequencies for the first four modes of IDG of the dimensions shown, for a kept constant and varying values of the slot aspect ratio h/a.

Figure 4-4

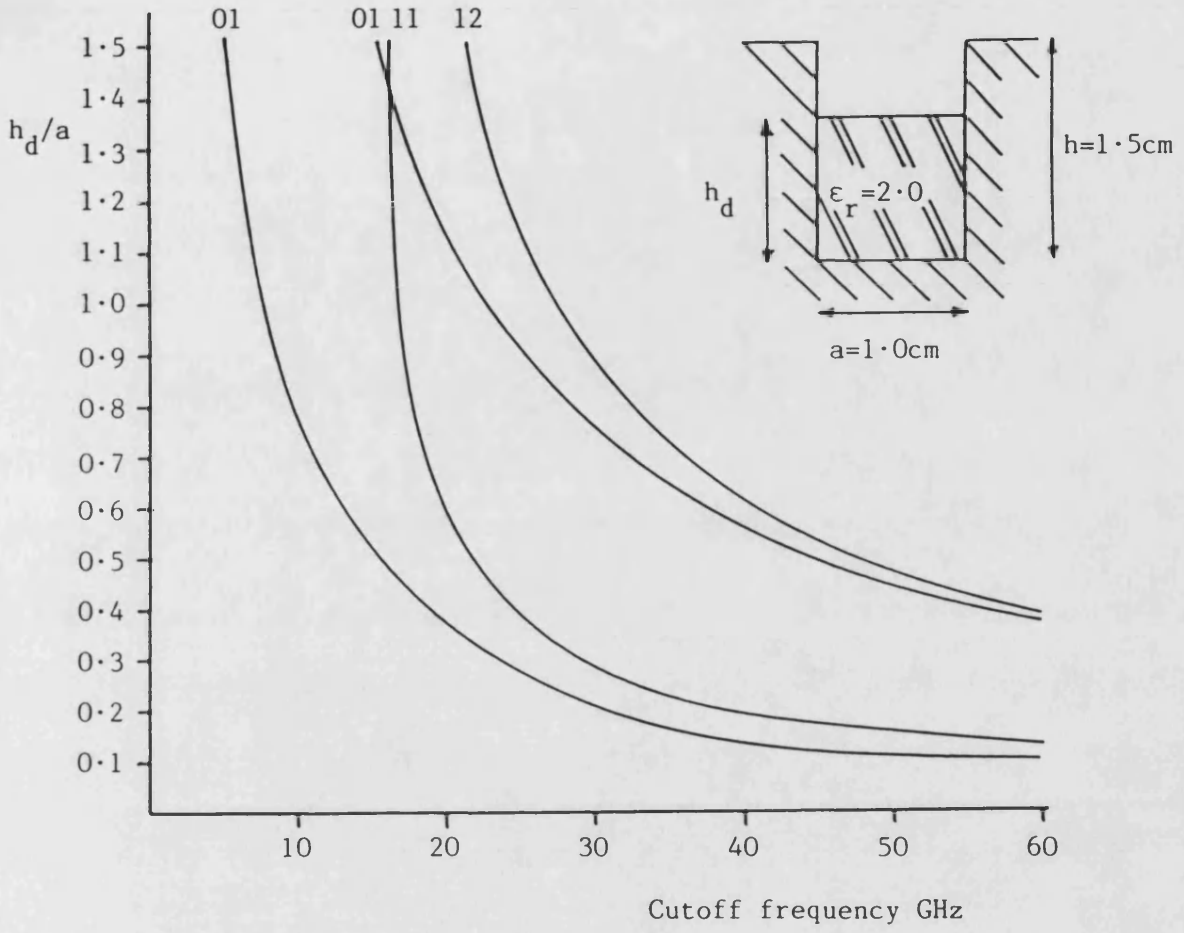

The computed cutoff frequencies for the first four modes of IDG of the dimensions shown, for slot dimensions kept constant and varying values of the dielectric insert depth.

Figure 4-5

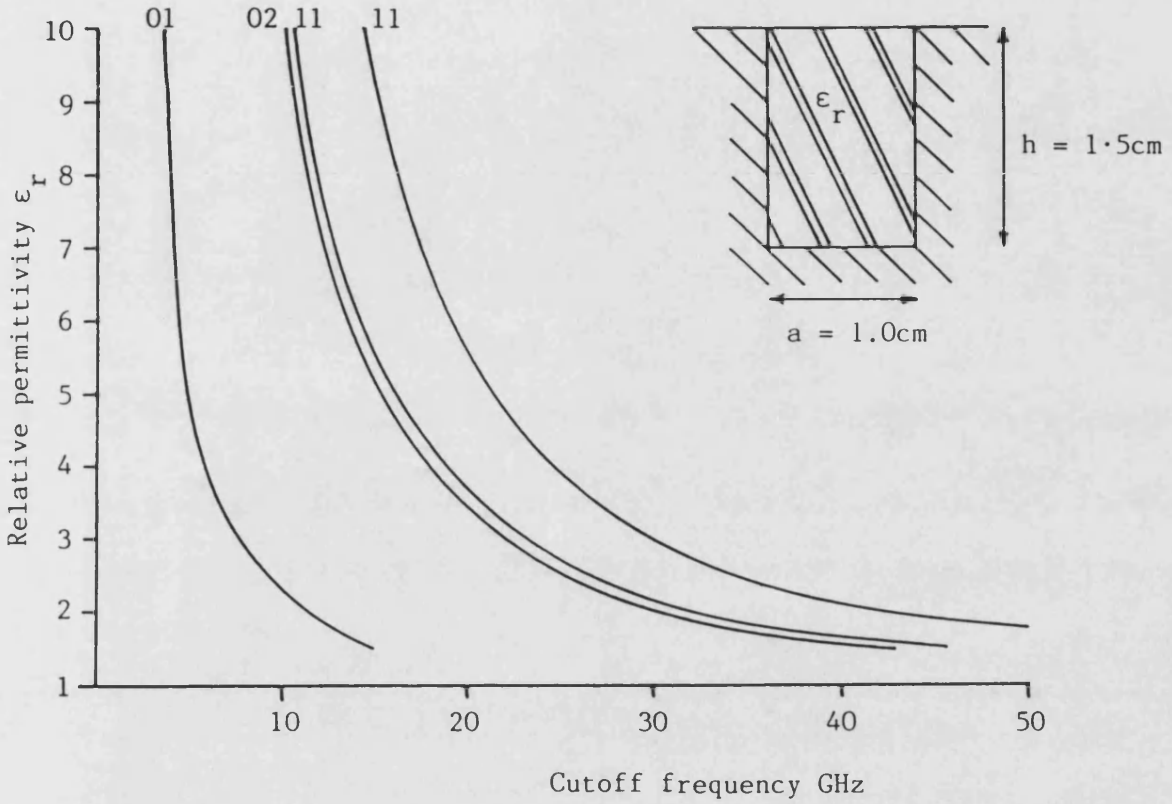

The computed cutoff frequencies for the first four modes of IDG of the dimensions shown, for varying values of relative permittivity.

Figure 4-6

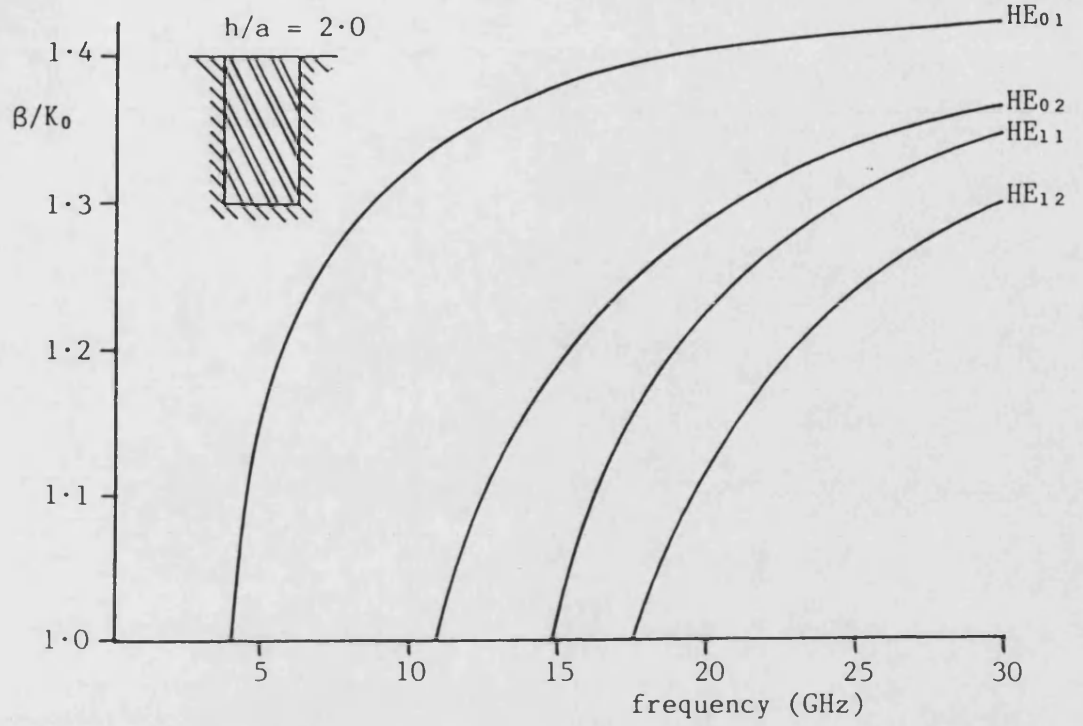

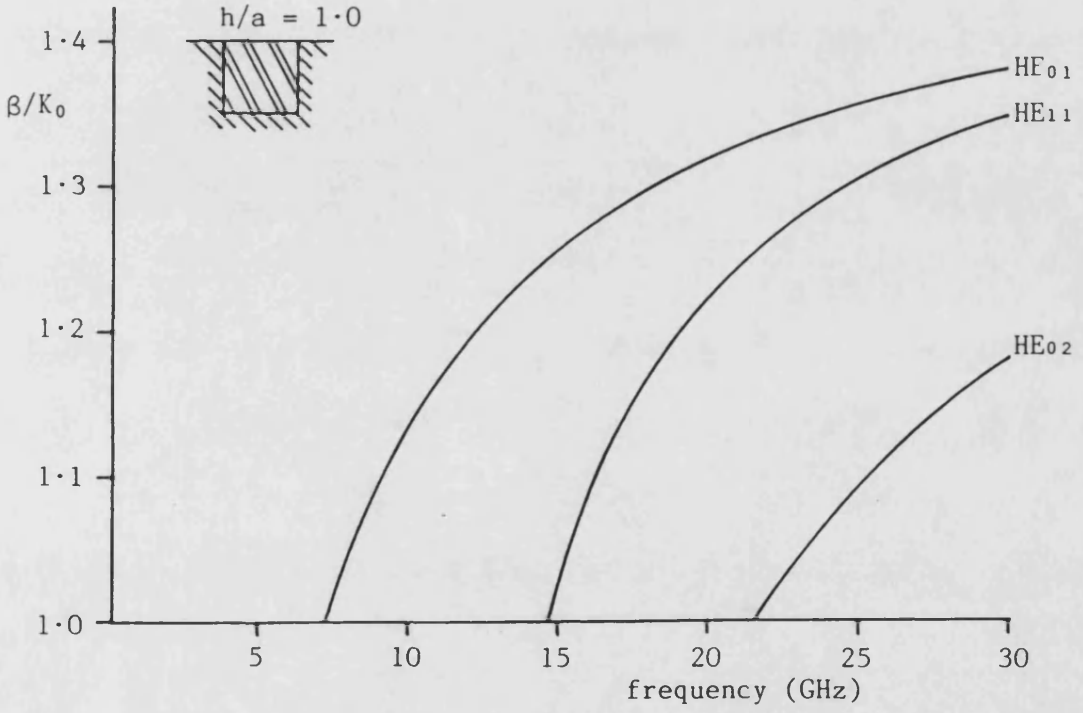

The computed dispersion curves for two samples of IDG, identical apart from the aspect ratios, with a =1·0cm, εr =2·0.

Figure 4-7

4-7 The Approximate Determination of Cutoff Frequencies

In the rigorous formulation of the dispersion equation, the field in the slot is constructed from a discrete set of components, each with an x-directed wavenumber kx = $(\frac{n\pi}{a})$ and an associated y-directed wavenumber kyn. An approximate value for the cutoff frequency of the higher order modes can be found from the cutoff frequency of the fundamental mode if the assumption is made that the slot field is composed of only one Fourier component. That is, the cutoff condition can be written as (since β = Ko)

$$(\varepsilon r - 1)\, kc^2 = kx^2 + ky^2 \qquad (4\text{-}7)$$

where kc is the cutoff wavenumber and kx and ky are the "effective" x and y-directed wavenumbers for a given mode.

The field variation across the slot, between the two perfectly conducting surfaces will be that of a standing wave, with kx = $(\frac{n\pi}{a})$. The value of ky gives rise to an electrical length in the slot of:

$$\theta = ky\, h \qquad (4\text{-}8)$$

This electrical length is found from the application of transverse resonance and is the length of short-circuited line required to provide an input admittance equal and opposite to the air admittance at the discontinuity. If the computed cutoff frequency of the HE_{01} mode for a particular guide is foc then from (4-7)

$$\theta = h\sqrt{\varepsilon r - 1}\ \frac{2\pi\, foc}{C} \qquad (4\text{-}9)$$

The input admittance for the line is a cotangent function. If the simplifying assumption is made that the frequency variation of this term is faster than that of the air region susceptance then to a

first order approximation the air region susceptance can be assumed constant. For resonance then, the slot electrical length will always be that of (4-9) within a factor of π. Thus for an HEnm or EHnm mode define:

$$kx = (\frac{n\pi}{a}),\ ky = \theta + (m - 1)\pi \qquad (4\text{-}10)$$

Given the cutoff frequency of the fundamental mode, then the cutoff frequency of a higher order mode can be found approximately from the application of (4-10) and (4-7). The cutoff frequencies of the higher order even modes of an X-band IDG sample with a = 1.016 cm, $h/a = 1.5$ and $\varepsilon r = 2.08$ were determined in this way and are given in Table 4.3. By comparison with the computed dispersion curves for the same guide given in Fig. 4-3, it can be seen that these values are useful over a moderate frequency range. The susceptance of the air region is assumed constant at all frequencies which of course it is not. Thus as the frequency increases, i.e. the order of the mode increases, the approximate value determined in this manner can be expected to become less accurate.

These approximate cutoff values can be used to aid the computation of the higher order mode solutions. The ability of the program for complex β to locate a solution is dependent upon the definition of the search area in the β plane. For large search areas the program speed can be severely reduced and so an approximate knowledge of the location of the solution which reduces the search area is useful.

		m			
		1	2	3	4
n	0	4.71	14.20	23.67	33.13
	2	28.79	31.75	36.99	43.63
	4	57.02	58.57	61.55	65.75
	6	85.37	86.41	88.46	91.45

The Approximate Cutoff Frequencies
of the EHnm modes
for a = 1.016 cm, $^{h}/_{a}$ = 1.5 ε_r= 2.08

Table 4-3

4.8 Computation of the Field Components

Having solved the dispersion equation (4-1) for β, the amplitude coefficients for the basis sets can be found by placing β into the admittance operators and solving:

$$\begin{bmatrix} \underline{X} \\ \underline{Z} \end{bmatrix} = \begin{bmatrix} \underline{\underline{Y}} \end{bmatrix}^{-1} \cdot \begin{bmatrix} \underline{P_0} \\ \underline{o} \end{bmatrix} \qquad (4\text{-}11)$$

The amplitude coefficients for the field amplitudes Exn etc can then be evaluated enabling the field components given by (3-11) and (3-26) to be calculated. The derivation of the amplitude coefficients for each region is given in Appendix III, and for convenience the results are summarised in Table 4.4.

The dispersion equation was solved for the X-band IDG (a = 1.016 cm, h/a = 1.5, εr = 2.08) for a frequency of 30 GHz. From Figure 4-3, which gives the dispersion curves for this guide it can be seen that at 30 GHz four propagating modes are possible. Indeed four solutions are found for the dispersion equation. These along with the amplitude coefficients calculated from (4-11) are given in Table 4.5. It is noted that, as expected, there is a 90^{o} phase shift between the TE ($\underline{X}$) and TM ($\underline{Z}$) components. The amplitude coefficients are normalised to X_0.

The field equations (3-11) and (3-26) for each of the four solutions are shown plotted as the magnitude over the transverse guide cross section in Figures 4.8 to 4.11. The isometric plots are shown for two different projections for each set of field components. It should be noted that each plot has been individually scaled by the computer plotting routine and so there is no amplitude correlation between the various plots.

$$Exn = \underline{X}^T \cdot \underline{Pn}$$

$$Eyn = \frac{-\cot\sqrt{U^2 - n^2}(\pi h/a)}{\sqrt{U^2 - n^2}} \left(n\,\underline{X}^T \cdot \underline{Pn} + j(a/n\pi)\beta\,\underline{Z}^T \cdot \underline{Pn} \right)$$

$$Ezn = (1/n)\,\underline{Z}^T \cdot \underline{Pn}$$

$$Hxn = \frac{n\cot\sqrt{U^2 - n^2}(\pi h/a)}{\sqrt{U^2 - n^2}} \left(\frac{-(a/\pi)\beta}{U}\,\underline{X}^T \cdot \underline{Pn} + \frac{1}{jU}\left(\frac{U^2 + \overline{\beta}^2 - n^2}{n^2} \right) \underline{Z}^T \cdot \underline{Pn} \right)$$

$$Hyn = \frac{1}{jU} \left(j\beta(a/\pi)\,\underline{X}^T \cdot \underline{Pn} + \underline{Z}^T \cdot \underline{Pn} \right)$$

$$Hzn = \frac{\cot\sqrt{U^2 - n^2}(\pi h/a)}{\sqrt{U^2 - n^2}} \left(-jU\,\underline{X}^T \cdot \underline{Pn} + \frac{(a/\pi)\beta}{U}\,\underline{Z}^T \cdot \underline{Pn} \right)$$

$$ex(\rho) = \underline{X}^T \cdot \underline{P}(\rho)$$

$$ey(\rho) = \frac{-1}{j\,Ky(\rho)} \left(\rho\,\underline{X}^T \cdot \underline{P}(\rho) + j\beta(\pi/a\rho)\,\underline{Z}^T \cdot \underline{P}(\rho) \right)$$

$$ez(\rho) = (\pi/a\rho)\,\underline{Z}^T \cdot \underline{P}(\rho)$$

$$hx(\rho) = \frac{1}{U\,Ky(\rho)} \left(-j(a/\pi)\beta\,\underline{X}^T \cdot \underline{P}(\rho) + \left(\frac{Ko^2 - \rho^2}{\rho^2} \right) \underline{Z}^T \cdot \underline{P}(\rho) \right)$$

$$hy(\rho) = \frac{1}{jU} \left(j(a/\pi)\beta\,\underline{X}^T \cdot \underline{P}(\rho) + \underline{Z}^T \cdot \underline{P}(\rho) \right)$$

$$hz(\rho) = \frac{-1}{U\,Ky(\rho)} \left((a/\pi)(Ko^2 - \beta^2)\,\underline{X}^T \cdot \underline{P}(\rho) + j\beta\,\underline{Z}^T \cdot \underline{P}(\rho) \right)$$

The amplitude coefficients obtained for the slot and air field components (The magnetic components are normalised to Yoo")

Table 4-4

β = 8·877392 (rad/cm) X_0 = 1·000000 j0·000000 X_2 = -0·200432 j0·000000 X_4 = -0·049328 j0·000000 Z_0 = 0·000000 j0·000000 Z_2 = 0·000000 j0·072169 Z_4 = 0·000000 j0·060709
β = 8·286919 (rad/cm) X_0 = 1·000000 j0·000000 X_2 = -0·190990 j0·000000 X_4 = -0·049910 j0·000000 Z_0 = 0·000000 j0·000000 Z_2 = 0·000000 j0·087351 Z_4 = 0·000000 j0·058391
β = 7·238387 (rad/cm) X_0 = 1·000000 j0·000000 X_2 = -0·159321 j0·000000 X_4 = -0·053189 j0·000000 Z_0 = 0·000000 j0·000000 Z_2 = 0·000000 j0·149733 Z_4 = 0·000000 j0·042879
β = 6·386717 (rad/cm) X_0 = 1·000000 j0·000000 X_2 = 7·088640 -j0·000937 X_4 = -3·238700 j0·000041 Z_0 = 0·000000 j0·000000 Z_2 = 0·001767 j13·948428 Z_4 = -0·000736 -j5·700577

The values of propagation constant and normalised basis amplitude terms obtained by solving the dispersion equation for:

a = 1·016cm, h = 1·524cm, ε_r = 2·08 - j0·000416, f = 30 GHz

Table 4-5

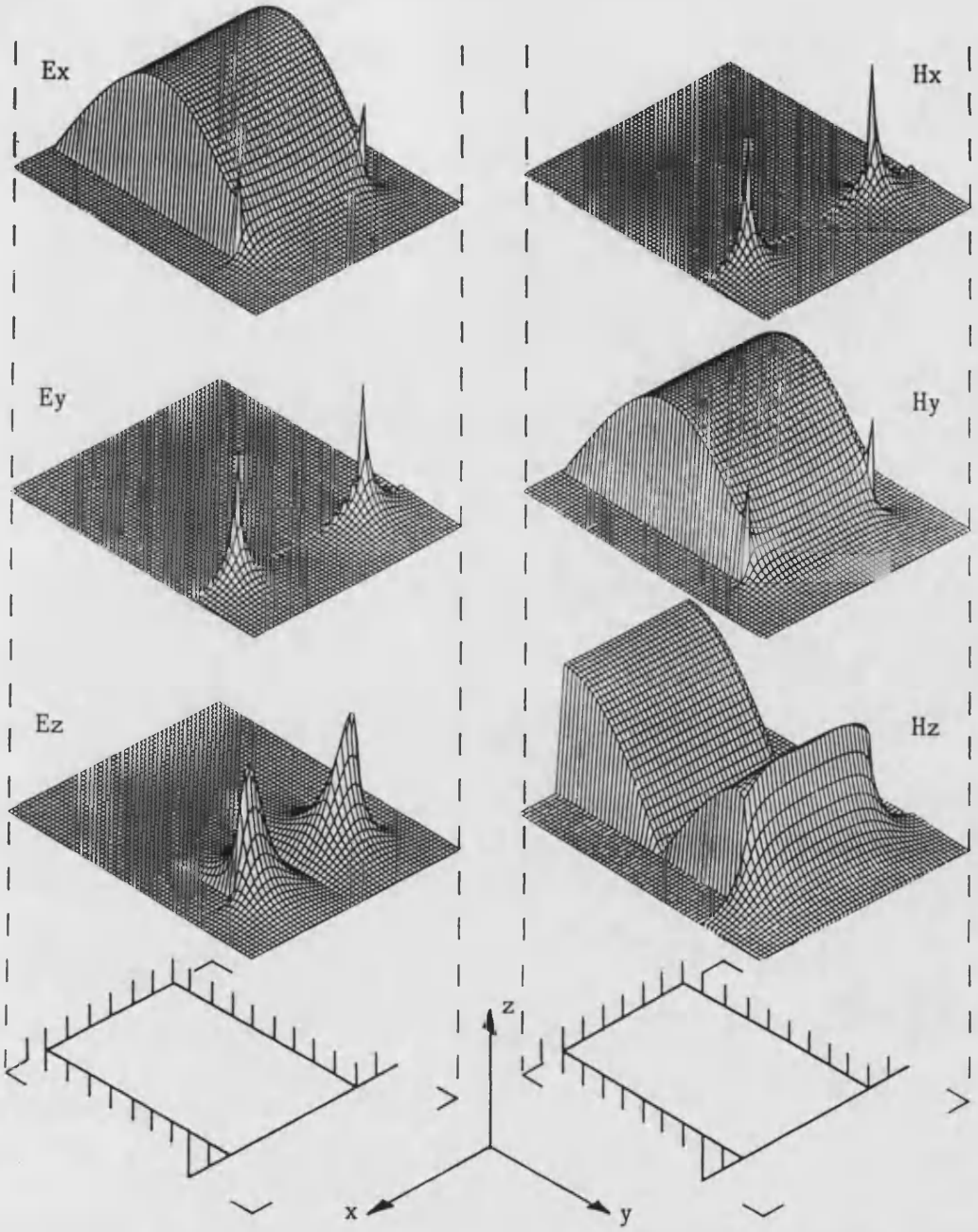

The field components of the fundamental HE_{01} mode, plotted as the magnitude values over the transverse guide section.

Figure 4-8(a)

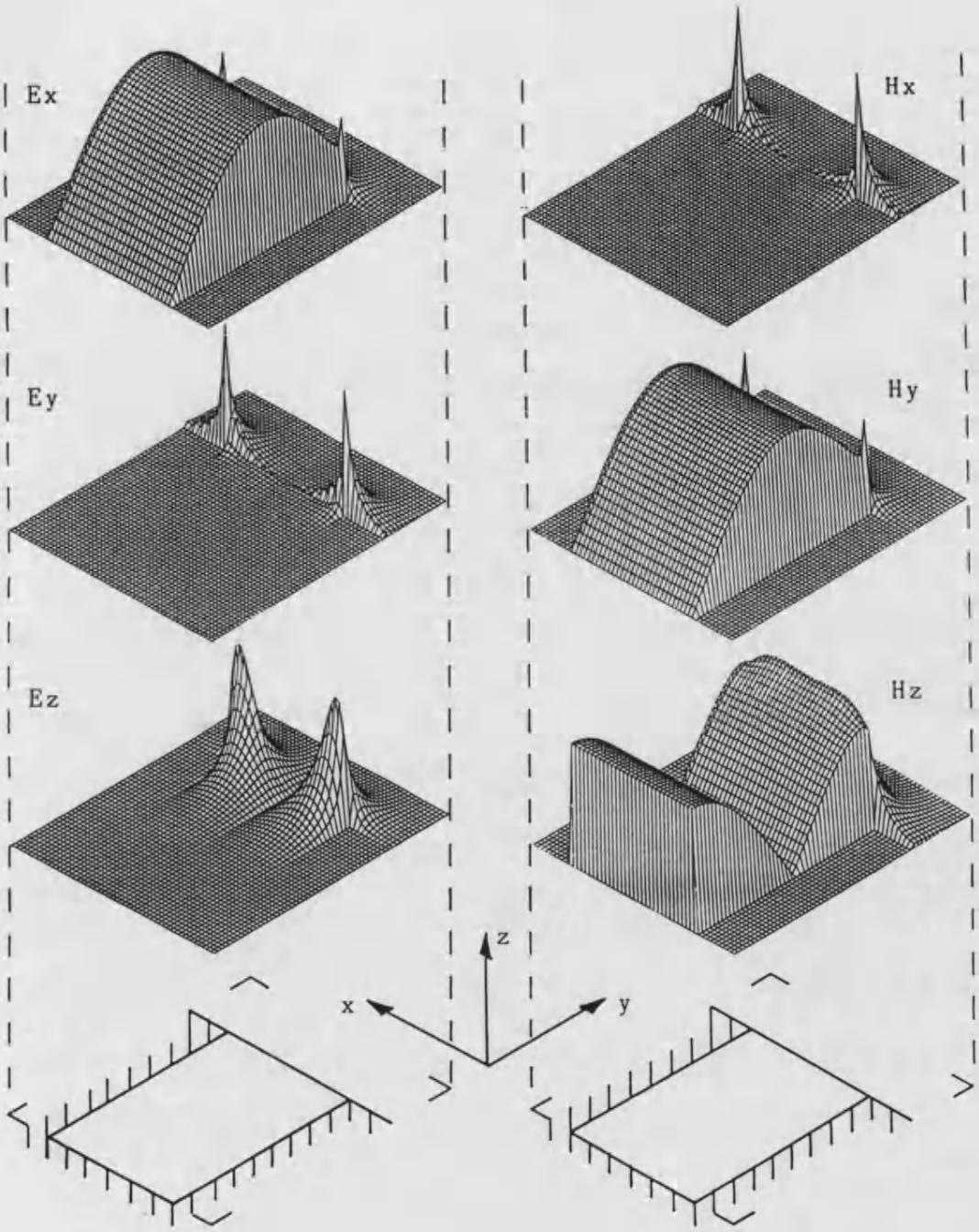

The field components of the fundamental HE_{01} mode, plotted as the magnitude values over the transverse guide section.

Figure 4-8(b)

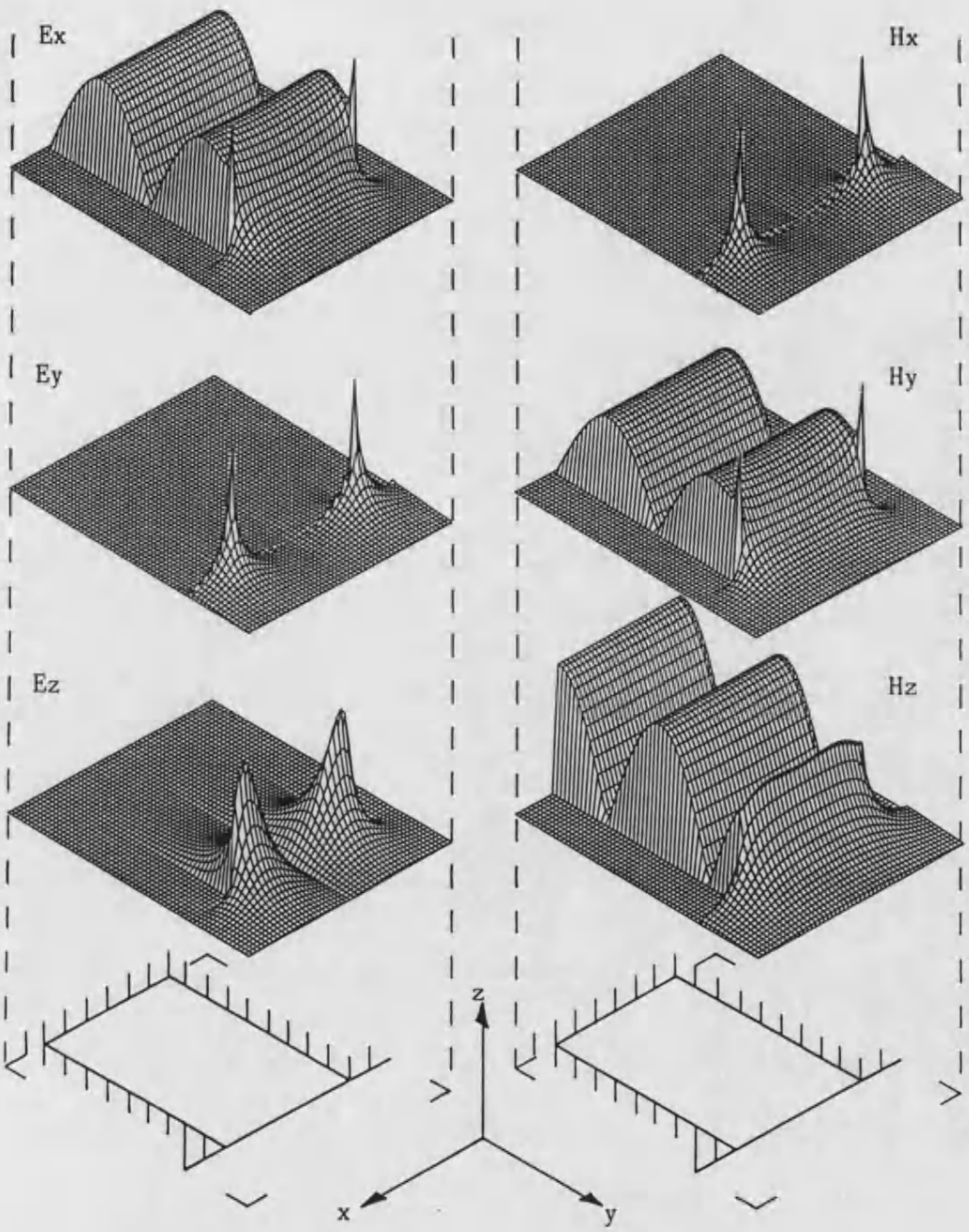

The field components of the HE_{02} mode, plotted as magnitude values over the transverse guide section.

Figure 4-9(a)

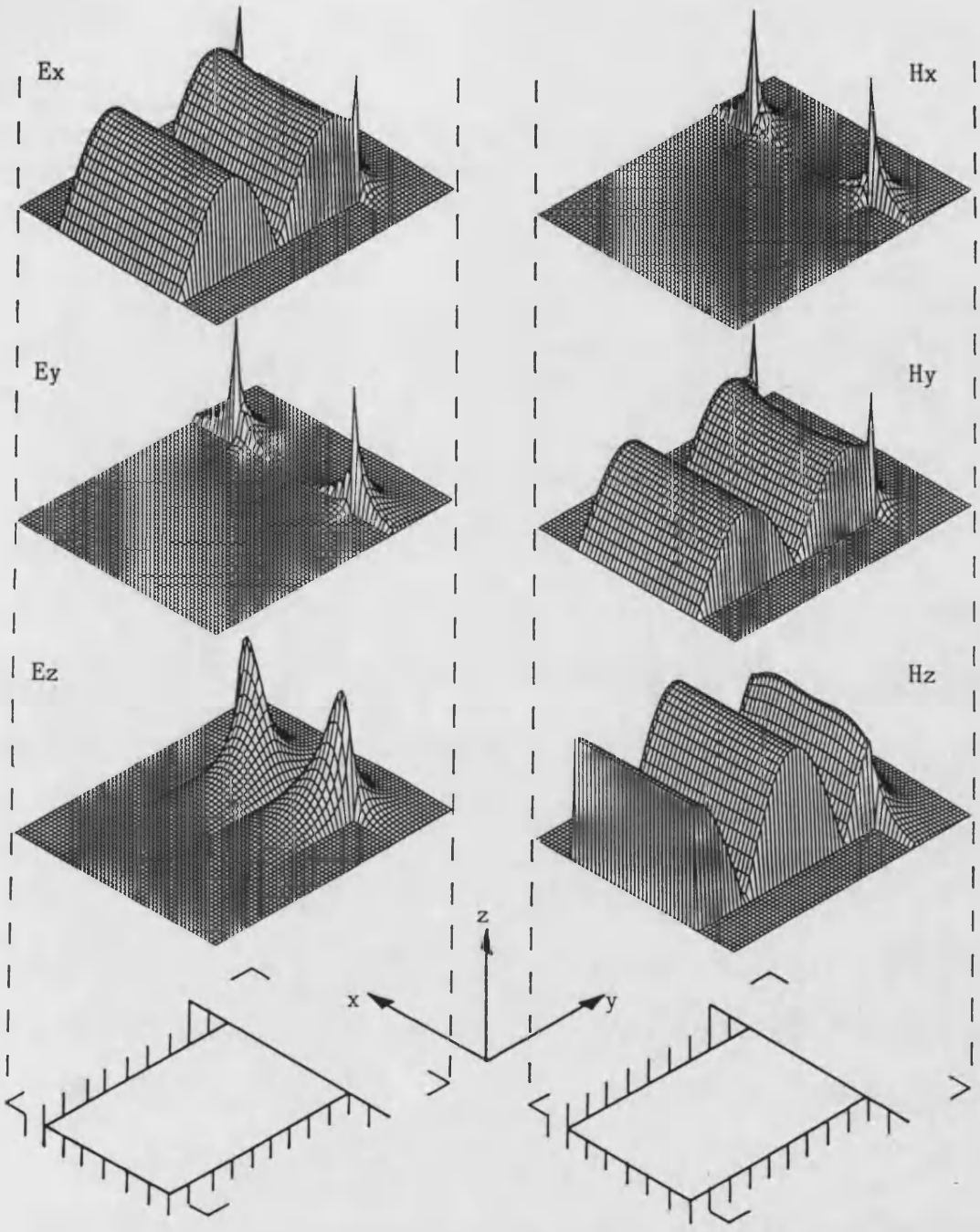

The field components of the HE_{02} mode, plotted as magnitude values over the transverse guide section.

Figure 4-9(b)

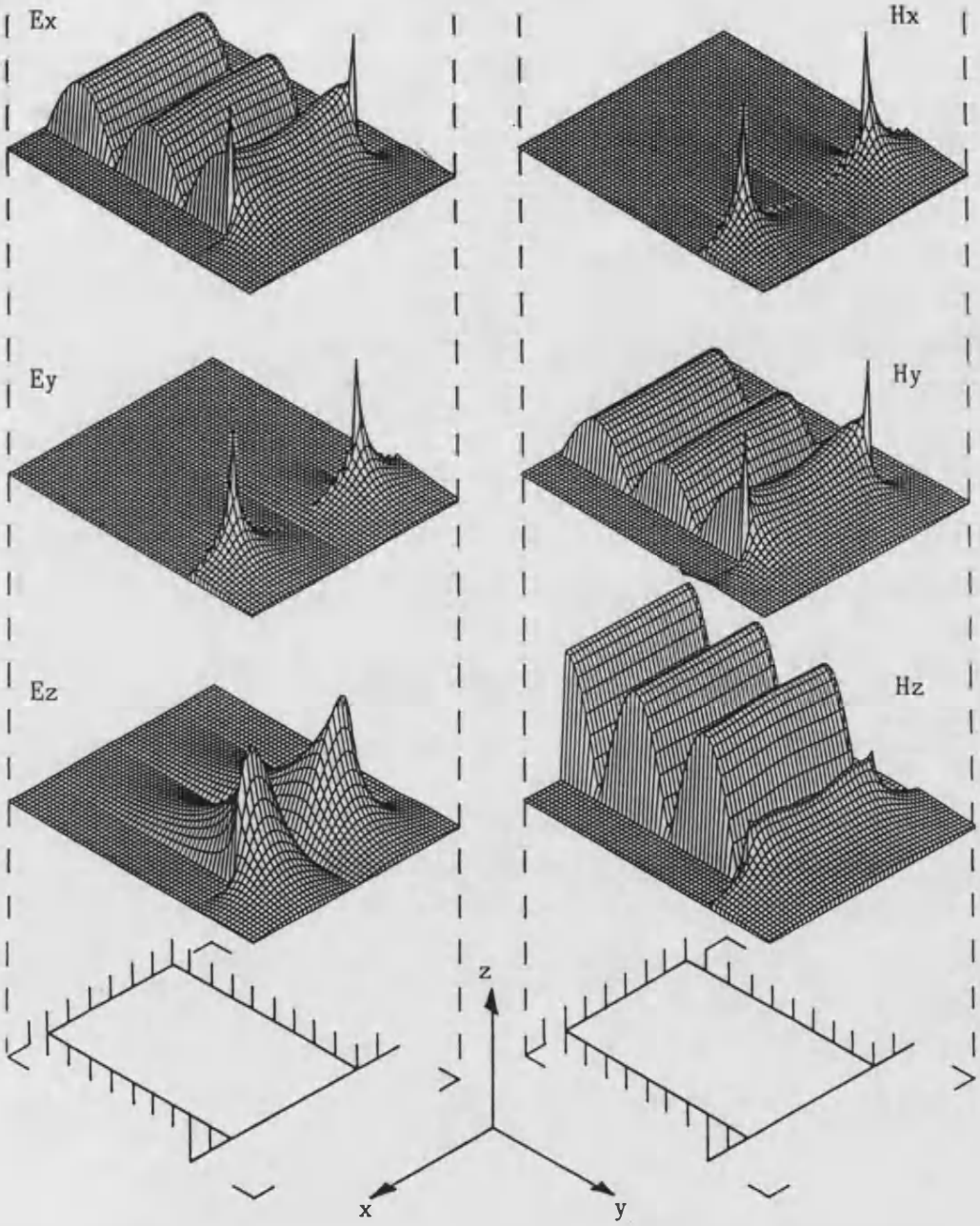

The field components of the HE_{03} mode, plotted as magnitude values over the transverse guide section.

Figure 4-10(a)

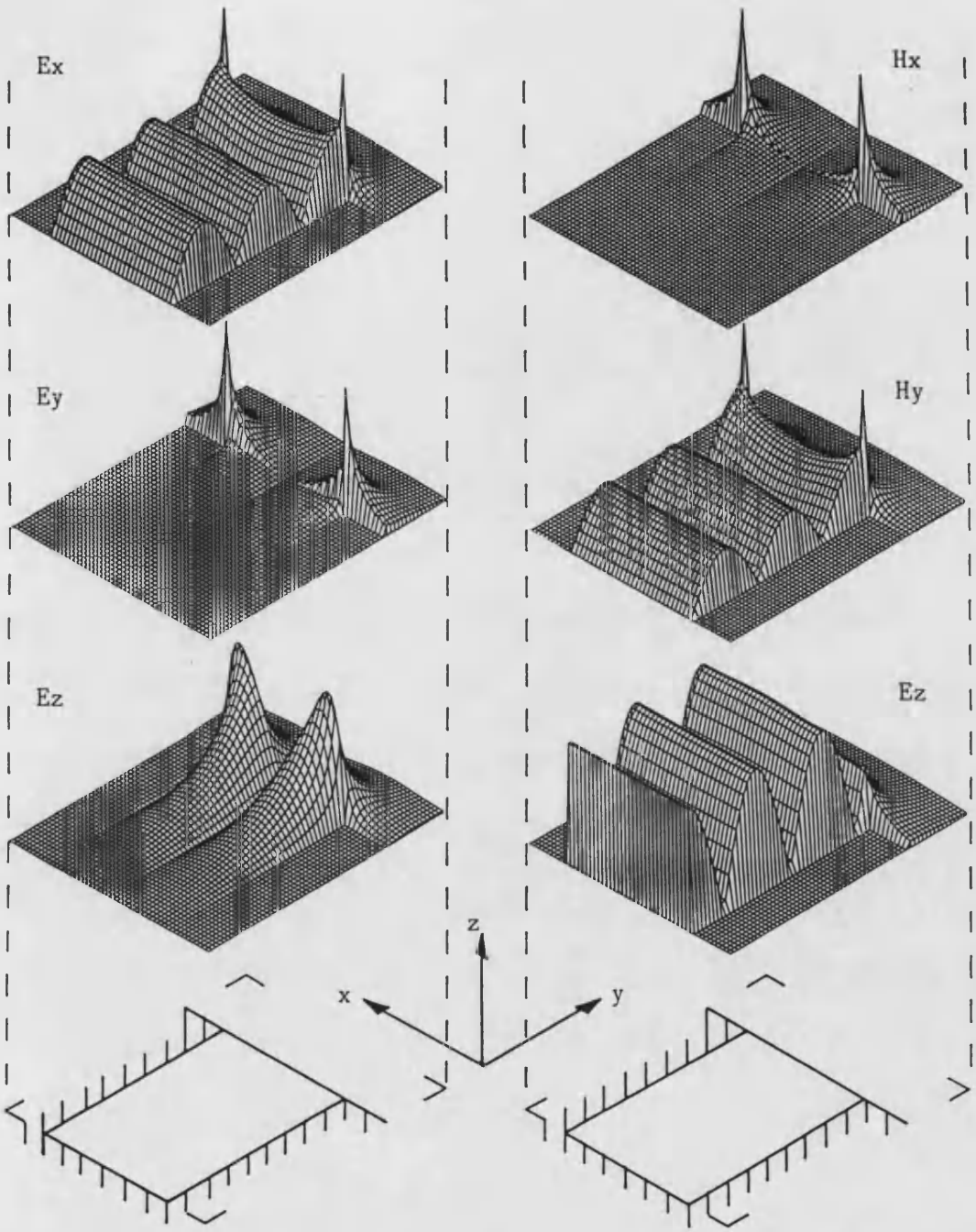

The field components of the HE_{03} mode, plotted as magnitude values over the transverse guide section.

Figure 4-10(b)

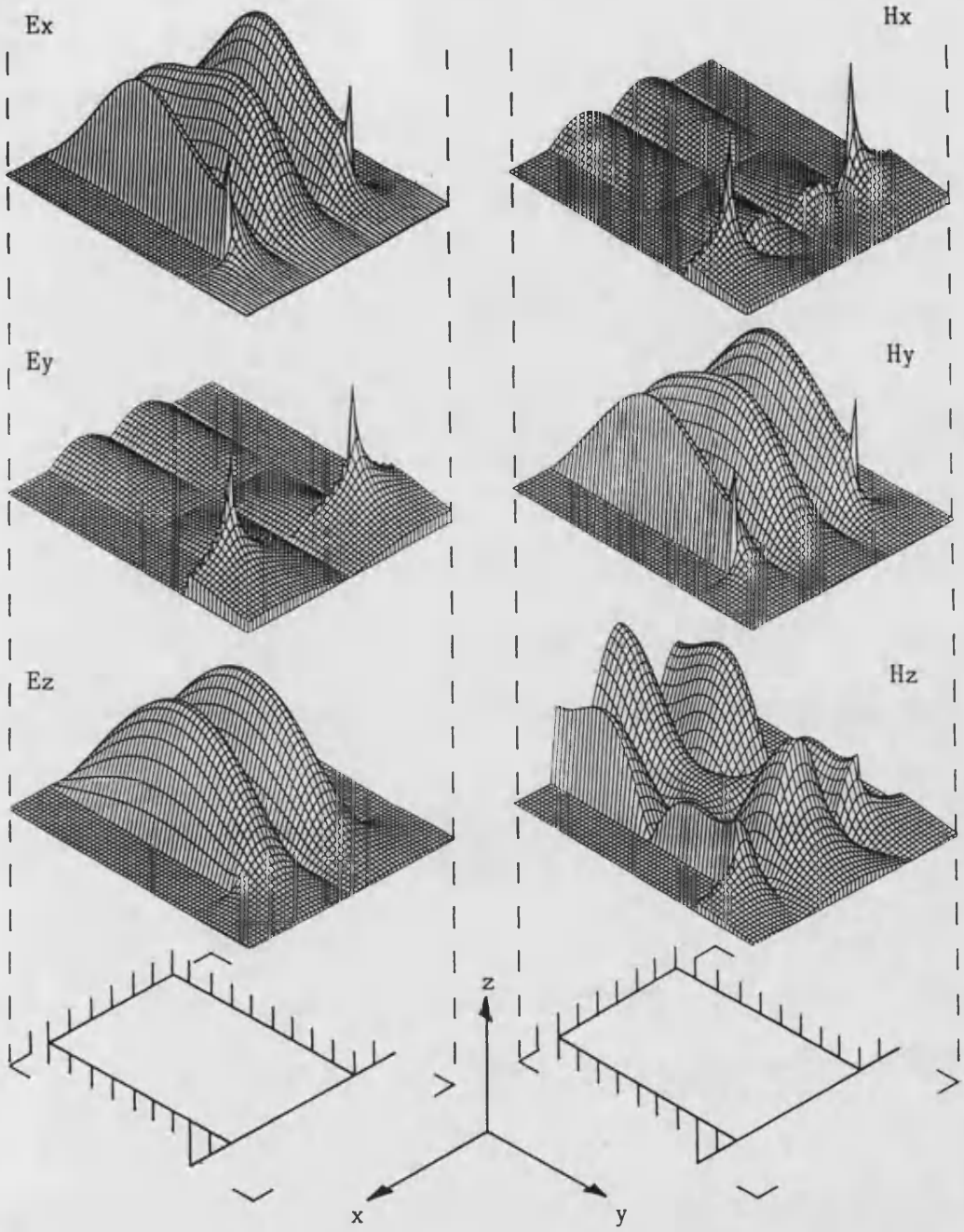

The field components of the HE_{21} mode, plotted as magnitude values over the transverse guide section.

Figure 4-11(a)

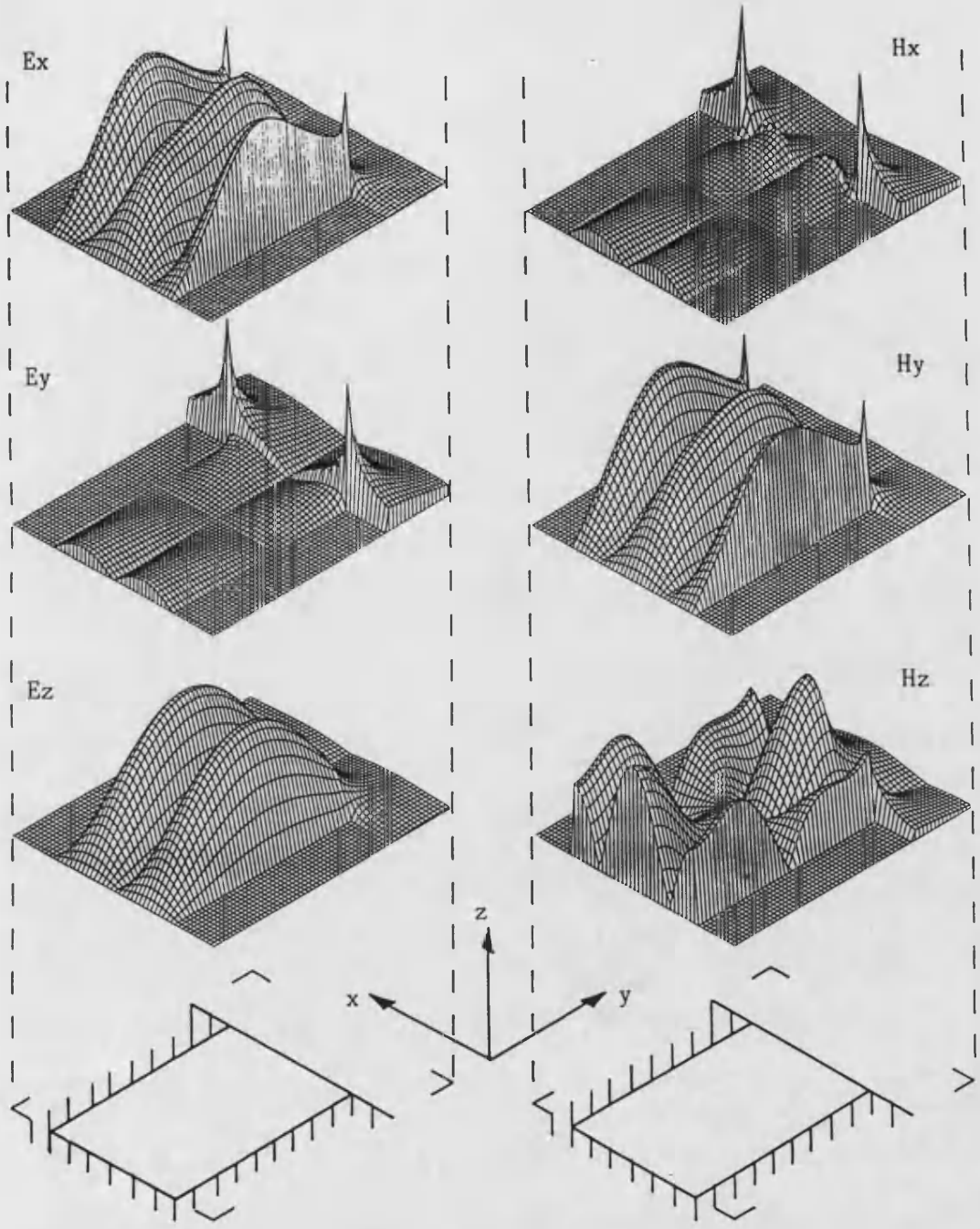

The field components of the HE_{21} mode, plotted as magnitude values over the transverse guide section.

Figure 4-11(b)

When plotting these fields the discontinuity must be taken into account. Problems can arise because one set of basis terms has been used to derive the fields in two regions that have different boundary conditions. This problem has been discussed by Lewin [4]. To illustrate the problem consider as an example the Ey field component. In the slot assuming perfect conductors Ey must vanish at the walls ($x = \pm a/2$). Thus the potential functions $\phi en(x)$ are chosen to satisfy this requirement. In the air region the presence of the ground plane means that Ey can be finite everywhere. At the plane of the discontinuity the edge condition require that Ey be a maximum at the edge. This condition cannot be satisfied by any superposition of the $\phi en(x)$ and so the field distribution at $y = o$ obtained by using them will be inaccurate. Thus, the field expansion in terms of slot modes is only strictly correct for $y \leq o^-$ and the expansion in terms of our modes, for $y \geq o^+$. At $y = o$ the field expansion must be chosen that can best model the singular behaviour.

The field plots clearly show the hybrid nature of the modes. It is noted that in the slot the dominant field components are those associated with TE wrt y behaviour, i.e. Ex, Hy and Hz. The other three field components are only excited in the vicinity of the interface, in order to satisfy the boundary conditions imposed by the singularity. The concentration of the fields at the edge by the discontinuity can be clearly seen in the transverse field components. As expected the z-directed field components which do not "see" the discontinuity show no singular behaviour.

4.9 The Partially Filled Slot

The amplitude coefficients and field expressions can be found for the partially filled slot case in much the same way as for the filled slot. In order to accentuate the difference, a guide was analysed with $a = 1.016$ cm, $h/a = 1.5$ and a dielectric depth of $a/2$ of $\varepsilon r = 4.0$.

The computed data for a frequency of 14 GHz is giv
the associated field plots are given in Fig. 4-12.

The effect of lowering the dielectric in the slot
field and hence reduce the significance of the dis
components are very small. In fact the Ez field c
negligible within the accuracy of the computer pro

Frequency = 14 GHz

β = 4·05644 (rad/cm) β/Ko = 1·382

X_0 = 1·000000 j0·000000
X_2 = -0·141860 j0·000000
X_4 = -0·016720 j0·000000

Z_0 = 0·000000 j0·000000
Z_2 = 0·000000 j0·000000
Z_4 = 0·000000 j0·000000

a = 1·016cm h/a = 1·5

dielectric depth = a/2, ε_r = 4·0

The computed values and parameters for a sample of partially filled IDG.(used for the field plots of figure 4-12)

Table 4-6

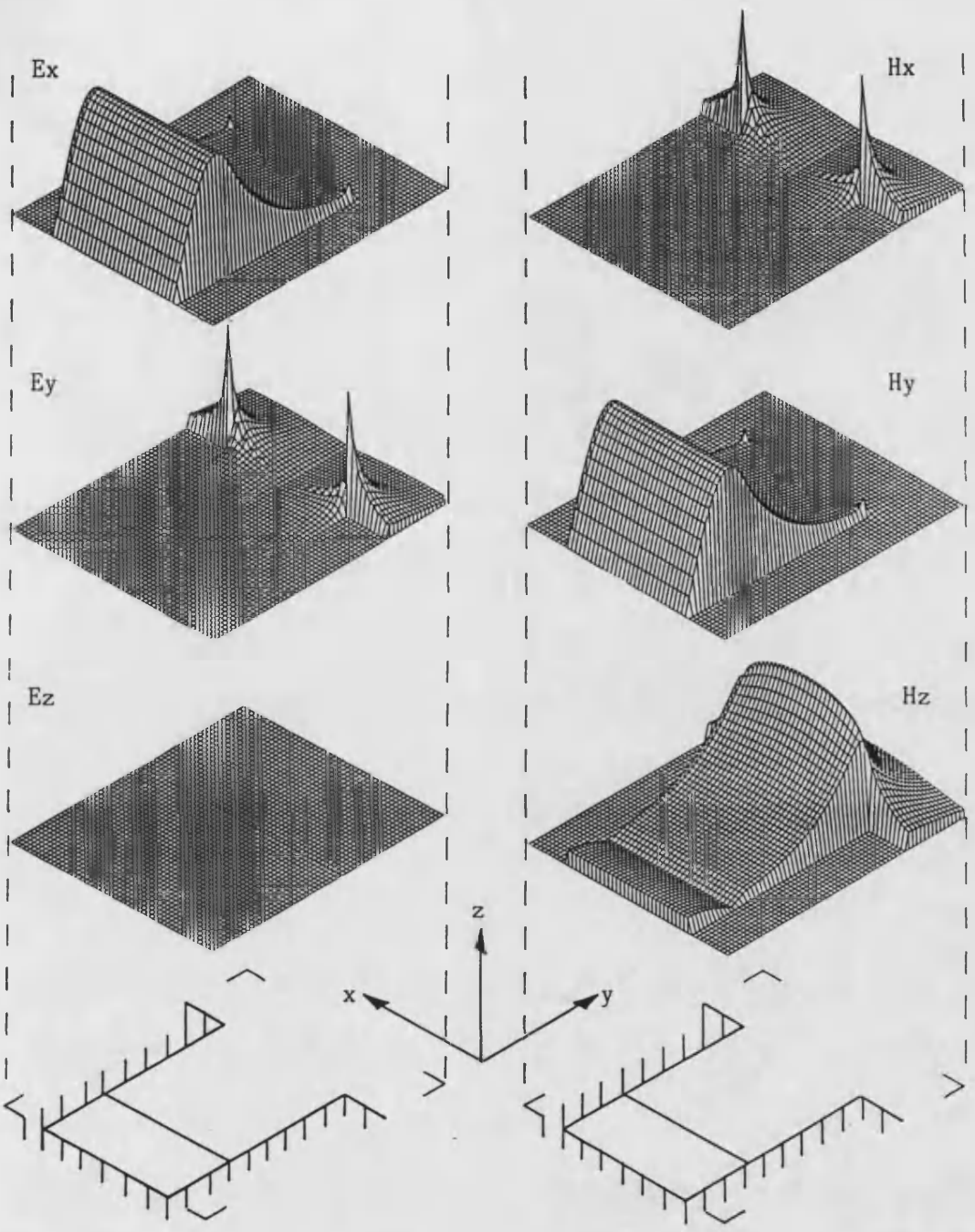

The field components for the HE_{01} mode, plotted as magnitude values over the transverse guide section for the partially filled slot case.

Figure 4-12

4-10 Comparison with Measured Results

In order to assess the accuracy of the computed results comparison with measured results was necessary. For ease of measurement and availability of equipment most of the measurements were carried out at X-band (8 - 12.4 GHz) although one sample was measured at Q-band (26 - 40GHz).

The initial test pieces were provided by Marconi Research Laboratories and consisted of brass pieces into which slots had been machined. A drawing of one of the pieces as supplied is given in Fig. 4.13. In order to facilitate the transition from rectangular waveguide to IDG the slots were kept at the standard rectangular waveguide width (1.016 cm at X-band). Two slot depths were supplied with the depth equal to the width and with the depth one and a half times the width. The dielectric inserts for these slots were machined from P.T.F.E. The square section dielectric insert could be placed in the deeper slot to form a partially filled slot and so three different IDG geometries could thus be measured. At Bath University several of the supplied blanks were machined with the deeper slot ($a = 1.016$ cm, $h/a = 1.5$) so that by bolting several sections together longer lengths of IDG could be obtained. The pieces were also drilled and tapped to allow rectangular waveguide to be connected directly to them. A discussion of the rectangular waveguide to IDG transition used is given in the next chapter. A section of IDG with $a = 3.556$ mm, $h/a = 1.5$ and with P.T.F.E. filling was also made for measurement at Q-band.

The dispersion characteristics of the IDG samples were measured by using the resonant section technique. If a section of transmission line is terminated at each end with an iris (or some other coupling mechanism) such that the coupling is very weak (say 20 dB transmission

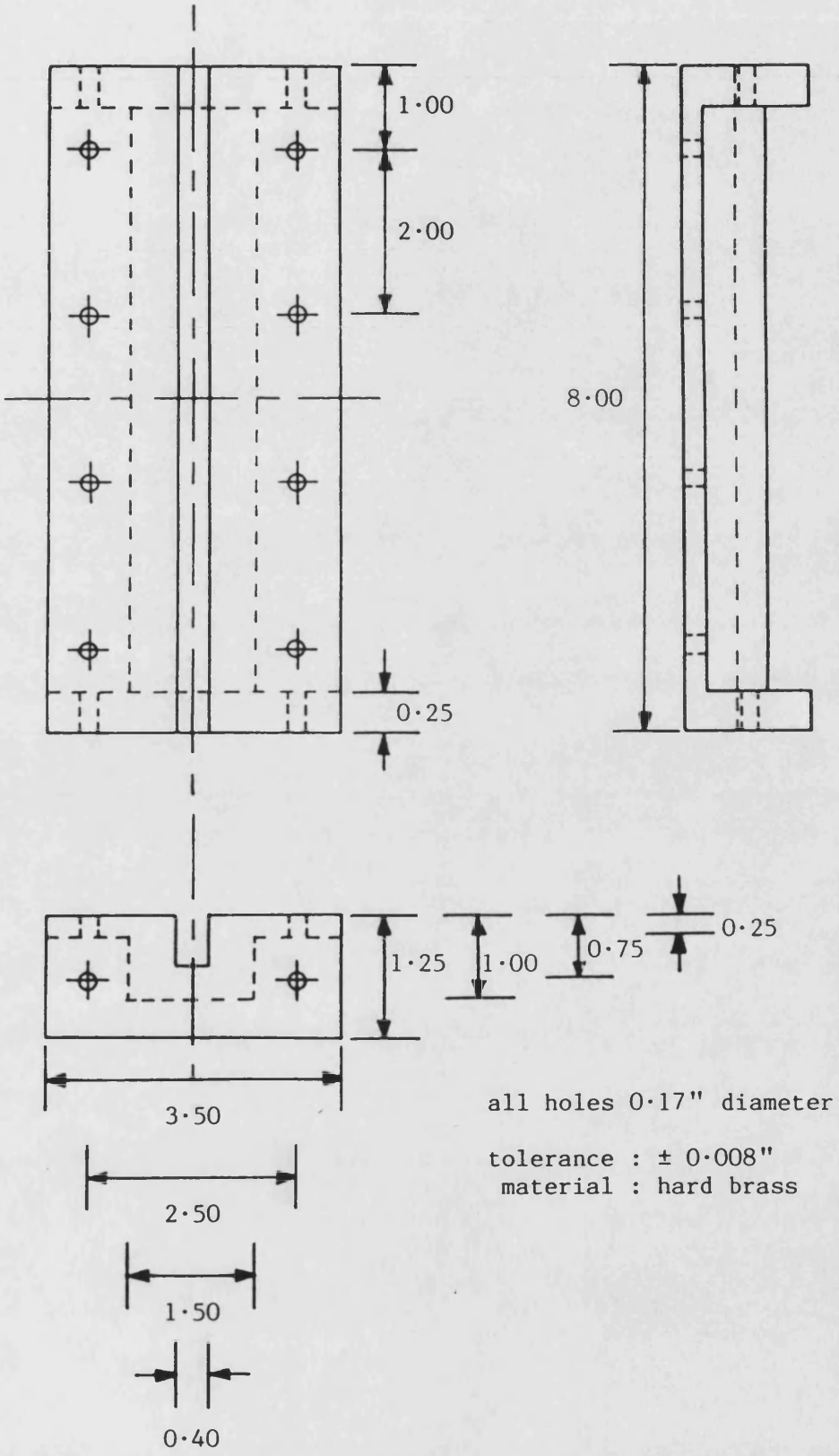

The X-band test pieces as supplied by Marconi Research Laboratories.

Figure 4-13

loss through each iris), then the section will virtually be short-circuited at each end. This structure will thus only support standing waves that have "zero" electric field at each end. This limits the fields in the section to those that satisfy

$$\frac{n\lambda g}{2} = L \qquad (4\text{-}12)$$

where λg = guided wavelength

n = integer

L = length of resonant section

Thus only discrete frequencies, corresponding to guided wavelengths that satisfy (4-12) will be able to propagate unattenuated through the section. The swept frequency transmission response of a single section of IDG excited by weak coupling at each end is shown in Fig. 4-14. The centre frequency of each resonant peak could thus be measured enabling λg of each resonant frequency to be determined. In order to determine the guided wavelength λg for each frequency the integer n in (4-12) had to be evaluated. This was carried out by tuning the source to a resonant frequency and measuring the guide wavelength with a field probe. Due to imperfect coupling and field fringing effects the value of λg will not give an integer value of n in (4-12) but will be close to one. Since successive resonant frequencies must correspond to successive values of n, the guide wavelength can be measured for several resonant frequencies to determine n correctly. Having determined λg correctly the guide dispersion β/k_0 can be calculated as $\lambda_0/\lambda g$.

This method is capable of measuring the dispersion characteristic correctly as long as the guide only supports a single propagating mode. Table 4.5 gives the measured dispersion results for three

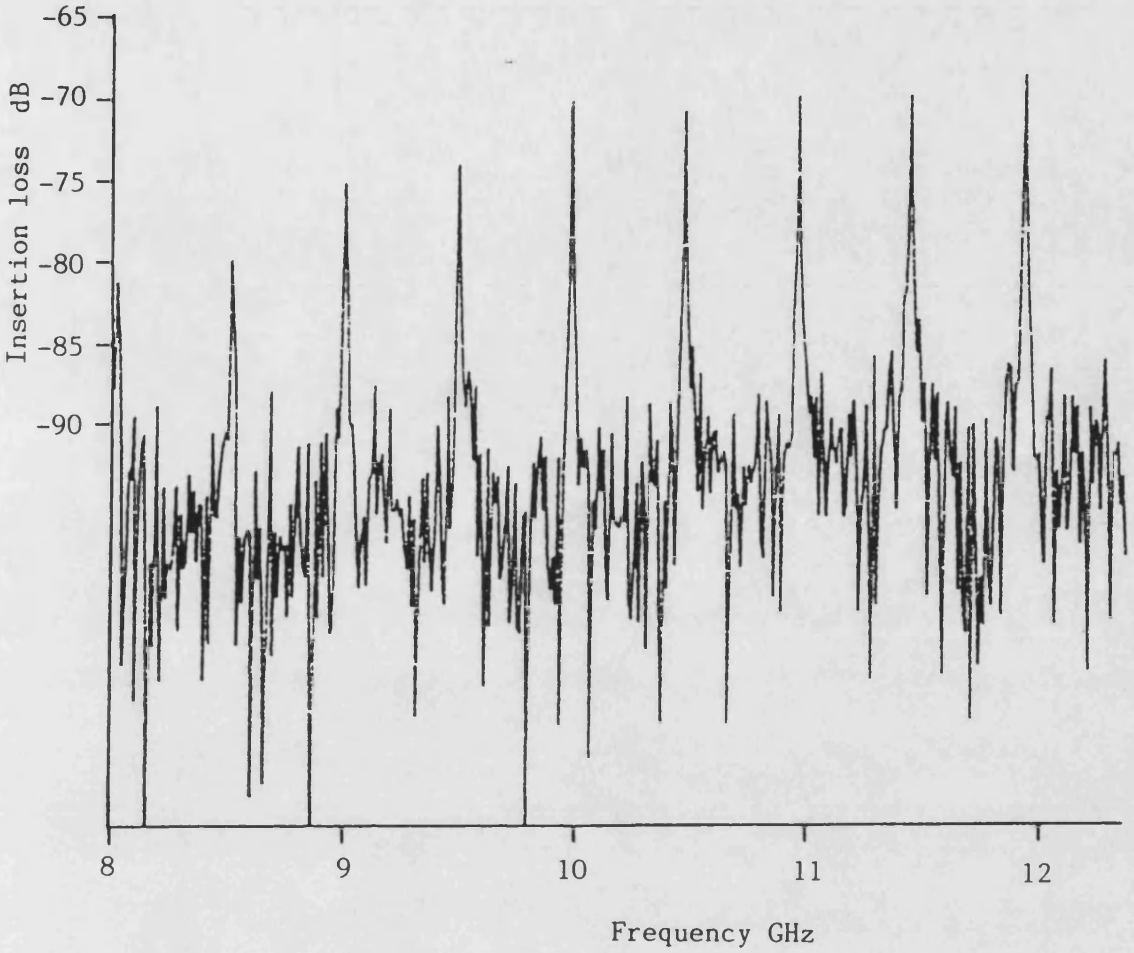

The measured insertion loss of a resonant section of IDG used to determine the dispersion characteristics (measured on a HP8510A network analyser).

Figure 4-14

fo(GHz)	Ko(rad/cm)	λo (cm)	λg (cm)	λo / λg
6·51	1·36	4·603	4·064	1·132
7·01	1·47	4·275	3·695	1·157
7·51	1·57	3·995	3·387	1·180
7·99	1·68	3·751	3·126	1·201
8·48	1·78	3·535	2·903	1·218
8·98	1·88	3·340	2·709	1·233
9·47	1·99	3·165	2·540	1·246
9·96	2·09	3·010	2·391	1·259
10·46	2·19	2·867	2·258	1·270
10·96	2·29	2·737	2·139	1·279
11·45	2·40	2·618	2·032	1·289
11·94	2·50	2·510	1·935	1·297
12·44	2·60	2·410	1·847	1·305
12·93	2·71	2·318	1·767	1·312

(a)

fo(GHz)	Ko(rad/cm)	λo (cm)	λg (cm)	λo / λg
7·84	1·64	3·824	3·695	1·035
8·39	1·76	3·573	3·387	1·055
8·93	1·87	3·359	3·126	1·075
9·45	1·98	3·173	2·903	1·093
9·96	2·09	3·009	2·709	1·110
10·48	2·19	2·861	2·540	1·126
10·98	2·30	2·730	2·391	1·142
11·49	2·41	2·610	2·258	1·156
11·98	2·51	2·503	2·139	1·170
12·48	2·61	2·402	2·032	1·182
12·97	2·72	2·312	1·935	1·194
13·46	2·82	2·229	1·847	1·206
13·95	2·92	2·150	1·767	1·217

(b)

fo(GHz)	Ko(rad/cm)	λo (cm)	λg (cm)	λo / λg
7·32	1·53	4·098	4·064	1·009
7·83	1·64	3·831	3·695	1·037
8·33	1·74	3·598	3·387	1·062
8·83	1·85	3·394	3·126	1·086
9·34	1·96	3·212	2·903	1·106
9·83	2·06	3·049	2·709	1·125
10·33	2·16	2·902	2·540	1·143
10·83	2·27	2·770	2·391	1·159
11·32	2·37	2·648	2·258	1·173
11·81	2·47	2·538	2·139	1·187
12·31	2·58	2·436	2·032	1·199
12·80	2·68	2·342	1·935	1·210

(c)

The measured dispersion values for the three X-band IDG geometries.

Table 4-7

IDG geometries. In each case the resonant length was 20.32 cm long with

a) $a = 1.016$ cm $h/a = 1.5$ dielectric depth = h

b) $a = 1.016$ cm $h/a = 1.5$ dielectric depth = a

c) $a = 1.016$ cm $h/a = 1.0$ dielectric depth = a = h

In Table 4.6 the measured results for the Q-band sample are presented. The graphical comparison of these results with the computed values is given in Figs. 4-15 and 4-16.

fo(GHz)	Ko(rad/cm)	λo (cm)	λg (cm)	λo / λg
26.89	5·63	1·115	0·898	1.242
27·23	5·71	1·101	0·885	1.244
27·55	5·78	1·088	0·872	1·248
27·88	5·85	1·075	0·860	1·250
28·21	5·91	1·063	0·848	1·254
28·54	5·98	1·050	0·836	1·257
28·87	6·05	1·039	0·825	1·259
29·20	6·12	1·027	0·814	1·262
29·53	6·19	1·015	0·803	1·264
29·86	6·26	1·004	0·793	1·266
30·19	6·33	0·993	0·782	1·270
30·52	6·40	0·982	0·773	1·270
30·85	6·46	0·972	0·763	1·274
31·19	6·54	0·961	0·753	1·276
31·52	6·61	0·951	0·744	1·278
31·84	6·68	0·941	0·735	1·280
32·18	6·74	0·932	0·727	1·282
32·51	6·82	0·922	0·718	1·284
32·84	6·88	0·913	0·710	1·286
33·16	6·95	0·904	0·702	1·288
33·50	7·02	0·895	0·694	1·290
33·83	7·09	0·886	0·686	1·292
34·17	7·16	0·877	0·678	1·294
34·50	7·23	0·869	0·671	1·295
34·82	7·30	0·861	0·663	1·299
35·16	7·37	0·853	0·656	1·300
35·49	7·44	0·845	0·649	1·302
35·83	7·51	0·837	0·642	1·304
36·16	7·58	0·829	0·636	1·303
36·48	7·64	0·822	0·629	1·307
36·81	7·72	0·814	0·623	1·307
37·15	7·79	0·807	0·617	1·308
37·49	7·86	0·799	0·610	1·310
37·82	7·92	0·793	0·604	1·313
38·15	7·99	0·786	0·598	1·314
38·47	8·07	0·779	0·593	1·314
38·80	8·13	0·773	0·587	1·317
39·12	8·20	0·766	0·581	1·318
39·47	8·27	0·760	0·576	1·319
39·81	8·34	0·753	0·570	1·321

IDG cross section : 3·556mm x 5·334mm

dielectric : P.T.F.E.

Length of resonant section : 30·52cm

The measured dispersion values for the Q-band sample of IDG.

Table 4-8

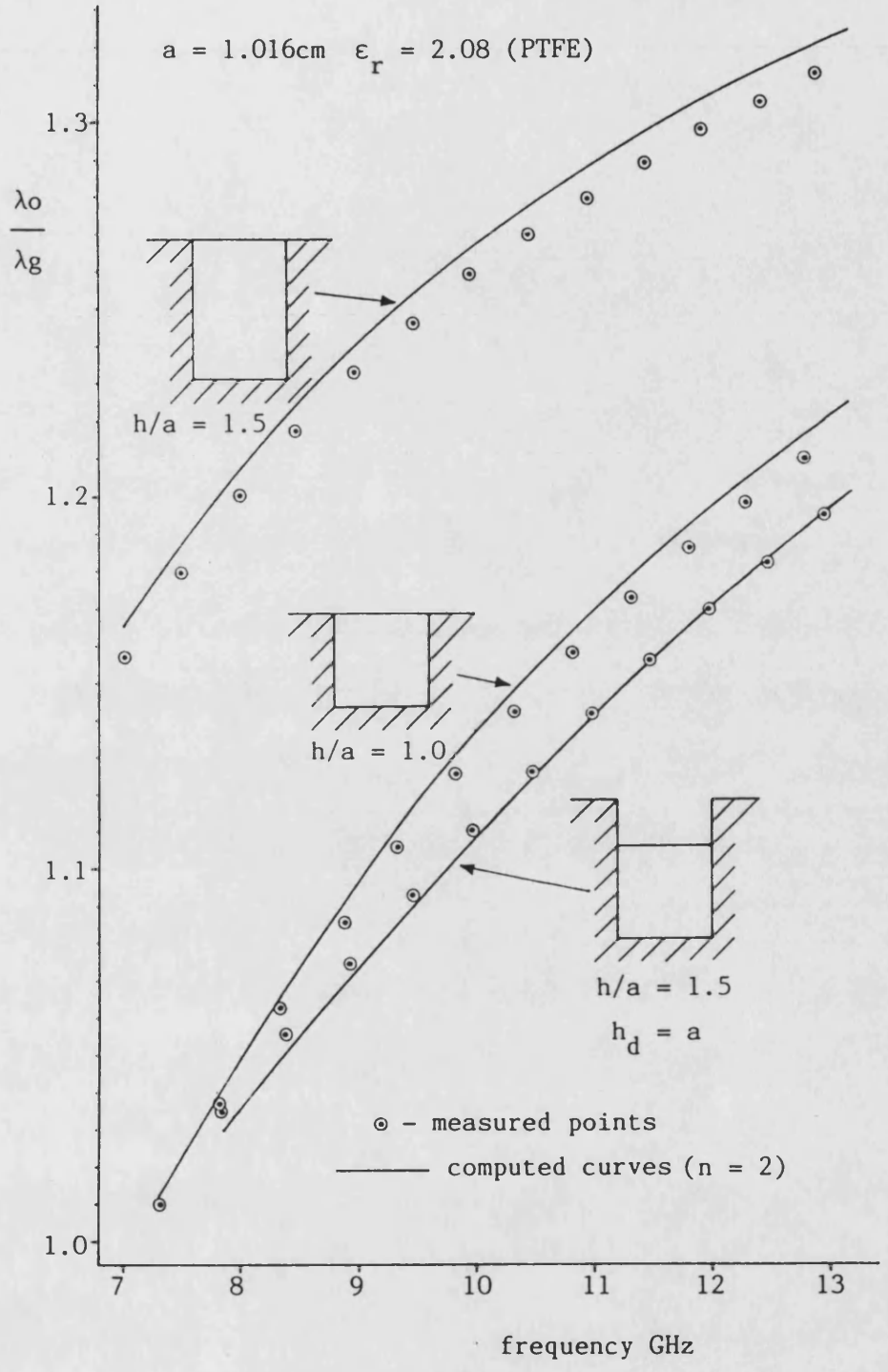

The comparison between the measured and computed dispersion values for the three X-band guides measured.

Figure 4-15

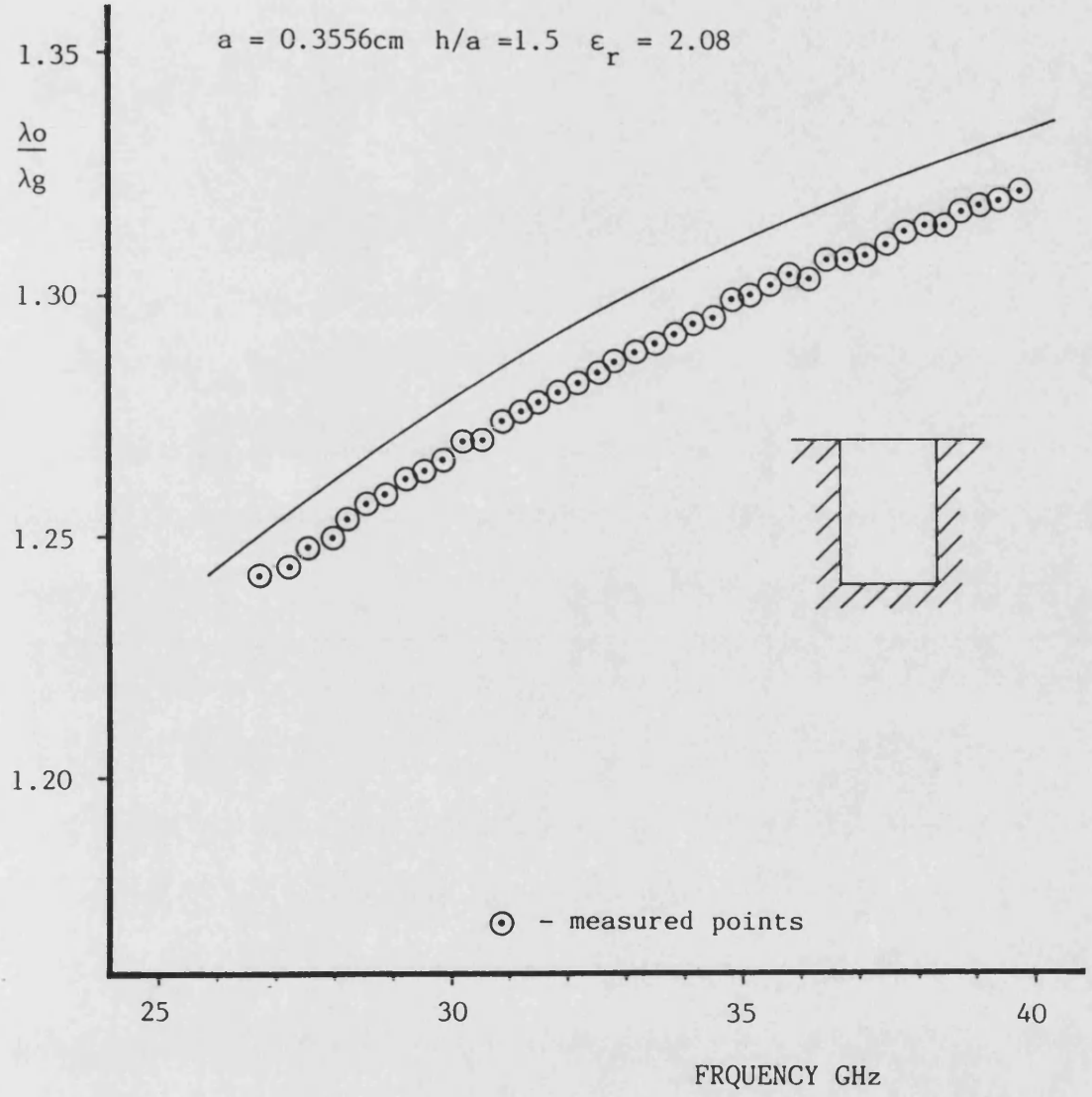

A comparison of the computed and measured dispersion results for a sample of IDG at Q-band.

Figure 4-16

4-11 The Sensitivity of the Dispersion Equation to the Dielectric Permittivity

Whilst the mechanical tolerances of the slot can be maintained during production the dielectric material may vary considerably from batch to batch. The dielectric material used for all the measured samples was PTFE (teflon) which has a quoted relative dielectric constant of 2.08 [5]. In order to measure the dielectric constant of a particular sample, a piece of the material was machined to the internal dimensions of Q-band waveguide (3.51 mm x 7.1 mm). A section of waveguide with a removable short circuit termination that could butt right up to the dielectric sample was then manufactured. With this component the phase change due to the inclusion of the dielectric sample in front of the waveguide short could be observed. From this data the dielectric constant of the sample could be ascertained by the method given in [6]. The measured results are given in Table 4.7. From these results it can be seen that the measured values fell within 2% of the assumed value. Due to the experimental scatter of the results it was decided to use the quoted value of 2.08.

However in order to see how the dispersion equation was influenced by ε_r, the dispersion curves for the Q-band sample were computed using the second order expansion for dielectric constant values of $\varepsilon_r = 2.08 \pm 2\%$. The resultant curves are shown in Fig. 4.-17, in comparison with the measured values for this guide. It was found that a ± 2% variation in the value of ε_r taken gave rise to a ± 1% variation in the computed value of β.

Thus in this case it is meaningless to quote agreement between computed and measured results as being better than 1% due to the uncertainty in the dielectric constant. It is noted that use of the average value

GUIDE WAVELENGTH (cm)	SHIFT IN STANDING WAVE PATTERN (cm)	DIELECTRIC CONSTANT
1.7074	0.4047	2.0576
1.4946	0.3385	2.0396
1.3828	0.3185	2.0558
1.2862	0.3161	2.0807
1.1966	0.3102	2.0509
1.1390	0.3147	2.0408
1.0793	0.3442	2.0872
1.0315	0.3393	2.0607
0.9766	0.3374	2.0571
0.9196	0.3234	2.0409

average value = 2·0571

Dimensions of sample : 3.59 x 7.1 x 50.7 mm

The value of dielectric constant determined experimentially for a sample of P.T.F.E., measured at Q band frequencies.

Table 4-9

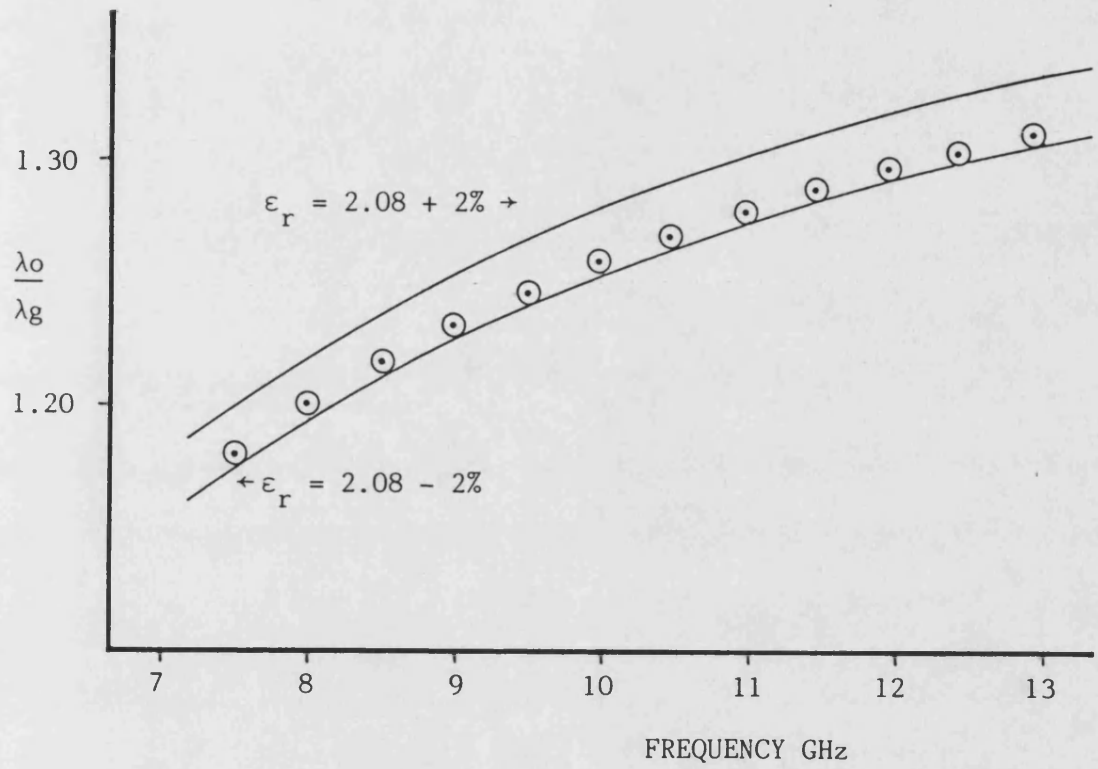

The mesaured dispersion values for an X-band sample of IDG, compared with the computed values with the relative permittivity taken as 2·08 ± 2%.

Figure 4-17

obtained from Table 4.7 for ε_r would give greater agreement between computed and measured values.

4-12 Conclusion

This chapter has been concerned with the solution of the dispersion equation. The solution for β has led to the determination of the amplitudes of the expansion terms and thus the field components themselves.

Two computer methods have been outlined for real or complex solutions of β, and both are rapidly convergent with the number of expansion terms taken. The accuracy of the solutions has been demonstrated by comparison with measured results and are within the measurement uncertainty.

For the guide geometries considered the field solutions were found to be predominantly LSE with the fundamental mode being defined as HE_{01}. The next mode to propagate was HE_{02} for a deep slot and HE_{11} for a shallow slot. The optimum slot width to depth ratio for maximum monomode bandwidth was found to be approximately 1.4. The monomode bandwidth was also dependent upon the permittivity of the dielectric used and was favoured by a low value.

The field plots for several mode solutions have been presented which show graphically the LSE nature of the field. The TM wrt y components are excited by the discontinuity in the field at $y = 0$ and are of little influence over the remaining cross-section. In fact, when the dielectric is lowered in the slot to reduce the influence of the singularity on the field, the TM components are almost negligible.

4-13 References

[1] Abramowitz and Stegun, "Handbook of Mathematical Functions", Dover, 1965, p. 887.

[2] J.F. Traub, "Iterative Methods for the Solution of Equations", Prentice Hall, 1964, p. 210.

[3] R.F. Harrington, "Time Harmonic Electromagnetic Fields", McGraw-Hill 1961, p. 131.

[4] L. Lewin, "On the Inadequacy of Discrete Mode-Matching Techniques in some Wavweguide Discontinuity Problems", IEEE Trans Microwave Theory Tech., vol MTT-18, No. 7, July 1970, pp 364-372.

[5] S. Roberts and A. Von Hippel, "A New Method for Measuring Dielectric Constants and Loss in the Range of Centimetre Waves", J. Appl. Phys., vol 17, No. 7, 1946.

[6] G.W.C Kaye and T.H. Laby, "Tables of Physical and Chemical Constants", Longman, 1966, p.96.

CHAPTER FIVE

THE LOSS ANALYSIS OF IDG

5-1 Introduction

This chapter is concerned with the evaluation of the IDG loss characteristics. Whilst an accurate knowledge of the propagation characteristics is necessary for circuit design, it is the level of loss that will determine the applicability of IDG and its acceptance by the system engineer. The sources of loss are threefold, consisting of radiation, dissipation by the dielectric media and conducting surfaces. Each of these contributions is discussed and it is ascertained that the ideal IDG structure, propagating above cutoff, will not suffer radiation loss.

Computed loss curves are obtained for various guide structures to ascertain the dominant cause of loss and to suggest ways of avoiding it. In particular good correlation is shown with measured results. A simple rectangular waveguide to IDG transition is described and shown to have a good performance.

The loss from bends has been an unfortunate characteristic of many open structures and has limited their practical application. IDG must be shown to offer considerable improvements in this area and to address this, two 90^{o} bends were made and measured. These initial results were very promising.

In the final part of this chapter the computed loss of IDG is compared with theoretical loss of Image Line and Insular guide, since these are the competing structures for high frequency integrated circuit design.

5-2 The Radiation Field

In chapter 3 the TRD formulation for the surface wave solutions of IDG was developed. A discrete set of solutions for β was obtained, determined by the resonant frequencies of the transverse equivalent network for each value of $\beta = \beta s$. The air region is unbounded and so it can support a continuum of plane waves or rays. These plane waves are free to propagate in any direction in the three dimensional space and being a solution to the Helmholtz equation, must satisfy the condition

$$k_0^2 = \omega^2 \mu_0 \varepsilon_0 = kx^2 + ky^2 + \beta^2 \qquad (5\text{-}7)$$

In the discrete mode formulation the fields in the air region were written as a Fourier expansion in x, as the superposition of plane waves each corresponding to a value of $kx = \rho$, $o \leq \rho < \infty$. From (5-7) the value of ky was then fixed to be

$$ky = \sqrt{k_0^2 - \rho^2 - \beta s^2} \text{ when } k_0^2 > \rho^2 + \beta s^2 \qquad (5\text{-}2a)$$

$$ky = -j\sqrt{\beta s^2 + \rho^2 - k_0^2} \text{ when } k_0^2 < \rho^2 + \beta s^2 \qquad (5\text{-}2b)$$

The signs of the square roots are chosen to satisfy the radiation condition that energy must either propagate away from the guide or be evanescent.

For a bound field solution the power flow transverse to the guide must be purely reactive (in the lossless case) requiring that condition (5-26) is satisfied for all ρ. Therefore since ρ is summed over the range of real values $o < \rho < \infty$ then bound mode solutions are only possible for $k_0^2 < \beta s^2 < \varepsilon r\, k_0^2$. Other discrete solutions are possible for $\beta^2 < k_0^2$. These have, for some values of ρ, spectral components corresponding to real power flow away from the guide and

are the so called leaky waves. The cutoff condition can thus be identified as $\beta = k$ above which the modes are fully bound and below which the modes become increasingly "leaky".

In a physical IDG structure, the dielectric medium in the slot will dissipate a small proportion of the field. Thus the modal fields will be reduced in amplitude and for a forward travelling mode the solution for β will contain a small imaginary part:

$$\beta = \beta' - j\beta'' \qquad (\beta', \beta'' > o) \tag{5-3}$$

where the single prime denotes a real component and the double prime denotes an imaginary component. Rewriting (5-1) in terms of complex quantities and equating the real and imaginary parts gives:

$$k_0^2 = \rho^2 + ky'^2 + \beta'^2 - ky''^2 - \beta''^2 \tag{5-4a}$$

$$o = ky'ky'' + \beta'\beta'' \tag{5-4b}$$

Condition (5-3) requires that:

$$ky'\, ky'' > o$$

so that permissible values for ky are:

$$ky(\rho) = ky' + jky'' \quad \text{for} \quad \beta'^2 + \rho^2 < k_0^2 + \beta''^2 \tag{5-5a}$$

$$= -ky' - jky'' \quad \text{for} \quad \beta'^2 + \rho^2 > k_0^2 + \beta''^2 \tag{5-5b}$$

The solution (5-5a) describes an outward propagating wave that increases exponentially away from the guide. This can be explained schematically as a propagating field with the real poynting vector at an angle θ to the z-axis as shown in Fig. 5-1. The leaky wave, as a steady state solution to Maxwell's equations is of infinite amplitude at infinity. From Fig. 5-1 this requires an infinitely large source located at $z = -\infty$. In a physical structure the source will be of finite power

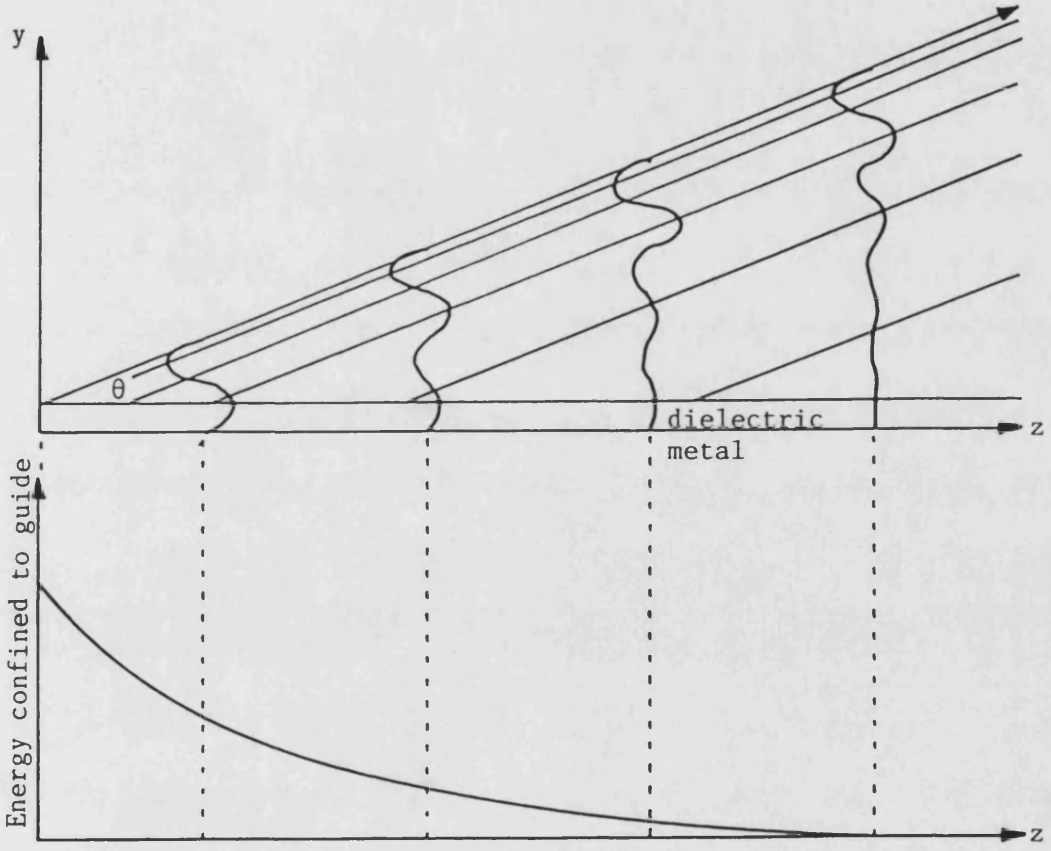

A schematic diagram to illustrate the exponential increase of the field away from the guide when $\mathrm{Re}|E \times H^*|$ has a component directed away from the guide.

Figure 5-1

and position so that, as shown in Fig.5.1 the outward wave only appears to grow in the segment of angle θ and is zero thereafter. Thus the leaky wave in a physical system does not violate the radiation condition.

The solution (5-5b) indicates a wave that enters the guide from the air region. This can be viewed as the tilting of the poynting vector into the guide to compensate for the energy lost in the dielectric by dissipation. Another way of stating this is that when the amplitude of the field components in the slot are reduced by absorption, energy must be redistributed between the air and slot regions in order to maintain the continuity of the transverse components at the interface.

Leaky waves are not normalisable in the usual way since they would contain an infinite amount of energy. They thus cannot be used to define discontinuities in the guide. The leaky wave is a consequence of the formulation and so if radiation is to be included in an analysis the full continuum over all of the partial waves must be considered.

It is apparent from the previous section that the discrete surface modes are not the only field solutions that can satisfy (5-1). Without β being fixed by a resonance condition there are two independent parameters in (5-1). The transverse field can be constructed from the superposition of plane waves travelling at all angles in the x-y plane. Thus by summing all these components over $o \leq kx < \infty$ and $o \leq ky < \infty$ β can be anywhere in the range $-j\infty > j\beta > jo$, $o < \beta \leq k_0$. This continuous range of spectral components forms the radiation field. The individual plane waves can propagate unattenuated to infinity and thus appear to violate the radiation condition. However, the radiation field is excited as a continuum, and so it is the

superposition of all the spectral components and not the individual elements that must satisfy this criterion. Thus since a physical field can only contain a finite amount of power, the integral of the field over the transverse section must converge to a finite value.

The complete IDG field can thus be constructed from a discrete set of bound mode functions with $k_0 < \beta < \sqrt{\epsilon r} k_0$, and a continuum of radiation modes in the range $-j\infty \geq \beta \geq j\alpha, o \leq \beta \leq k_0$. Any arbitrary field can be obtained from these solutions. Moreover, the individual components can be normalised such that:

$$\int_0^{\infty}\int dx\, dy \quad \psi s\,(x,y)\psi r(x,y) \;=\; \delta sr \qquad (5\text{-}6a)$$

$$\int_0^{\infty}\int dx\, dy \quad \psi(x,y\ kx,ky)\ \psi\ (x,y,kx',ky') = \delta(kx - kx')\ \delta(ky - ky') \qquad (5\text{-}6b)$$

where ψs, ψr are discrete solutions and ψ is a component of the continuum.

The inclusion of the radiation continuum is beyond the scope of this thesis. The derivation and normalisation of the continuum is however given in [1]. It is useful though to include briefly the formulation of the radiation mode functions.

The problem of diffraction can be viewed from two standpoints. Either a single spectral component incident from the air region onto the edge discontinuity will excite a complete set of slot modes, or a single slot mode will excite the continuum in the air region. Since in most practical applications the sources to be analysed (such as diodes) will be on the interface plane or in the air region it is convenient to adopt the former approach. Consider the even excitation

by a single ray in the air region with transverse wave numbers kx, ky. The x-dependence of the total field can be obtained as an even Fourier series in kx so that the ray will have the x dependence;

$$\phi(x) = \cos(kx\ x) \tag{5-7}$$

The ray, impinging upon the dielectric/air interface will set up a standing wave in the y-direction. The phase shift of this reflection will depend upon the angle of incidence of the ray, so that the y-dependence of the ray in the air region can be written:

$$\chi(y) = \sin\ (ky\ y + \alpha\ (kx,\ ky)) \tag{5-8}$$

where α is the "phase shift" at y = o.

The component of the continuum in the air region, with Fourier amplitude A(kx,ky) is thus:

$$\psi(x,y,kx,ky) = \frac{2}{\pi} A(kx,ky)\cos(kx\ x)\ \sin(kyy + \alpha\ (kx,ky)) \quad \text{for } y > o \tag{5-9a}$$

This function satisfies the boundary conditions for a y-directed Hertzian magnetic potential and gives solutions for TE fields wrt y. An analogous expression is found for the TM field. The ray will be diffracted at the 90°metal edge into the slot and so will excite a discrete set of slot components analogous to those excited in the bound mode formulation. A standing wave in the y-direction is set up between the slot floor and the interface, which is continuous at y = o so that the field can be written

$$\psi(x,y,\ kx,ky) = \sqrt{\frac{2}{\pi}}\ \sin\ (\alpha(kx,ky))\ \sum_{n}^{\infty} Qn(kx)\ \phi hn(x)\ \frac{\sin kyn(y+h)}{\sin\ knh} \quad \text{for } y \leq o \tag{5-9b}$$

The Fourier amplitudes Qn are found by the continuity of (5-9a) and

(5-9b) at y = o and the orthogonality of the ϕhns. It is readily proven that the mode functions (5-9) are orthogonal over the transverse guide section and are normalised to satisfy (5-6b) [1].

The ideal IDG structure, such as that analysed here, in invariant with z. Therefore the z-dependence of the incident and diffracted components will be the same. Since for a bound wave $\beta > k_0$, any diffracted components must be reactive in the air region so that radiation cannot occur. Thus the theoretical IDG structure will not suffer from radiation loss when excited by a surface wave above cut-off. In a practical sample of IDG small corrugations in the side-walls are inevitable, along with material inhomogenities and radiative components may consequently be excited. However, in a well made guide these departures from the ideal case will be small and a consideration of radiation is neglected from the loss analysis presented here. Thus discussion of course, applies only to a straight section of IDG. As soon as bends, changes in cross-section or any other type of discontinuity is encountered, then, the complete field representation including the radiation continuum must be used.

5-3 Dielectric Loss

In a medium with finite conductivity σ, a conduction current $J = \sigma E$ will exist, resulting in energy loss due to joule heating. That is, a medium with finite conductivity will dissipate energy when placed in an electromagnetic field. With this current term, Maxwell's curl equations become:

$$\nabla \times E = -\mu_0 \frac{dH}{dt} \qquad \nabla \times H = \varepsilon_0 \varepsilon_r \frac{dE}{dt} + \sigma E \qquad (5\text{-}10)$$

Eliminating H from these equations gives

$$\nabla^2 E - \mu_0 \sigma \frac{dE}{dt} - \mu_0 \varepsilon_0 \varepsilon_r \frac{d^2 E}{dt} \qquad (5\text{-}11)$$

which for a harmonic time variation $e^{j\omega t}$ gives:

$$\nabla^2 E + (\omega^2 \mu_0 \varepsilon_0 \varepsilon_r - j\omega\mu_0\sigma)E = 0 \qquad (5\text{-}12)$$

The first term in the brackets gives the propagating terms, and the second, a damping term, corresponding to the decay in amplitude due to dissipation. This equation can be simplified by writing the permittivity as a complex quantity:

$$\varepsilon_r = \varepsilon_r' - j\,\varepsilon_r'' = \varepsilon_r \left(1 - \frac{j\sigma}{\omega\,\varepsilon_0 \varepsilon_r}\right) \qquad (5\text{-}13)$$

The imaginary part of ε is often expressed in terms of the real part by the loss tangent so that,

$$\varepsilon'' = \varepsilon_r \tan\delta, \qquad \varepsilon = \varepsilon_r(1 - j \tan\delta).$$

Thus the loss characteristics of a medium can be expressed as a complex value of dielectric constant. The permittivities and loss tangents for several dielectric materials are given in Table 5.1. It can be seen that generally the loss tangent is largest for materials of high permittivity.

material	ε_r	tanδ	ε''
P.T.F.E	2·08	0·0002	0·000416
Polythene	2·24	0·00667	0·01494
Perspex	2·50	0·0083	0·02075
Polystyrene	2·54	0·0012	0·003048
Al_2O_3 (98%)	8·3	0·00032	0·002656
Sapphire	9·0	0·0002	0·0018
"ECOMAX 3GDK" casting resin	5·4	0·0008	0·00432

The typical permittivity values of some dielectric materials

Table 5-1

Since the transverse field confinement to the dielectric in IDG is largely due to the metal sidewalls enclosing it, the material can be chosen primarily for its low loss tangent. This is in marked contrast to image line for example, where a high permittivity material is required to maximize the field confinement to the guide and so minimize the radiation loss from bends. Ultimately the materials used in IDG will be determined by the fabrication techniques available.

For the low frequency test pieces used in this work, P.T.F.E. was used throughout. This material has a permittivity that is almost invariant with frequency and temperature, has a low $\tan\delta$, and is relatively easy to machine. However, for the high frequency circuits for which IDG is intended the small slot size may necessitate the use of casting resins, extrusion or sintering. Thus the choice of dielectric material may be governed by its suitability for the fabrication process rather than its electrical properties.

5-4 Conductor Loss

The guide analysis developed in chapter two assumed metal surfaces that behave as perfect conductors, in order to simplify the boundary conditions. In a perfect conductor, with infinite conductivity, no potential difference or current can exist and so the current component at the boundary;

$$\underline{J}s = \hat{n} \times \underline{H} \text{ , } \hat{n} = \text{unit inward normal to surface} \qquad (5\text{-}14)$$

must lie on the surface of the conductor. For a physically realisable conductor the conductivity σ, although large, will be finite and so a current will flow into the metal and dissipate energy by joule heating.

From equation (5-12) it can be seen that for a large value of conductivity the conduction current is far greater than the displacement current, so that propagation into a good conductor is heavily damped. The field propagation into a conductor will decay as $\exp(-\sqrt{j\omega\mu_0\sigma}\, z)$ where z is the ordinate into the surface. Since the field decays rapidly into the conductor it can be considered to be concentrated at the surface. The exponentially decaying current distribution can be approximated by a layer of constant current distribution of thickness δs. The requirement that the total current contained in the layer be the same in both cases gives

$$\int_0^\infty e^{-\sqrt{j\omega\mu_0\sigma}\, z}\, dz = \delta s\,(1 + j) \qquad (5\text{-}15)$$

so that $\delta s = \left(\frac{2}{\omega\mu_0\sigma} \right)^{\frac{1}{2}}$

δs is known as the "skin depth" and for metals at microwave frequencies is of the order 10^{-5} cm. Thus the current components at microwave frequencies can be considered to be localised at the surface of a conductor. The conductor surface can be characterised as having an impedance per unit area of

$$Zm = \frac{1 + j}{\sigma \delta s} \quad \Omega\ m^{-2} \qquad (5\text{-}16)$$

so that the resistive part of the surface impedance is equal to the d.c. resistance per unit area of metal of thickness δs. The tangential electric field components induced by the current flow at the conductor surface will be:

$$\underline{Et} = Zm\ \underline{Js} = Zm\ A \times \underline{H} \qquad (5\text{-}17)$$

For metals Zm will be small and the electric field components will be of an order two smaller than the transverse magnetic components. Thus for good conductors the finite conducting surface is a small perturbation from the case of a perfect conductor and so the surface currents can be calculated from the loss-free fields.
This approximation only holds for small values of Zm and so is only valid for small losses.

If αc is the attenuation due to conductor loss in nepers/cm then each field component will decay along the guide as $\exp(-\alpha_c z)$. Thus if the power in the guide field at $z = 0$ is P_0, then the power at any other section z along the guide will be given by

$$Pz = P_0 \exp(-2\alpha_c z) \qquad (5\text{-}18)$$

The rate of decrease of power along the guide is:

$$\frac{dPz}{dz} = -2\alpha_c P_0 \exp(-2\alpha_c z) \qquad \text{WATTS/cm} \qquad (5\text{-}19)$$

This power loss corresponds to the power dissipated in conductors, Pc, so that:

$$Pc = 2\alpha_c P_0 \exp(-2\alpha_c z) \qquad (5\text{-}20)$$

$$\therefore \quad \alpha_c = -\frac{1}{2} \frac{Pc}{P_0 \exp(-2\alpha_c z)}$$

$$= -\frac{1}{2} \frac{\text{ENERGY DISSIPATED BY CONDUCTING SURFACES}}{\text{ENERGY PROPAGATED ALONG GUIDE}} \qquad (5\text{-}21)$$

The currents induced in the metal walls will be dissipated by the real part of the surface resistance:

$$Rm = \sqrt{\frac{\omega\mu_0}{2\sigma}} \qquad (5\text{-}22)$$

so that the time averaged power loss per unit length of guide is given as:

$$Pc = \frac{Rm}{2} \int_{\text{SIDEWALLS}} Js \cdot Js^* \, d\ell = \frac{Rm}{2} \int_{\text{SIDEWALLS}} (n \times H) \cdot (n \times H^*) \, d\ell \qquad (5\text{-}23)$$

$$= \frac{Rm}{2} \int n \times |H|^2 \, d\ell$$

The power flow along the guide can be evaluated as the time averaged Poynting vector over the transverse guide cross-section:

$$P = \tfrac{1}{2} \int_{\text{CROSS-SECTION}} \text{Re}\,(E \times H^*) \cdot \hat{n}z \, da \qquad \text{WATTS/cm}^2 \qquad (5\text{-}24)$$

5-5 The Evaluation of the Conductor Loss Components

The integral in (5-23) may be split into three contributions Pf, Psw, Pg which correspond to the contributions from the slot floor, slot sidewalls and the ground plane respectively. Due to the symmetry of the field, the integrals need only be computed over one half of the guide cross-section and so from (5-23):

$$Pf = \frac{Rm}{2} \int_{o}^{a/2} [Hz(x,-h)Hz^*(x,-h) + Hx(x,-h),Hx^*(x,-h)]dx \quad (W/cm) \tag{5-25a}$$

$$Psw = \frac{Rm}{2} \int_{-h}^{o} [Hz(a/2,y)Hz^*(a/2,y) + Hy(a/2,y)Hy^*(a/2,y)]dy \quad (W/cm) \tag{5.25b}$$

$$Pg = \frac{Rm}{2} \int_{a/2}^{\infty} [Hz(x,o)H^*z(x,o) + Hx(x,o)Hx^*(x,o)]dx \quad (W/cm) \tag{5.25c}$$

Similarly, the Poynting vector integral (5-24) can be split into the integrals over the slot and air regions as Ps and Pa respectively so that (5-21) can be written as:

$$\alpha_c = \frac{-1}{2} \frac{Pf + Psw + Pg}{Ps + Pa} \tag{5-26}$$

By substituting the expressions for the field components obtained in chapter 3, into (5-24) and (5-25), then the following expressions are obtained:

$$Pf = \frac{Rm}{2} \sum_{n=o,2}^{\infty} \frac{(Hzn\ Hzn^* + Hxn\ Hxn^*)}{\cos knh \cos knh^*} \tag{5-27a}$$

$$Psw = \frac{Rm}{a} \sum_{\substack{n=o,2 \\ m=o,2}}^{\infty} \left\{ \frac{Hzn\, \overset{*}{Hzm}\, \delta n\, \delta m\, (-1)^{\frac{m+n}{2}}}{\cos knh\, \cos \overset{*}{k}mh} \left(\frac{\sin(kn + \overset{*}{k}m)h}{kn + \overset{*}{k}m} + \frac{\sin(kn - \overset{*}{k}m)h}{kn - \overset{*}{k}m} \right) \right.$$

$$\left. + \frac{Hyn\, \overset{*}{Hym}\, \delta n\, \delta m (-1)^{\frac{m+n}{2}}}{\sin knh\, \sin kmh} \left(\frac{\sin(km - \overset{*}{k}m)h}{kn - \overset{*}{k}m} - \frac{\sin(kn + \overset{*}{k}m)h}{kn + \overset{*}{k}m} \right) \right\}$$

(5-27b)

$$Pg = \frac{Rm}{2} \int_0^{\infty} dp\, (hz(p)\overset{*}{hz}(p) + hx(p)\overset{*}{hx}(p)) - \frac{Rm}{2} \sum_{n=o,2}^{\infty} (Hzn\, \overset{*}{Hzn} + Hxn\, \overset{*}{Hxn})$$

(5-27c)

$$Ps = \tfrac{1}{4}\, Re \sum_{n=o,2}^{\infty} \frac{Exn\overset{*}{Hyn}}{\sin knh\, \sin \overset{*}{k}nh} \left(\frac{\sin(kn - \overset{*}{k}n)h}{kn - \overset{*}{k}n} - \frac{\sin(kn + \overset{*}{k}n)h}{kn + \overset{*}{k}n} \right)$$

$$- \sum_{n=2,4}^{\infty} \frac{\overset{*}{Hxn}\, Eyn}{\cos knh\, \cos \overset{*}{k}nh} \left(\frac{\sin(kn + \overset{*}{k}n)h}{kn + \overset{*}{k}n} + \frac{\sin(kn - \overset{*}{k}n)h}{kn - \overset{*}{k}n} \right)$$

(5-27d)

$$Pa = \tfrac{1}{4} \int_0^{\infty} \frac{Re\, (ex(p)\overset{*}{hy}(p) - \overset{*}{hx}(p)\, ey(p))}{|\, ky''(p)\, |}\, dp \qquad (5\text{-}27e)$$

These expressions were used in the computation of the conductor loss values given in the next sections. The integral Pa was evaluated numerically and the first three expansion terms were used in the evaluation of the amplitude terms.

5-6 Correction for Surface Imperfections

In the previous section the conducting surfaces were replaced with perfectly flat sheets of material with resistance Rm per unit area and thickness δs. Physically realisable surfaces will have been machined, extruded, electroformed or manufactured in some other way, and so will not have perfectly flat surfaces. Corrosion and oxidation will also roughen the surface from its ideal state. The effect of surface undulations will be to effectively increase the area over which the surface currents flow and thus increase the dissipation. That is, the contour for the line integral in equation (5-23) is increased from the ideal value. When the size of the surface undulations is small in comparison with the skin depth the surface is still effectively flat. When however the surface undulations are of the same order as the skin depth then the effective area of the surface can be greatly increased. Thus it can be expected that the discrepancy between the theoretical and measured conductor loss will increase with frequency as the skin depth decreases.

Benson has carried out extensive experimental work into the causes of attenuation of practical rectangular metal waveguides [2] and has concluded that surface roughness is the dominant cause for the discrepancy between measured and computed values. The ratio of the measured to computed attenuation constants for various rectangular guides at several frequencies is given for several metals in Table 5.2. This was taken from Benson [3]. It can be seen that the ratio increases with frequency as expected. Since the loss in rectangular air filled guides is due to the conductors, the values given in Table 5.2 can be used as correction parameters to account for surface roughness.

material	value of measured to calculated attenuation					
	9·375 (GHz)	27 (GHz)	35 (GHz)	70 (GHz)	140 (GHz)	203 (GHz)
Copper	1·034	1·39	1·56	1·7–2·5	2·1–2·5	-
Brass (60/40)	1·014	1·24	1·29	1·4	-	-
Standard silver	-	-	1·20–1·55	1·4	1·3	2·2

The ratio of measured to calculated attenuation for rectangular waveguide made from different metals (taken from [3])

Table 5-2

metal	$\rho \times 10^{-8}$ (Ωm)
copper	1·73
brass (Cu 90 Zn 10)	3·90
brass (Cu 70 Zn 30)	6·20
aluminium	2·87
gold	2·44
silver	1·63

The values of resistivity for some common metals

Table 5-3

The effect of dimensional tolerances upon the guide loss can be predicted by changing the guide dimensions slightly in the loss program. The computed conduction loss has an inverse square-root dependence upon the value of conductivity used. The values of conductivity given in table 5.3 are for "pure" materials. In practice the metal will contain small amounts of impurities and a layer of corrosion, which will increase the conductivity. Thus the computed values underestimate somewhat the real losses.

5-7 The Determination of the Q-factor

The measurement of low values of loss is often most accurately achieved by determining the unloaded Q-value of a resonant circuit. Thus it is useful to be able to express the previously computed value of α as a Q value. If a length of transmission line is excited in one mode only then the unloaded Q can be defined as:

$$Q = \omega \frac{< W >}{< Pd >} \tag{5-28}$$

where: $< W >$ = time averaged total energy stored in the propagating mode, per unit length (J/cm)

$< Pd >$ = time averaged power lost from propagating mode per unit length in W/cm.

If $< Pf >$ = time average power flow along guide then

$$\alpha = \tfrac{1}{2} \frac{< Pd >}{< Pf >} \tag{5-29}$$

and so:

$$Q = \frac{1}{2\alpha} \omega \frac{< W >}{< Pf >} \tag{5-30}$$

The group velocity can be expressed as

$$Vg = \frac{< Pf >}{< W >} = \frac{\lambda o}{\lambda y} \frac{C}{\sqrt{\epsilon r}} \tag{5-31}$$

leading finally to

$$Q = \frac{1}{2\alpha} \frac{k_o^2}{\beta} \sqrt{\epsilon r} \tag{5-32}$$

5-8 The IDG to Rectangular Waveguide Transition

Any practical implementation of IDG into integrated circuits will require interfaces to rectangular waveguide, or circuits contained in rectangular waveguide. For fundamental mode excitation the slot field in IDG is very similar to that of rectangular waveguide and so all that is required is an impedance match between the two. This can simply be achieved by the use of a dielectric taper as shown in Fig. 5-2. The measured SWR from the butt-joint between rectangular waveguide with and without a dielectric taper is shown in Fig. 5-3. It can be seen that the taper provides an acceptable broadband match. This transition was not optimised in any way. By reducing the impedance rate of change by increasing the length of the taper or by using a raised cosine profile for example could improve the broadband match.

It is worthwhile here to describe the measurement technique used to obtain the SWR curves of Fig. 5-3. The SWR measurement was carried out using the HP 8510 network analyser with the time-domain facility. The analyser was first calibrated for reflection measurement in rectangular waveguide. A length of IDG was then assembled which was as long as possible from the available pieces (24 ins. for X-Band dimensions). This section was terminated with a dielectric taper into a "matched" waveguide load, and then connected to the reference plane on the analyser. By displaying the measured $|S11|$ in the time-domain, the nature of the discontinuities could be ascertained. As expected there were two major contributions to the reflected signal, from each end of the IDG section. By placing microwave absorbing material at the load end of the IDG section, the reflected signal from this end was made as small as possible.

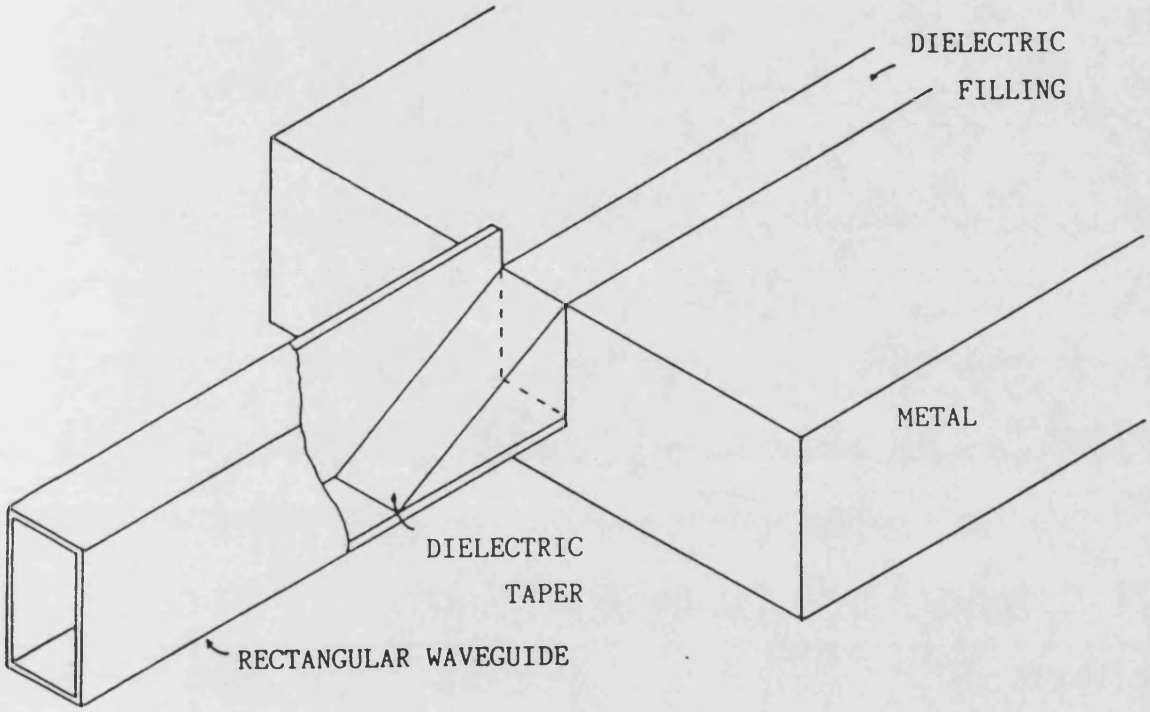

The rectangular waveguide to IDG transition

Figure 5-2

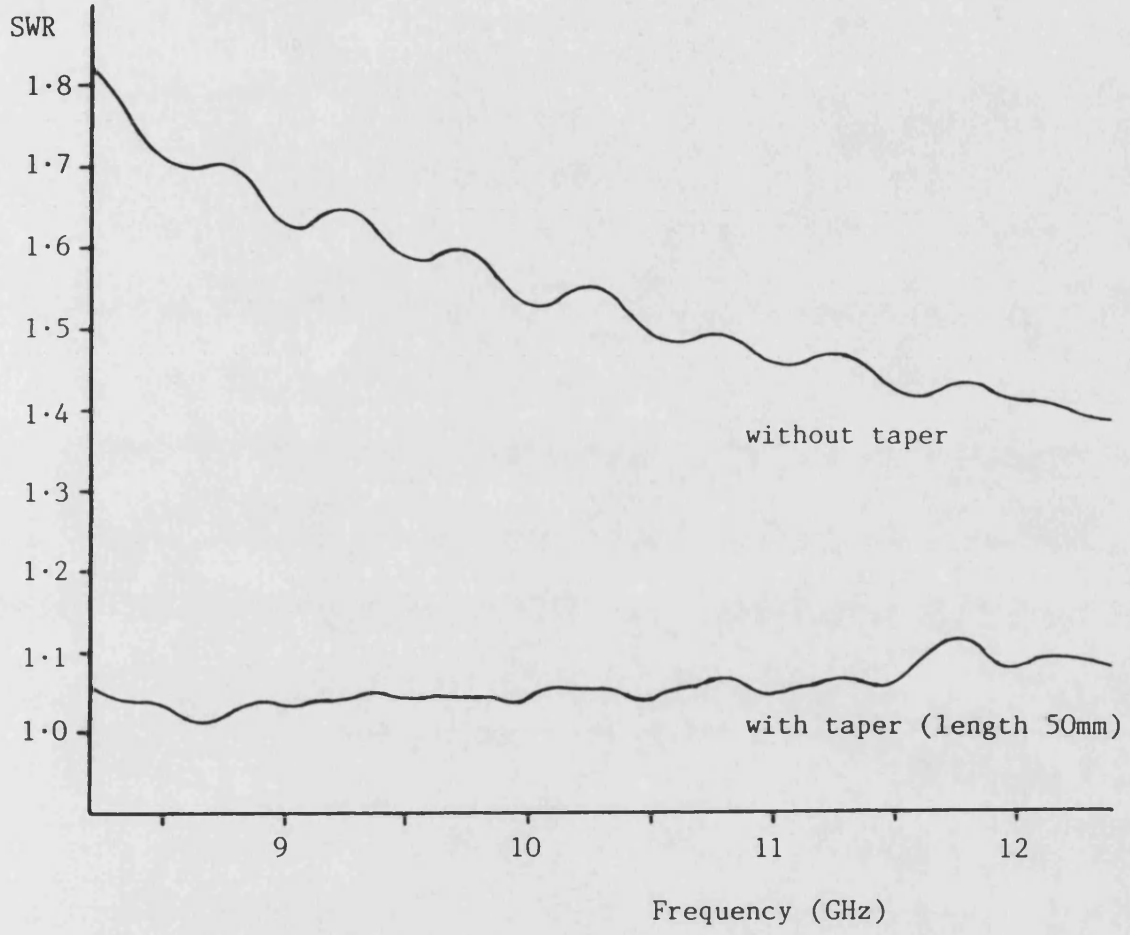

The measured reflection from a rectangular waveguide to IDG transition with and without a dielectric taper

IDG dimensions 1·016cm × 1·524cm with a PTFE insert

Figure 5-3

The time-domain gate facility was then used to remove the contribution to the measured $|S_{11}|$ of the far end altogether. The measured $|S_{11}|$ then closely approximated that of a transition to an infinitely long section of IDG.

5-9 The Measurement of Transmission Loss

The transmission loss of IDG was measured by the HP 8510 vector network analyser, using a substitution method and by determining the Q value of resonant sections of line.

The substitution method could only be used to measure the transmission loss of one particular IDG geometry since this was the only one available in three sections. The procedure was to measure the transmission loss (S_{21}) of a two-section length of line complete with transitions. A third section was then inserted between the two sections and the loss was measured again. The difference between these two readings, all other things remaining invariate, gave the loss of a single section of line. This method, as used on the analyser, was prone to errors, the major problem being that the interface to the machine took place via co-axial cables. The experimental set-up had to allow waveguide calibration at the nearest planes to the IDG transitions and then allow the insertion of two and three sections of IDG. It was thus extremely difficult to avoid cable bends between the calibration and measurement stages. This relative bending altered the phase behaviour of the lines which then produced an error in the calibration. Because a loss of the order of 0.1 dB was being measured this small change gave rise to an appreciable ripple on the measured results. The measured transmission loss difference between two and three sections of line as recorded on the analyser is shown in Fig. 5-4, with and without some "smoothing" of the trace. The effect of the smoothing was to low-pass filter the response and thus average out the ripple. The loss measurement was repeated several times to allow different cable bends, and although the ripple behaviour varied, the smoothed response was always similar. Thus it was felt that the smoothed trace could be taken to be indicative of the actual loss over a single section of IDG.

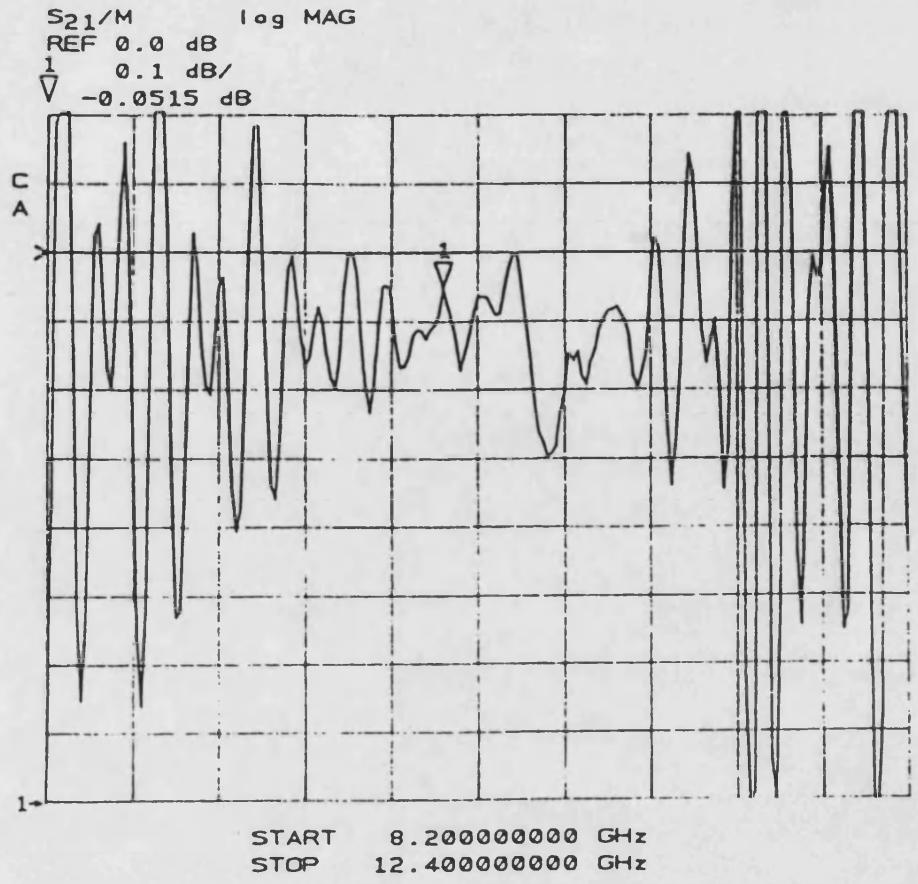

(a) WITHOUT SMOOTHING OF TRACE

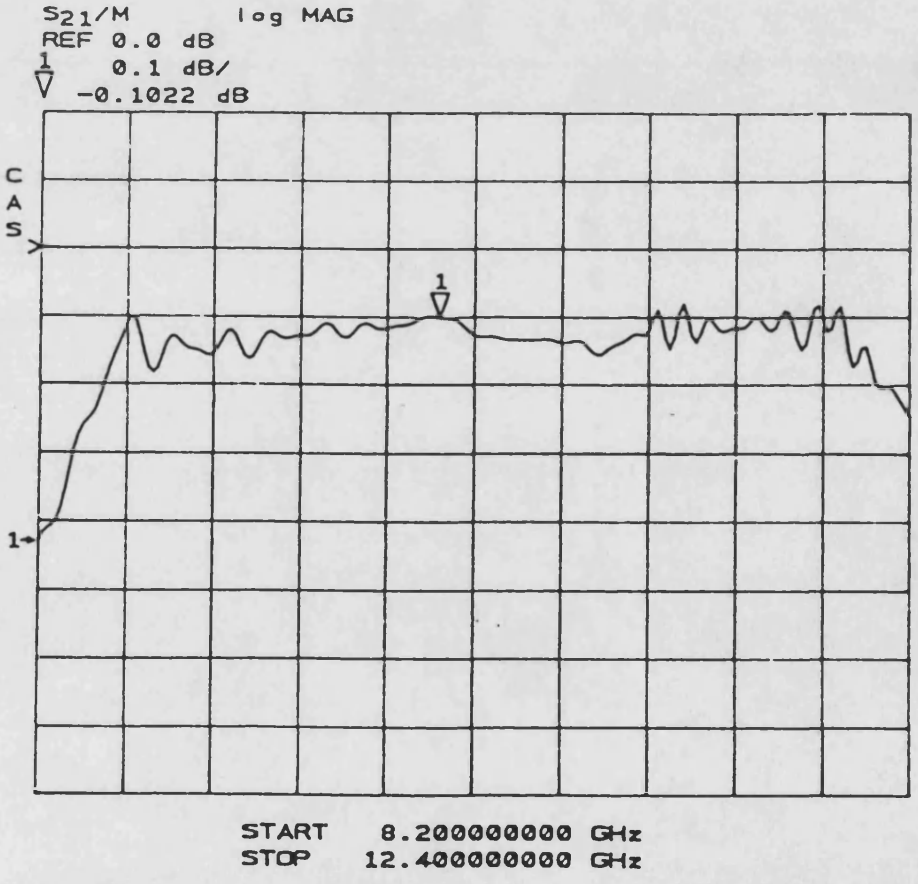

(b) WITH SMOOTHING OF TRACE

The transmission loss of a section of IDG measured by a substitution method using the HP8510 network analyser

Figure 5-4

An alternative way of determining the loss of a transmission line, which is more accurate for low loss measurements is to measure the unloaded Q factor of a resonant section. The measured Q of a resonant section of line will approach the unloaded Q if the coupling at each end of the line is small enough to provide a virtual short circuit (<- 20 dB) and the line is sufficiently long so that the losses in the end walls can be neglected. The Q-factor at each resonant frequency can be determined from the transmission response as:

$$Q = \frac{\text{centre frequency}}{\text{3 dB bandwidth}} \qquad (5\text{-}33)$$

and was measured using the same experimental set-up as described in Section 4-10 to determine the guide dispersion characteristics.

The coupling irises were made from copper foil which was made large enough to extend over the whole end face of the guide and several centimetres above it. They were clamped in as many places as possible to maximise the electrical contact and reduce the end losses. The coupling hole diameters were determined experimentally to provide an overall transmission loss through the resonant section of greater than 40 dB at all the measured frequencies. With these irises, the Q-value was measured for two resonant sections of different lengths and similar values were obtained, indicating that the end losses could be neglected. The same coupling irises were used for each guide geometry measured.

The measured Q values of three 8 inch resonant sections of IDG of various geometries are shown in Fig. 5-5. Although the partially filled slot example has a higher operating range it can be seen that the curves rise to a maximum and then decrease. This characteristic

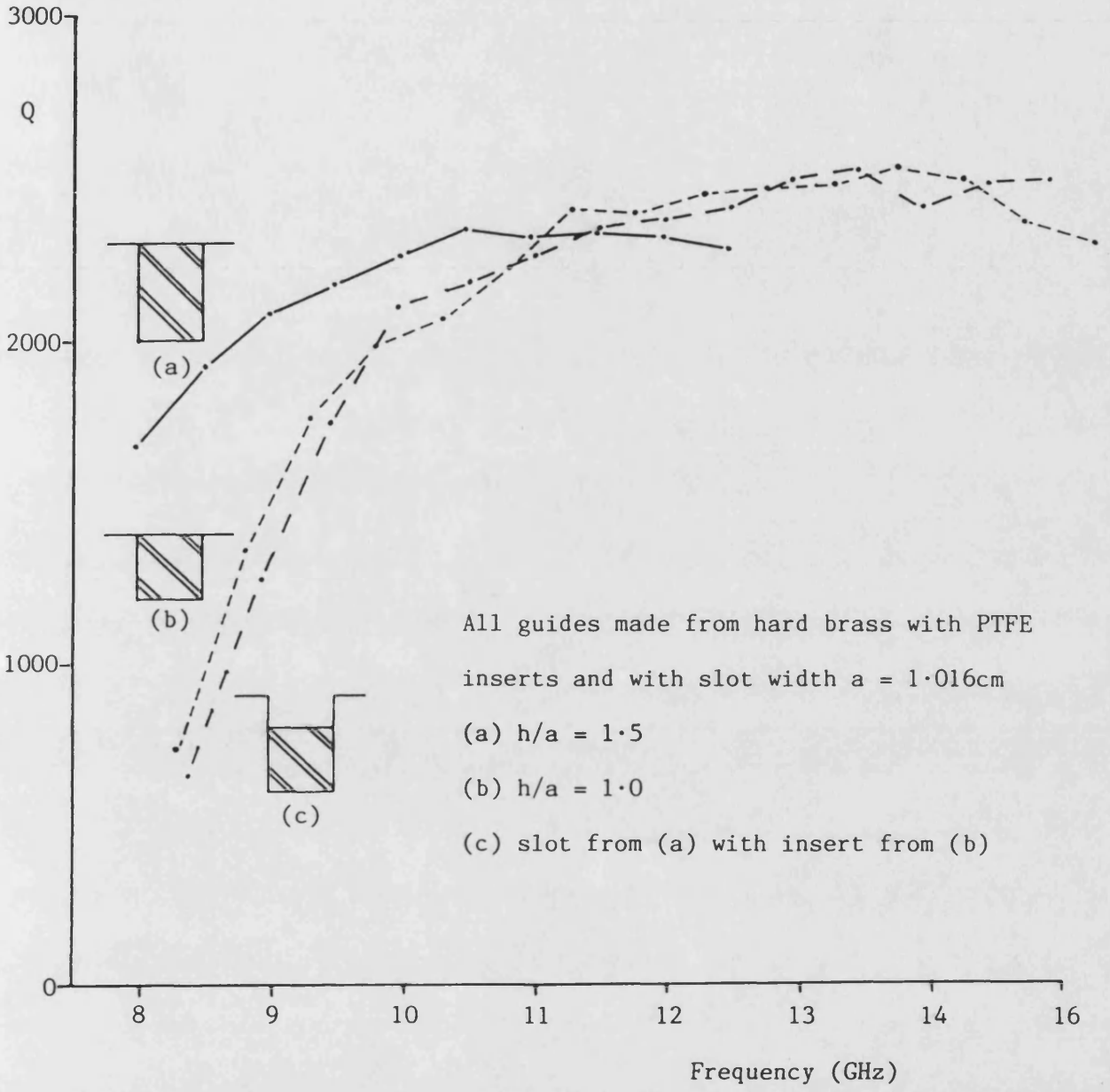

The measured Q values for three different IDG geometries

Figure 5-5

is consistent with the superposition of radiation losses which decrease with frequency and dissipation losses which increase with frequency.

Initially these radiation losses were thought to be caused by higher order mode excitation by the coupling irises, which were by no means regularly shaped or symmetrically placed in the slot region. To validate this hypothesis, the Q measurements were repeated using a diffraction grating rather than a single coupling hole. The grating was fabricated by drilling hundreds of small holes in a piece of copper foil with a p.c.b. drill. This foil was then sandwiched between the dielectric wedge of the waveguide transitions and the IDG section. The aim was that the hundreds of randomly placed small field excitations would cancel out any higher order modes whilst allowing the fundamental mode to couple through. Measurements with these gratings gave the same Q values as with the irises, leading to the conclusion that the radiation loss was inherent to the guide structure. IDG should ideally exhibit no radiation loss from a straight section above cutoff. The actual structures measured however, were not ideal and the PTFE inserts, being quite soft, were scored and pitted. Hence some radiation loss was to be expected.

5-10 The Computed Loss of IDG

The ideal IDG structure, as analysed here, will exhibit no radiation loss when excited above cutoff and so the computed loss will consist of dielectric and conductor loss components only. The dielectric loss was determined by solving the dispersion equation using a complex value of permittivity. This then gave a complex solution for β, the imaginary part of which was the attenuation in nepers/distance due to dielectric absorption. The solution for β enabled the field amplitude coefficients $\underline{X}$ and $\underline{Z}$ to be obtained. These values were then placed in Table 4.4 and equation (5-27) to evaluate the conductor loss components.

Any comparisons between the loss of different guide geometries must be made at the same frequency, and so the loss was computed for two sets of guides chosen to have the same cutoff frequency. The cutoff frequency of the fundamental HE_{01} mode is independent of the slot width. Therefore, in order to ascertain the effect of guide aspect ratio ($^h/a$) on the loss, several guides were analysed which had the same slot depth and dielectric but different slot widths. In order to assess the loss characteristics with different dielectric materials, three guides were analysed with the same slot width but with different material permittivities and slot depths, chosen so as to keep the cut-off frequency constant.

A useful parameter which gives the ratio of the guided power contained in the dielectric to the overall guided power is the confinement factor. This is defined here, using the notation of section 5-4 as:

$$cf.(\%) = \frac{Ps}{Ps + Pa} \times 100 \qquad (5\text{-}34)$$

The confinement factor can give an indication of the radiation losses

that are likely to be incurred at bends and other discontinuities. Generally a high confinement factor is required to minimize the loss from bends whilst a low value will reduce the dielectric and conductor loss components.

The conductor loss has a square root dependence upon the resistivity of the metal considered. The values of resistivity for some common metals have already been given in Table 5.3 but in order to show graphically the difference, the computed conductor loss for a particular sample of IDG is shown in Fig.5-6 for the various metals. The resistivity values used are for pure metals. In practice the surface finish of the metal due to impurities, oxidization and manufacturing process will lead to increased loss values and bring them closer together.

The overall loss of the four different guides of the same slot depth and various aspect ratios are shown in Fig. 5-7, with the loss components tabulated in Table 5.4. From the tables it can be seen that the variations in the overall loss are due to the conductor loss, with the dielectric loss remaining constant for the four guides. In order to gain an insight of the distribution of the conductor loss components in the guide it is instructive to sketch the current distribution in the guide associated with the fundamental mode. This can be achieved by using:

$$\underline{J}s = \hat{n} \times \underline{H} \qquad (5\text{-}35)$$

in reference with the field intensity plots of the previous chapter. The current distribution over one half of the conductor surface is sketched in Fig. 5-8. It can be expected that, since the currents are most concentrated near the edge of the guide that this will be the major area of dissipation. The conductor loss components in the

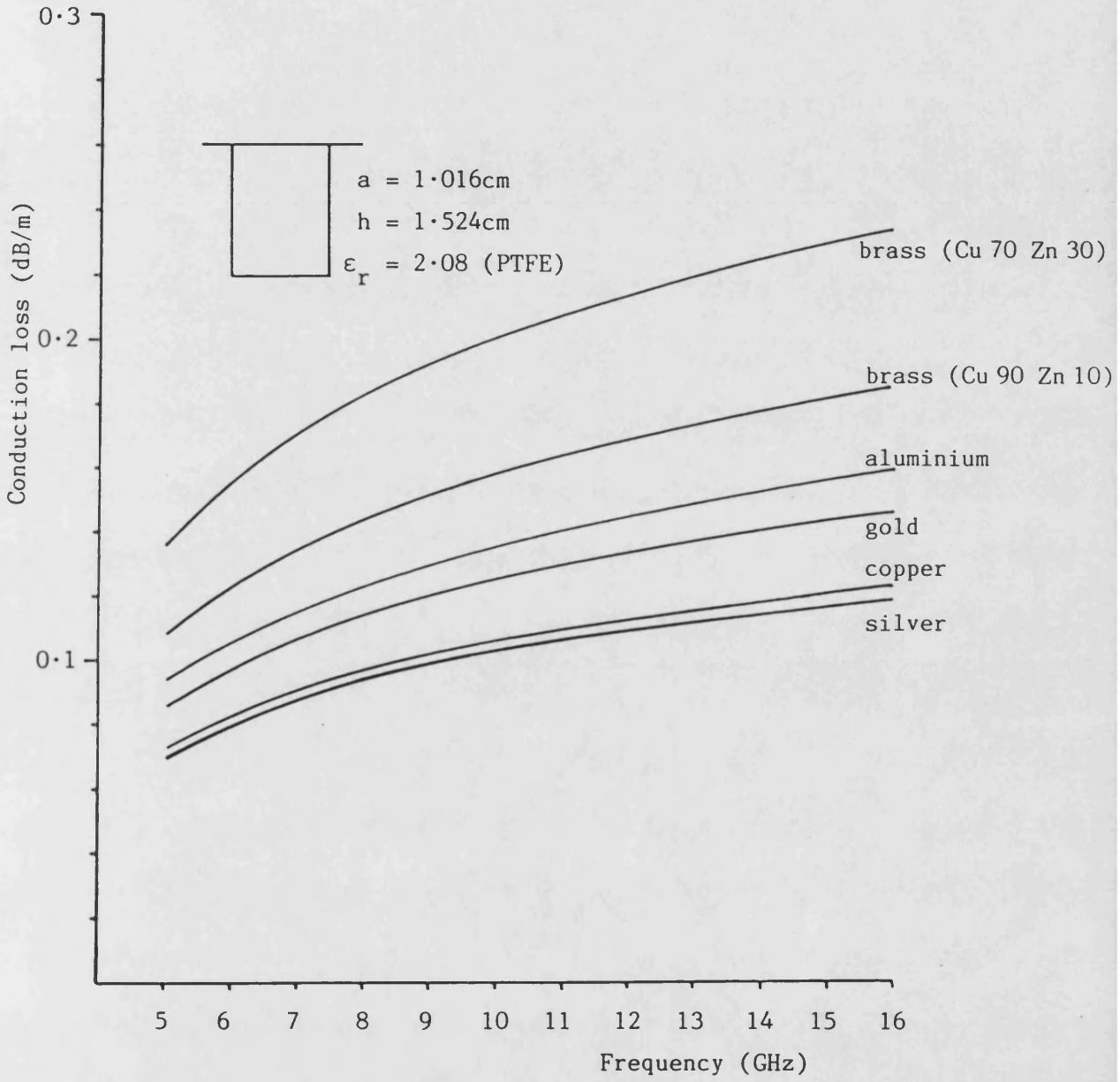

The computed conductor loss of an IDG sample of given dimemsions plotted for some different metals

Figure 5-6

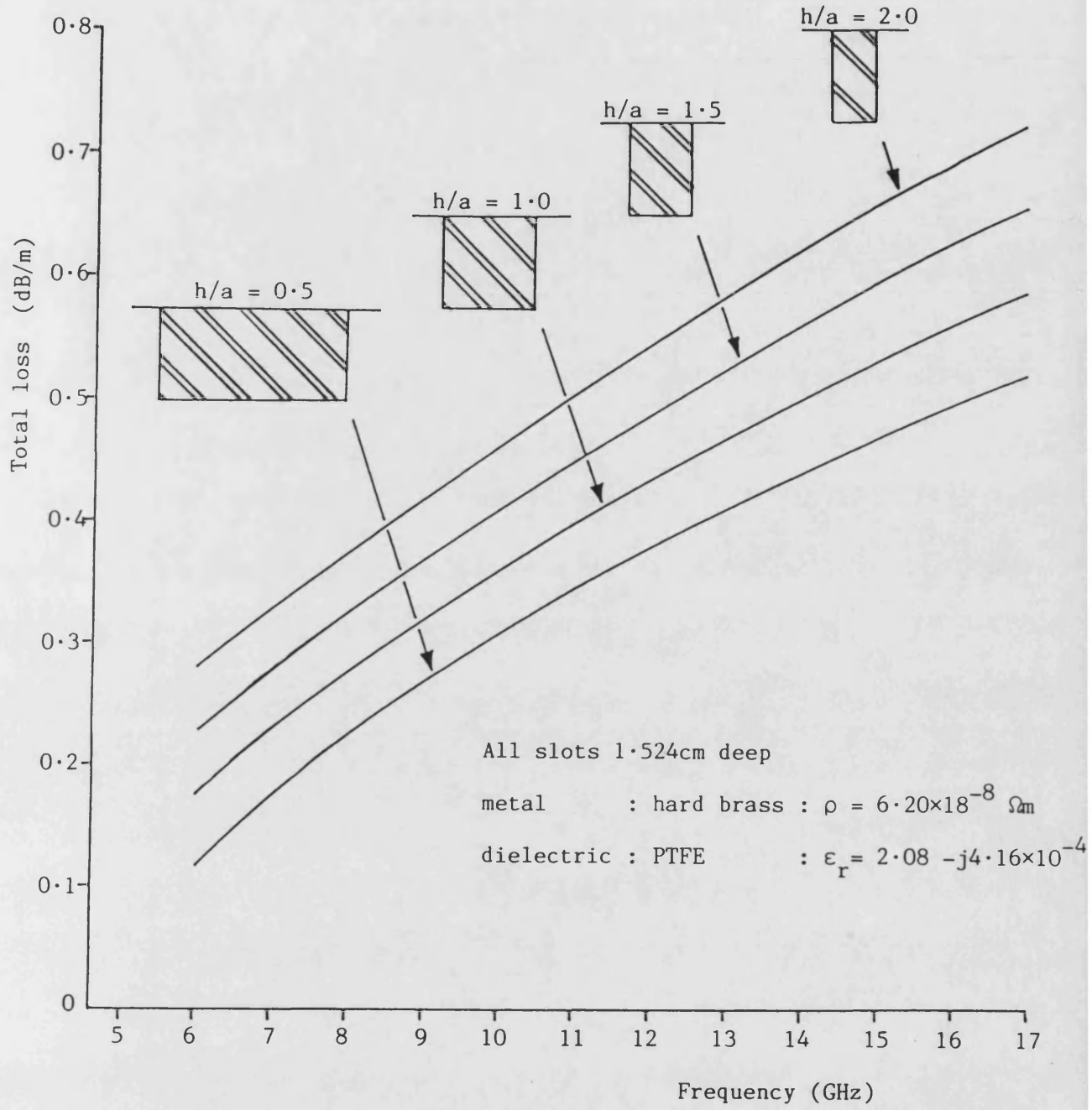

A comparison of the computed loss of four guides of different aspect ratios, made from the same materials and having the same cutoff frequencies

Figure 5-7

frequency (GHz)	conductor loss (dB/m)	dielectric loss (dB/m)	total loss (dB/m)	total loss (dB/λ)	Q-factor	confinement (%)
5·0	0·0558	0·0623	0·1181	0·0069	5453	33
6·0	0·0745	0·1096	0·1841	0·0085	3949	52
7·0	0·0828	0·1499	0·2327	0·0087	3467	64
8·0	0·0873	0·1869	0·2742	0·0087	3233	73
9·0	0·0898	0·2214	0·3112	0·0085	3108	79
10·0	0·0912	0·2539	0·3451	0·0083	3039	84
11·0	0·0921	0·2849	0·3770	0·0081	3001	87
12·0	0·0928	0·3147	0·4075	0·0078	2982	90
13·0	0·0932	0·3436	0·4368	0·0077	2974	92
14·0	0·0938	0·3719	0·4657	0·0075	2972	93
15·0	0·0943	0·3998	0·4941	0·0074	2974	94
16·0	0·0949	0·4272	0·5221	0·0072	2979	95

The computed loss values for IDG with: a = 3·048cm, h = 1·524cm (h/a = 0·5) $\varepsilon_r = 2{\cdot}08 - j4{\cdot}16\times10^{-4}$ (PTFE)

$\rho = 6{\cdot}20\times10^{-8}\,\Omega\,m$ (brass)

TABLE 5-4a

frequency (GHz)	conductor loss (dB/m)	dielectric loss (dB/m)	total loss (dB/m)	total loss (dB/λ)	Q-factor	confinement (%)
5·0	0·0955	0·0799	0·1754	0·0103	3657	43
6·0	0·1167	0·1208	0·2375	0·0108	3021	58
7·0	0·1274	0·1552	0·2826	0·0105	2816	67
8·0	0·1351	0·1882	0·3233	0·0101	2711	74
9·0	0·1411	0·2203	0·3614	0·0098	2652	80
10·0	0·1459	0·2516	0·3975	0·0094	2621	84
11·0	0·1499	0·2820	0·4319	0·0092	2606	87
12·0	0·1534	0·3116	0·4650	0·0089	2601	89
13·0	0·1566	0·3407	0·4973	0·0087	2604	91
14·0	0·1596	0·3692	0·5288	0·0085	2611	93
15·0	0·1624	0·3972	0·5596	0·0083	2620	94
16·0	0·1652	0·4249	0·5901	0·0082	2632	95

The computed loss values for IDG with: a = 1·524cm, h =1.524cm (h/a = 1·0) $\varepsilon_r = 2{\cdot}08 - j4{\cdot}16\times10^{-4}$(PTFE)
$\rho = 6{\cdot}20\times10^{-8}$ Ωm (brass)

TABLE 5-4b

frequency (GHz)	conductor loss (dB/m)	dielectric loss (dB/m)	total loss (dB/m)	total loss (dB/λ)	Q-factor	confinement (%)
5·0	0·1364	0·0916	0·2280	0·0133	2805	50
6·0	0·1593	0·1286	0·2879	0·0130	2470	63
7·0	0·1721	0·1597	0·3318	0·0122	2376	70
8·0	0·1826	0·1903	0·3729	0·0116	2331	76
9·0	0·1917	0·2207	0·4124	0·0111	2308	80
10·0	0·1997	0·2507	0·4504	0·0106	2298	84
11·0	0·2068	0·2804	0·4872	0·0103	2298	87
12·0	0·2133	0·3097	0·5230	0·0100	2304	89
13·0	0·2193	0·3385	0·5578	0·0097	2314	91
14·0	0·2249	0·3670	0·5919	0·0095	2326	92
15·0	0·2302	0·3951	0·6253	0·0093	2340	94
16·0	0·2352	0·4229	0·6581	0·0091	2356	95

The computed loss values for IDG with: a = 1·016cm, h = 1·524cm (h/a =1·5) $\varepsilon_r = 2{\cdot}08 - j4{\cdot}16\times10^{-4}$ (PTFE)
$\rho = 6{\cdot}20\times10^{-8}$ Ωm (brass)

TABLE 5-4c

frequency (GHz)	conductor loss (dB/m)	dielectric loss (dB/m)	total loss (dB/m)	total loss (dB/λ)	Q-factor	confinement (%)
5·0	0·1785	0·0999	0·2784	0·0162	2291	54
6·0	0·2024	0·1344	0·3368	0·0151	2097	66
7·0	0·2169	0·1635	0·3804	0·0139	2057	72
8·0	0·2300	0·1924	0·4224	0·0130	2044	77
9·0	0·2420	0·2215	0·4635	0·0124	2041	81
10·0	0·2530	0·2506	0·5036	0·0119	2046	84
11·0	0·2632	0·2797	0·5429	0·0114	2055	87
12·0	0·2728	0·3088	0·5816	0·0111	2068	89
13·0	0·2814	0·3371	0·6185	0·0108	2081	91
14·0	0·2896	0·3655	0·6551	0·0105	2097	92
15·0	0·2973	0·3936	0·6909	0·0102	2114	93
16·0	0·3048	0·4214	0·7262	0·0100	2132	94

The computed loss values for IDG with: a = 0·762cm, h = 1·524cm (h/a = 2·0) $\varepsilon_r = 2{\cdot}08 - j4{\cdot}16\times10^{-4}$ (PTFE)
$\rho = 6{\cdot}20\times10^{-8}$ Ωm (brass)

TABLE 5-4d

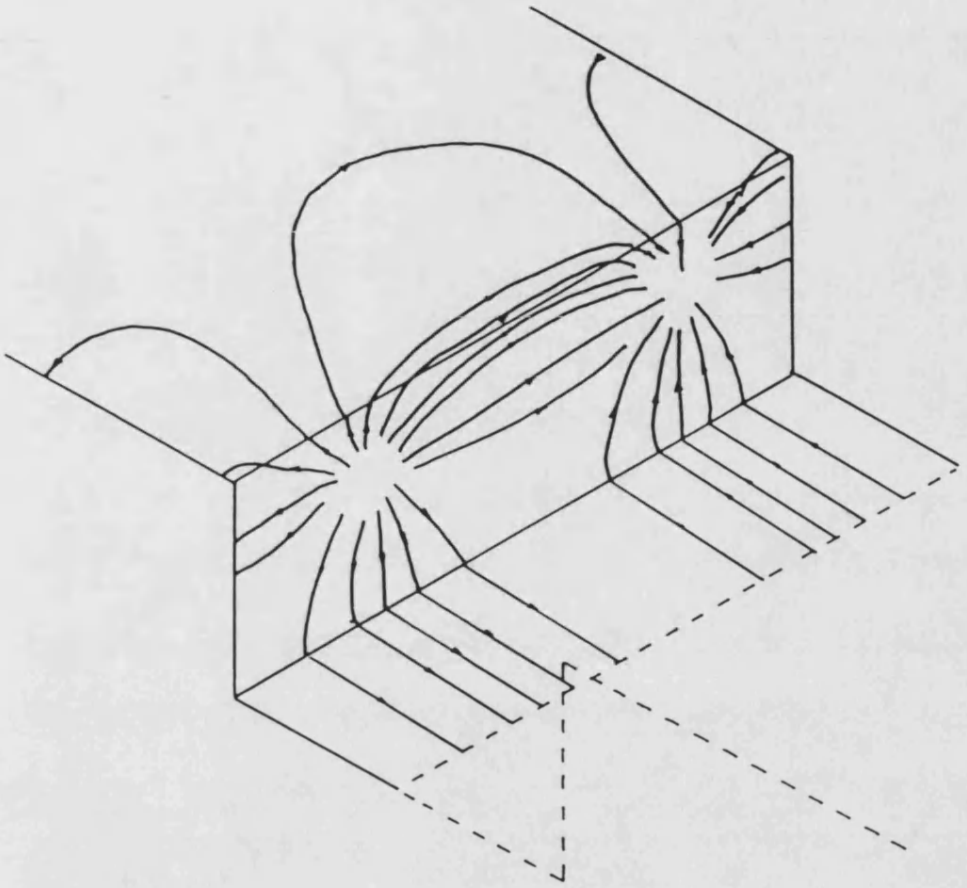

A sketch of the current distribution associated with the fundamental HE_{01} mode of IDG

Figure 5-8

ground plane, sidewalls and slot floor are tabulated in Table 5.5 for the four guides of Fig. 5-7 at 8 GHz. To further aid the discussion the confinement factor of these guides is plotted in Fig. 5-9.

It can be seen that the wider, more open guide has the lowest confinement factor but that all the guides tend to the same value with increasing frequency. This situation can be crudely explained with reference to the case of a dielectric filled parallel plate guide radiating into freespace. A narrower gap between the plates will increase the guide impedance and cause a larger reflection at the transition to the air region. However,as the frequency is increased (and $\beta \rightarrow \sqrt{\varepsilon_r}\, k_0$), and the radiation impedance becomes more reactive the reflection (and hence, confinement) becomes large for guides of all widths.

From Table 5.5 it can be seen that, as the aspect ratio is increased and the field confinement in the slot region increases the conductor loss also increases. As expected the major contribution to the conductor loss in all cases is from the slot sidewalls. As the aspect ratio is increased both the ground plane and slot floor components decrease with respect to the sidewall losses. This is due to the reduced field in the air region, in the case of the ground plane component, and to the relative reduction in slot floor areas in the case of the slot floor component.

To further illustrate the increase in field confinement to the slot with frequency, the real part of the z-directed poynting vector was plotted over the transverse cross-section for a particular guide for three different frequencies. This is shown in Fig. 5-10 and the shift in energy density from almost uniform just above cutoff to

aspect ratio (h/a)	conductor loss contributions normalised to Psw			total loss (dB/m)
	Psw	Pf	Pg	
0·5	1·0	0·4485	0·2424	0·2742
1·0	1·0	0·2409	0·2149	0·3233
1·5	1·0	0·1619	0·1892	0·3729
2·0	1·0	0·1208	0·1679	0·4224

Psw = conductor loss due to slot sidewalls

Pf = conductor loss due to slot floor

Pg = conductor loss due to ground plane

The relative contributions to the conductor loss arising from the slot sidewalls, floor, and ground plane, for the four guides of table 5-4 at 8·0 GHz.

Table 5-5

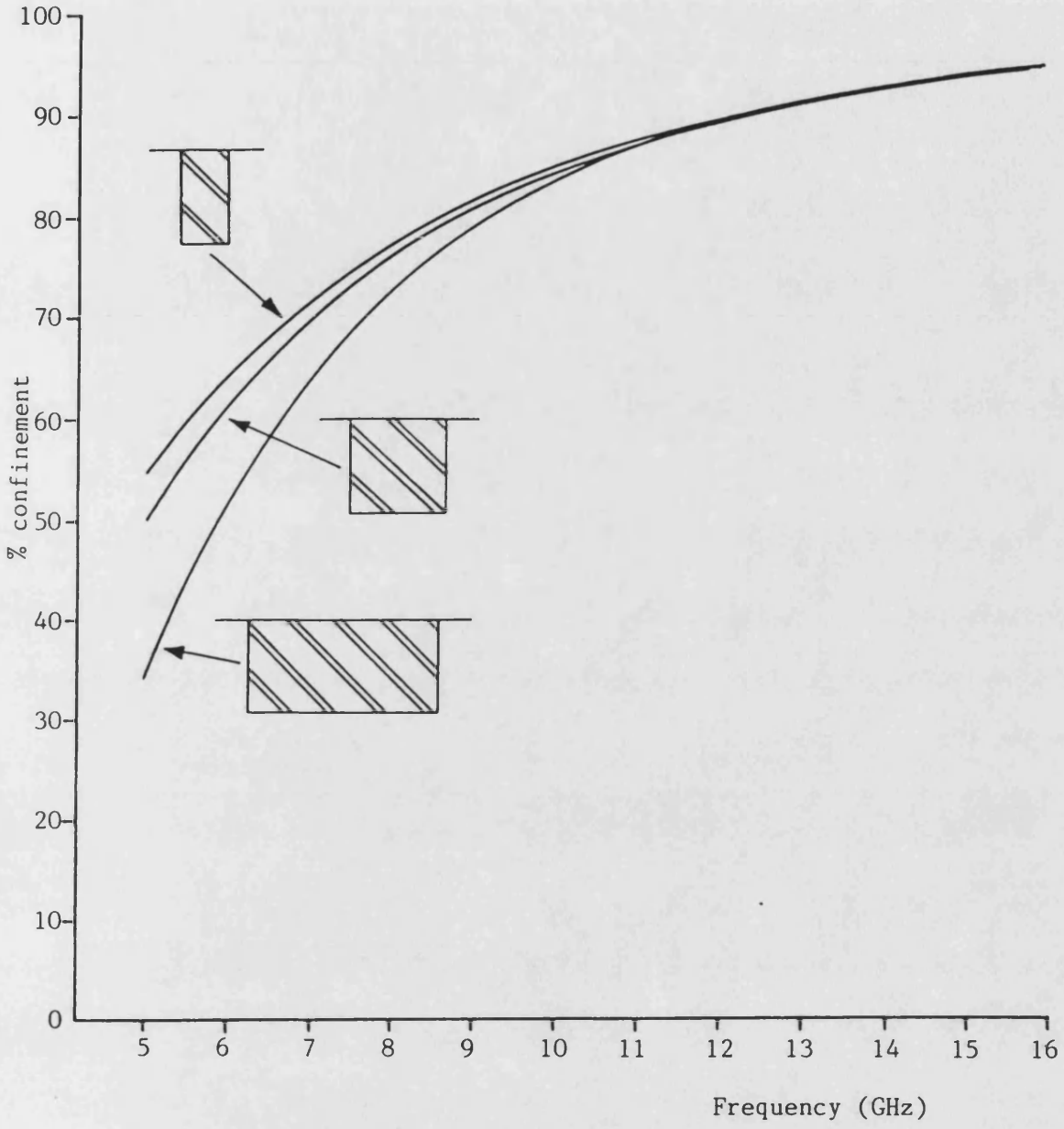

Plots of the confinement factor for three guides taken from tables 5-4

Figure 5-9

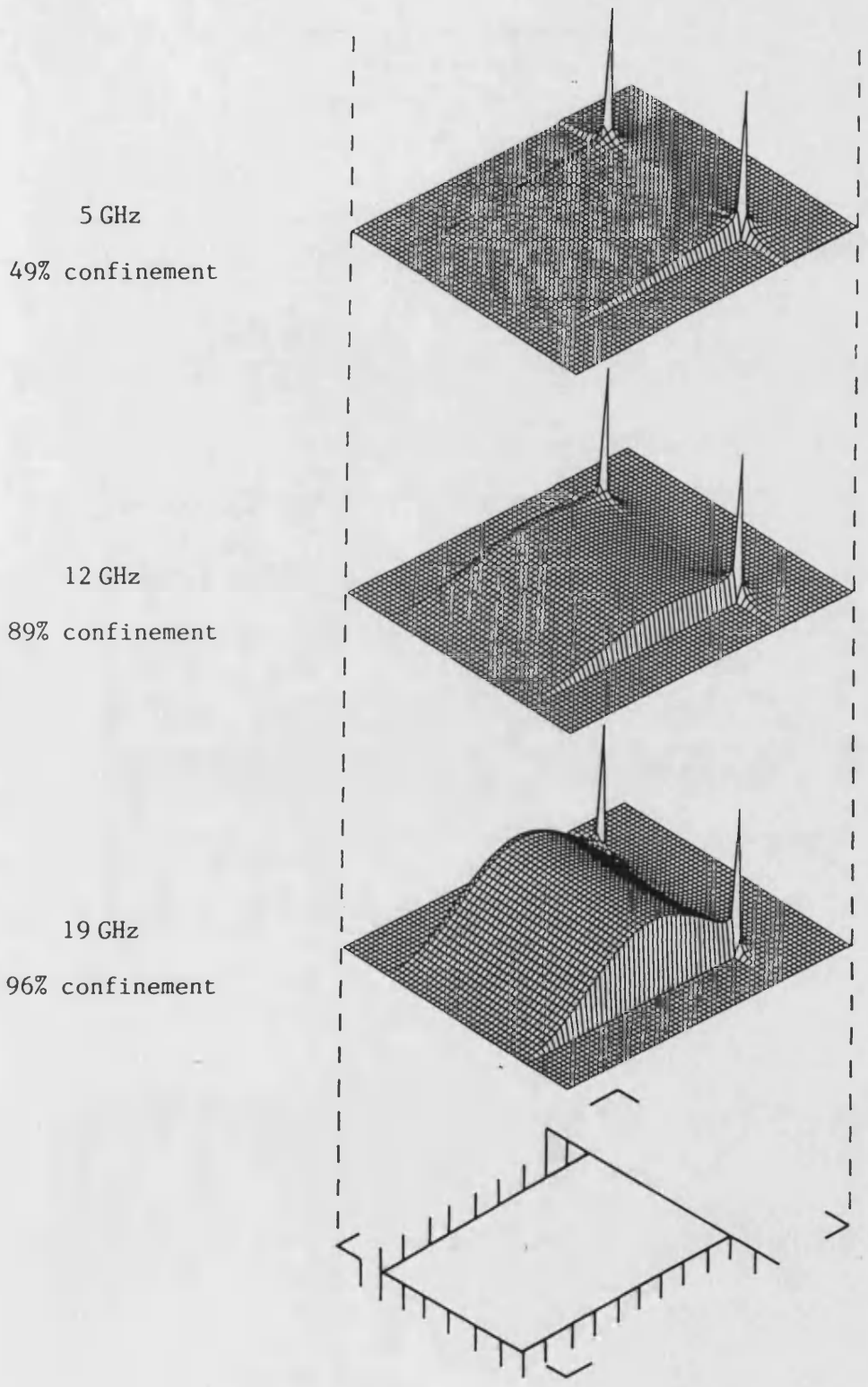

The magnitude of Re|E × H*| plotted over the transverse cross section of a guide at three different frequencies.

Figure 5-10

almost total confinement well above cutoff is clearly evident.

In Table 5.6 the computed loss values for three guides are given which have the following dielectric inserts:

P.T.F.E.:	$\varepsilon_r = 2.08 - j0.000416$	($\tan\delta = 0.0002$)
Polystyrene:	$\varepsilon_r = 2.54 - j0.00304$	($\tan\delta = 0.0012$)
Alumina:	$\varepsilon_r = 8.30 - j0.002656$	($\tan\delta = 0.00032$)

The slot depths were chosen so as to give the same cutoff frequency for each guide. The overall loss of these three examples are plotted in Fig. 5-11 and illustrate that the loss is dependent upon the $\tan\delta$ value of the dielectric and not the magnitude of the imaginary part of the permittivity. This is to be expected since the field is guided by a smaller volume of dielectric in a high permittivity guide which offsets the fact that the dissipation per unit volume may be higher. From this example it may appear that there is no real advantage to be gained by using a high or low permittivity dielectric as long as the $\tan\delta$ value is the same. Practically, however, it is easier to manufacture the lower permittivity structure. This is because the wavelength is reduced in a high dielectric material which increases the mechanical tolerances (which are a function of the guided wavelength).

The results of this section clearly indicate that the dominant source of loss in practical IDG samples (i.e. well machined slots, good conductors) is due to dissipation in the dielectric medium. The simplest way to reduce the guide loss is therefore to choose a dielectric material with a lower $\tan\delta$ value. Of the conductor loss components the highest dissipation is on the slot sidewalls, where the current flow is largest. One possible way of reducing the loss is thus to lower the dielectric in the slot and reduce the field at

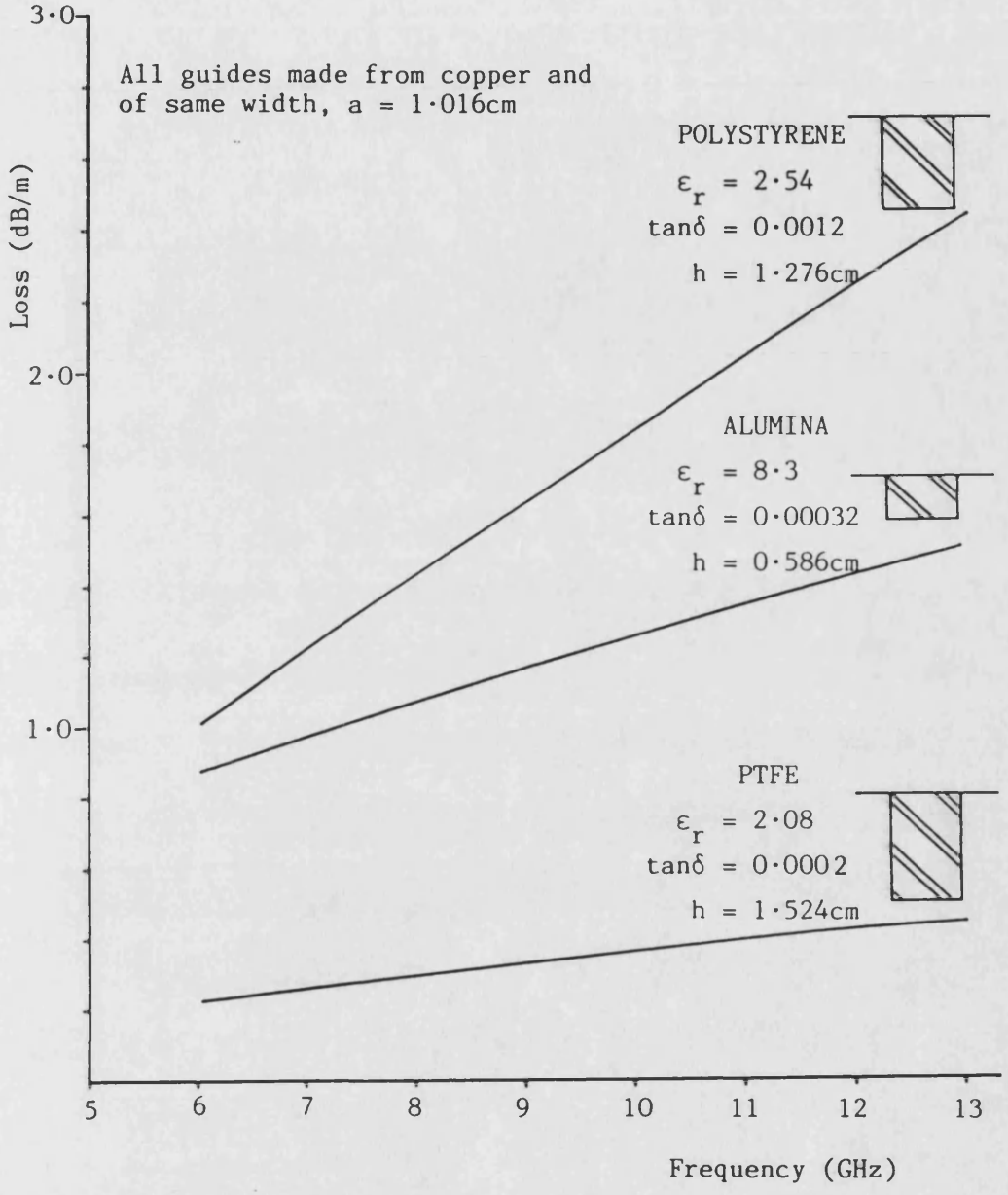

The computed loss for three guides with different dielectric inserts and slot depths so as to maintain the same cutoff frequency.

Figure 5-11

the slot edge, the region of highest current density. This is illustrated in the measured Q values of Fig. 5-5. This method increases the complexity of the manufacturing process. Another more practical way is to widen the slot so that the field at the sidewall is reduced. Care must then be taken to avoid the excitation of higher order modes since the monomode bandwidth is then reduced (see Fig. 4-4.).

5-11 Comparison with Measured Values

The loss components were computed for the X-band test pieces in order that a comparison could be made between the computed and measured results. The test pieces were constructed from hard brass and so a resistivity value of $\rho = 6.2 \times 10^{-6}$ Ω/m was used in the conductor loss calculations. However, since the exact nature of the brass composition was not known and the conductor loss components have a $\sqrt{\rho}$ dependence, a small error can be expected. Published values for brass lie in the range $3 - 7 \times 10^{-6}$ Ω/m according to the alloy. The dielectric material used was P.T.F.E. Again, an uncertainty in the value of permittivity of ± 2% can be expected to cause a small error. However both errors are small when compared to the accuracy of the analysis. The perturbation approach used to determine the loss values can be expected at best to give the order of the loss and its frequency dependence.

The loss was computed for two filled slots, with widths 1.016 cm and aspect ratios 1.5 and 1. The loss was measured by the substitution method and by determining the Q value as outlined in Section 5-9. The comparison between measured and computed values for the guides is shown in Figs.5-12, 5-13 and 5-14.

The agreement can be seen to be quite good, especially at the top end of the waveguide band. The discrepancy at the lower end is thought to be mainly due to the radiation loss of the guides, which is not accounted for in the analysis. It is noted however that in the regions of practical importance the correlation between measurement and theory is good and the computed values give usable results for design purposes.

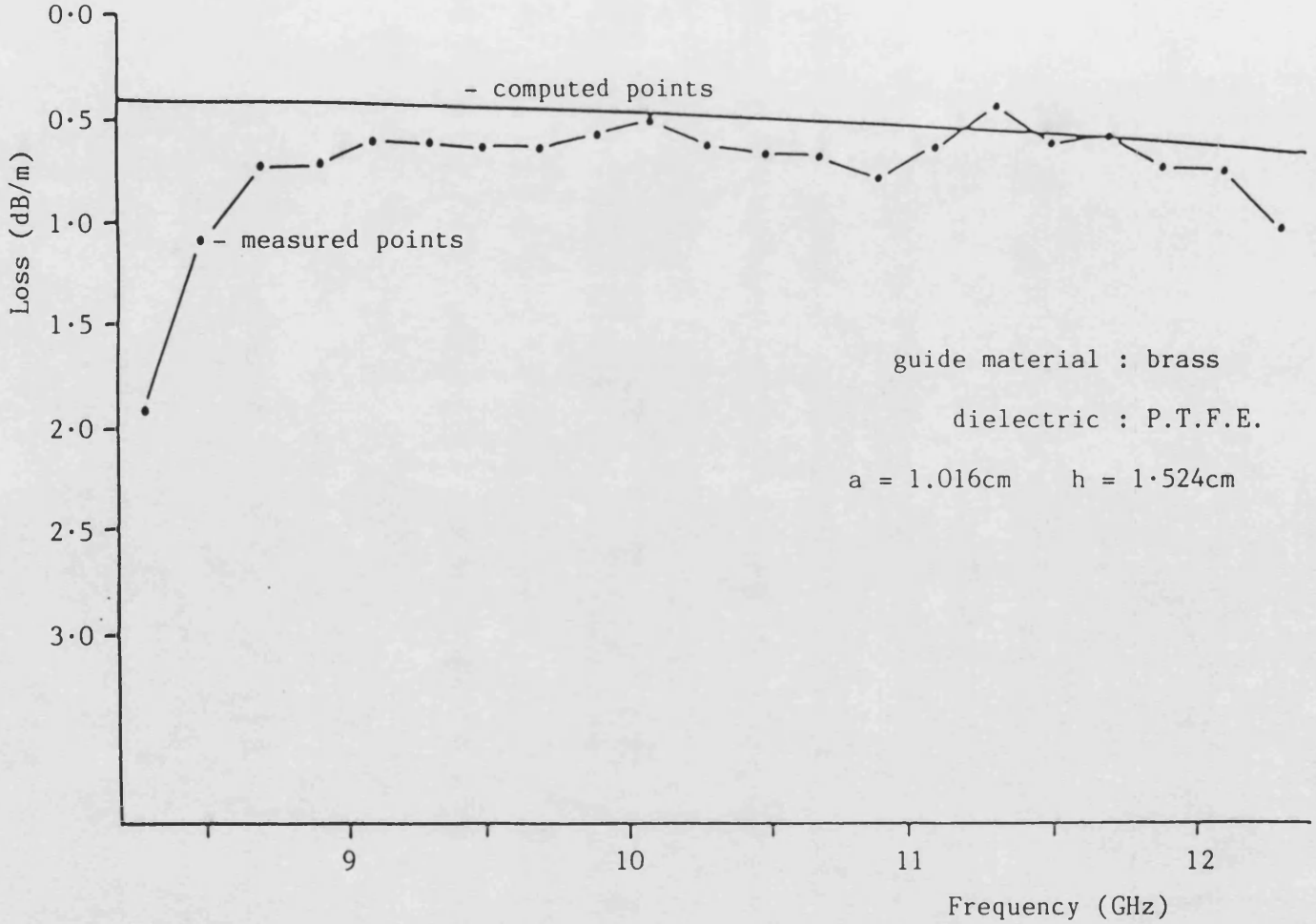

The measured and computed loss of a section of IDG

Figure 5-12

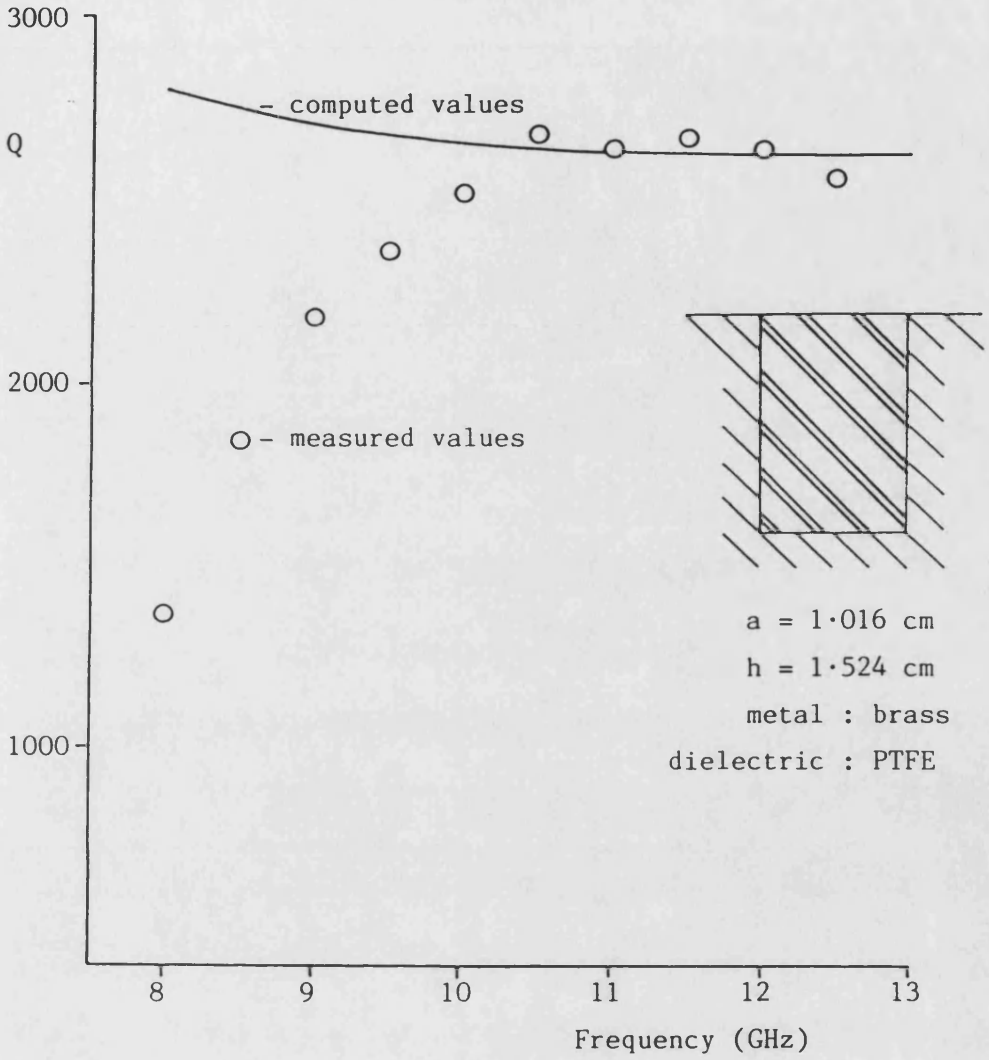

The computed and measured Q values for a resonant section of IDG

Figure 5-13

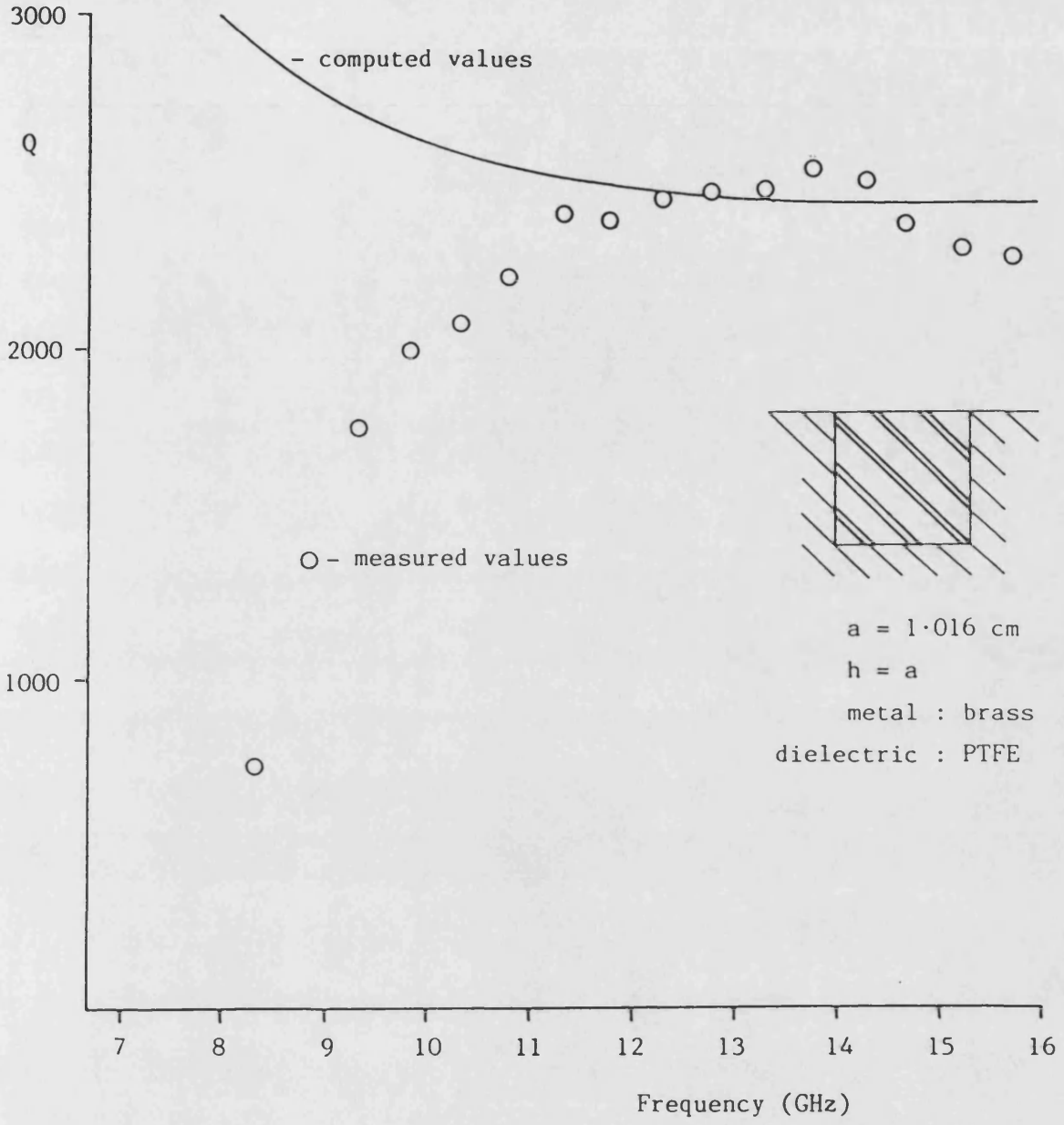

The computed and measured Q values for a resonant section of IDG

Figure 5-14

5-12 The Loss from Bends

A limitation of most dielectric waveguides with geometries simple enough for practical device fabrication is the loss from bends. Any open structure must suffer some radiation loss from bends since the field can extend far away from the guide. On a straight section all the field components (of a particular mode) have the same velocity with the constant phase fronts transverse to the guide axis. To propagate around a curved path whilst maintaining a constant phase front transverse to the curve, however, requires that all the field components have the same angular velocity. Since the field can extend far from the guide this implies that at some distance from the centre of the curvature the field components must have linear velocities in excess of the velocity of light. This is physically impossible and so such components must de-couple into either a radiation field or a lower velocity mode. By considering the proportion of the "straight" field that would be forced to exceed the freespace velocity on a bend, some estimate of the order of the bend loss can be made [4].

The perturbation of the guided field on a bend can be reduced by either increasing the field confinement, so that less field can extend transverse to the guide, or by increasing the radius of the bend, so that the linear velocity a certain distance from the guide is reduced. It it possible then, to choose a bend geometry such that the radiation loss is within an acceptable level. This has led to the derivation of a "minimum bend radius" as a design aid for the various open structures such as image line [5].

Even if the field on a bend is only a small perturbation of the straight line field, a discontinuity will exist at the transition between the two fields. The coupling between the phase front of the straightline field

with the "tilted" phase front of the bend field is given by the projection of one onto the other and indicates that the amount of coupling will decrease with decreasing bend radius. Thus the transition between the two fields can be viewed as an impedance step, as the "effective cross section" of the guide is changed. The loss of a bend will thus consist of two components. At each end of the bend there will be a reflection of incident power due to the field discontinuity, as well as the continual radiation loss as the field propagates along the bend.

The analysis of the bend structure involves computing the bend field and determining the coupling to the fundamental even mode on the straight sections. Since the field solutions have already been obtained rigorously for the straight geometry it is economic to use them in the construction of the bend field. Such a construction considers the field over any transverse plane to the bend axis to be the superposition of the transverse field solutions of the straight section. This is the so called "local modes" formulation [6]. The curved axis then causes a coupling between the local modes as they propagate around the bend. The major source of loss from the fundamental even mode will be the coupling to odd radiation modes. These will be excited by the asymmetry of the bend structure, as there are no bound odd modes propagating over the frequency range of interest. Such a rigorous bend analysis is not within the scope of the present work and so is not included here.

In order to obtain a practical evaluation of the loss from IDG bends, two 90^{o} bends were constructed and measured. For compatibility with the existing test pieces they were machined from brass with a PTFE filled slot of dimensions a = 1.016 cm, $^{h}/a = 1.5$. The minimum radius of the 90^{o} bend was dictated by the mechanical fixing to the

straight line sections and was 4.4 cm measured to the centre of the slot. The largest bend radius was governed by the cost of brass and was chosen to be 15 cm. The ratio of the bend radius to guide wavelength at 10 GHz for these bends was 1.9 and 6.3 respectively.

The insertion loss of these two bends, measured by a substitution method is shown in Fig.5-15. The accuracy of the measurement was again hindered by the bending of the coaxial cables on the network analyser. The system was calibrated for waveguide at the APC-7 to rectangular waveguide transitions. The transmission loss of two sections of IDG plus rectangular waveguide to IDG transitions was then measured and stored in the memory of the analyser. The bends were then individually inserted between the two sections, and the measured response was then divided by the memory to give the insertion loss of each bend. Relative cable bend between measurements was thus unavoidable. The Q values for the bend sections were measured in the same way as for the straight section, using the same irises. The measured values are given in Table 5.7 and are shown graphically in Fig. 5-16 with the straight line values also included as a comparison.

The Q value measurements clearly show the bend characteristic of decreasing loss with frequency. This is due to the increase in both field confinement and the electrical length of the bend radius as the frequency is increased, and is shown by the convergence of the straight line and bend values in Fig. 5-16. At 11 GHz the 15 cm radius bend has a similar Q-value to that of the straight section, indicating that the bend radiation loss has fallen to a negligible value. Assuming the same value of β as for the straight line, at 11 GHz the bend radius normalised to guide wavelength is 7. It is not good practice to make a judgement based on the results of only one measurement, but perhaps

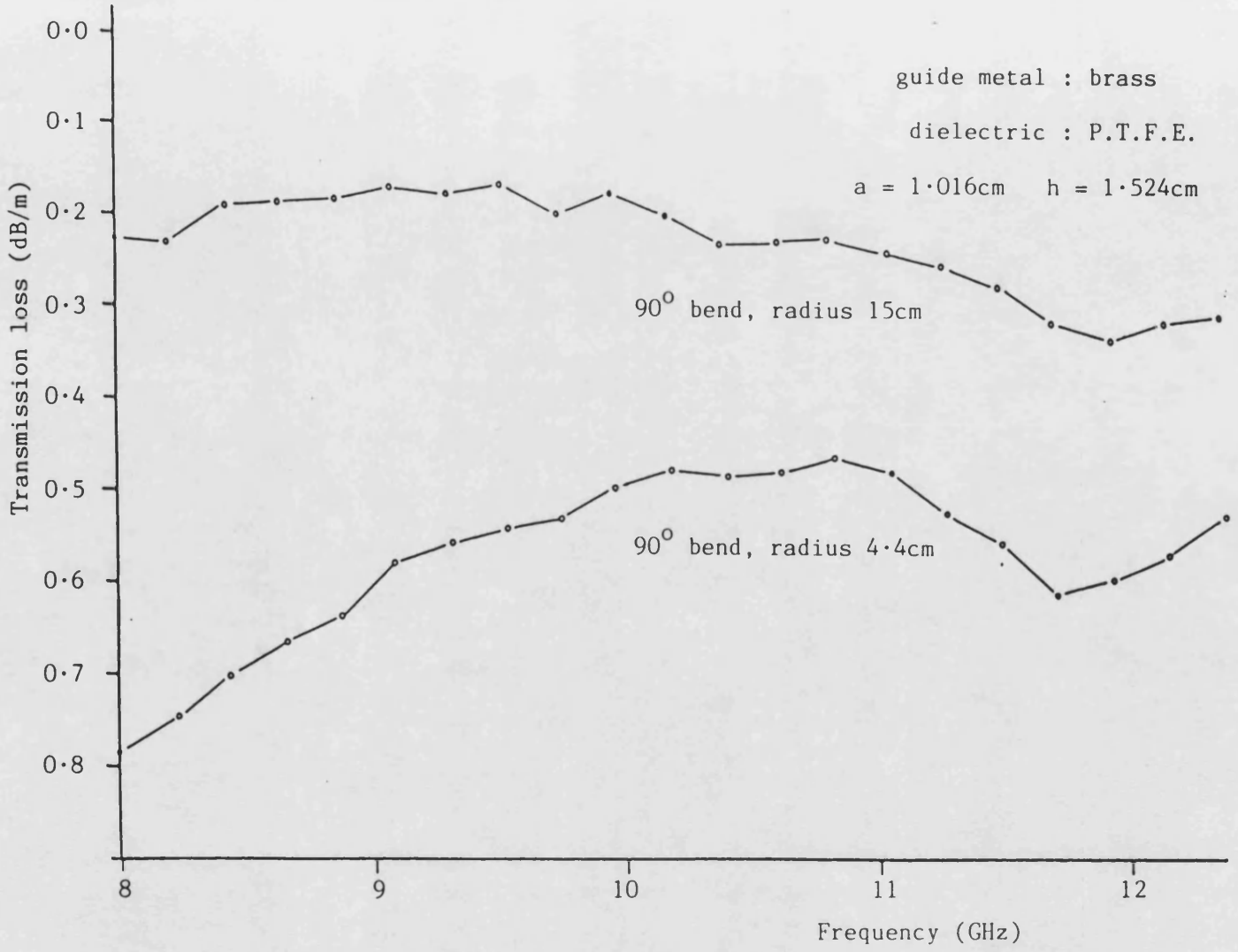

The measured transmission loss of the two 90° bends in IDG, measured using a substitution method.

Figure 5-15

this normalised value could provide a "minimum guide radius" figure for IDG of $^{h}/a = 1.5$ and $\varepsilon_r = 2.08$.

Whist the Q values of the straight and 15 cm radius bend sections are similar at 11 GHz, there is a marked difference in the substitution measurements at this frequency. The reason for this is that the Q-value gives a measure of the loss of a resonant section of line, whilst the substitution result also includes the loss of the transitions between the straight and curved sections. Assuming that the loss per unit length is identical for both the bend and straight line at 11 GHz, some estimate of the loss of these transitions can be made.

Straight line loss @ 11 GHz 0.6 dB/m (from Fig. 5-12)

Length of bend $= 2\pi \times 15/4 = 23.6$ cm

$\therefore$ Bend loss $= 0.236 \quad 0.6 = 0.14$ dB

Measured loss by substitution method @ 11 GHz $\simeq 0.25$ dB

$\therefore$ Insertion loss of each transition $= \frac{0.25 - 0.14}{2} = 0.055$ dB

This value corresponds to a return loss of 19 dB, which is a standing wave ratio (SWR) of 1.253 : 1.

The measured Q values for the 90^{o} bend of 4.4 cm radius were lower than would be expected from the substitution results. The Q value measurement is not very accurate for this bend since with an axial length of only 6 cm which is only 2 or 3 guide wavelengths at X-Band frequencies, the resonant length is not sufficiently long to enable the end losses to be neglected.

Although the 15 cm radius bend gave an acceptable performance, it's size would be rather impractical at X-Band frequencies. However, at frequencies above 100 GHz where IDG is intended for use, size is not a major concern and the normalised bend radii may even have to be larger, to reduce the fabrication difficulties.

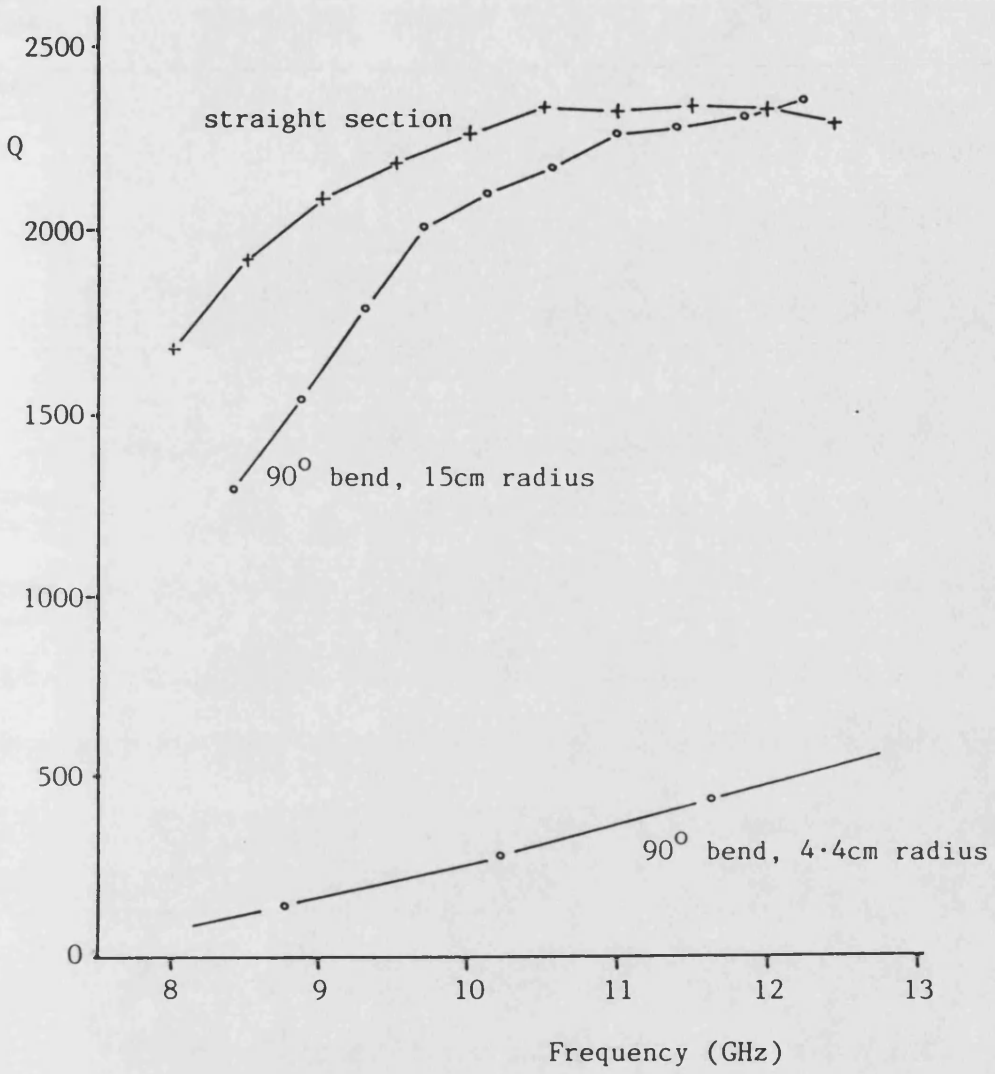

The measured Q values of two 90° bends compared with those obtained for a straight section. The guides are made from brass and PTFE with h/a = 1·5 and a = 1·016cm.

Figure 5-16

centre frequency at resonance (GHz)	Q
8·018	1685
8·512	1926
9·006	2094
9·501	2179
9·995	2261
10·490	2342
10·986	2318
11·482	2334
11·977	2319
12·473	2279

Straight section

(a)

centre frequency at resonance (GHz)	Q
8·417	1293
8·845	1539
9·273	1795
9·701	2010
10·128	2099
10·556	2172
10·983	2260
11·412	2270
11·839	2304
12·267	2347

90^{o} bend, radius 15cm

(b)

centre frequency at resonance (GHz)	Q
8·771	149
10.199	285
11·629	439

90^{o} bend, radius 4·4cm

(c)

The measured Q values of a straight section and two 90^{o} bends in IDG.

Guides made from brass with PTFE inserts. Slot cross section 1·016cm × 1·524cm.

Table 5-6

5-13 A Theoretical Comparison with Image and Insular Guides

Much work has been undertaken in recent years to demonstrate the feasibility of using Image and Insular Guides for high frequency integrated circuit construction. Gelsthorpe et al [7] have studied these media and have given the theoretical loss curves for guides designed to operate across W-Band (70 - 110 GHz). These loss curves were evaluated from the EDC method and so are only valid for guides well above cutoff when the radiation loss can be neglected. In order to minimize the radiation loss from bends in Image and Insular lines, a high permittivity material is necessary to increase the field confinement in the guiding layer. In [7] lines of permittivity 9.8 (alumina) were used in the analysis, their dimensions being chosen so as to give the same propagation characteristics at 90 GHz. Thus for comparison purposes the IDG structure was chosen to have approximately the same propagation characteristics at 90 GHz with alumina dielectric. The dimensions of the three structures and the dispersion curves over the W-Band range are shown in Fig. 5-17.

In order to compute the loss curves a dielectric loss tangent of 0.001 has been assumed. All the metal surfaces were taken as thick film gold with a conductivity of 24.7×10^6 s/m. The computed loss curves for three structures are given in Fig. 5-18. In comparing these results, it is noted that the IDG has a comparable loss to the image line, with an increase in both the dielectric and conductor loss components over image line at the lower frequencies. This is not unexpected since in IDG the increased conductor area over image line will produce greater field confinement in the dielectric as well as increasing the resistive losses by the wall currents. The conductor loss of the insular line can be seen to decrease with increasing

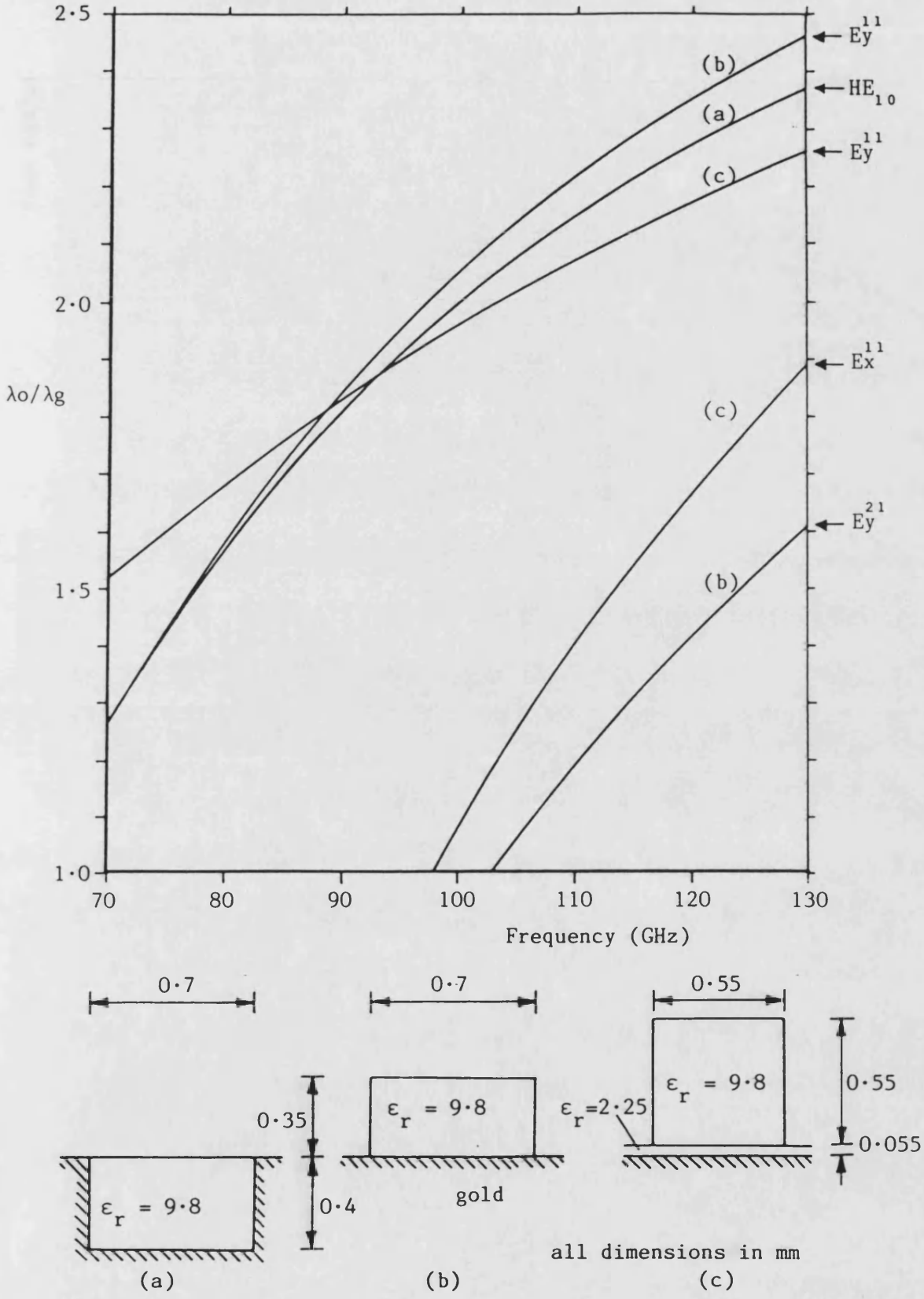

The dispersion characteristics and the dimensions of the three guides used for the loss comparion (curves (b) and (c) taken from [7])

Figure 5-17

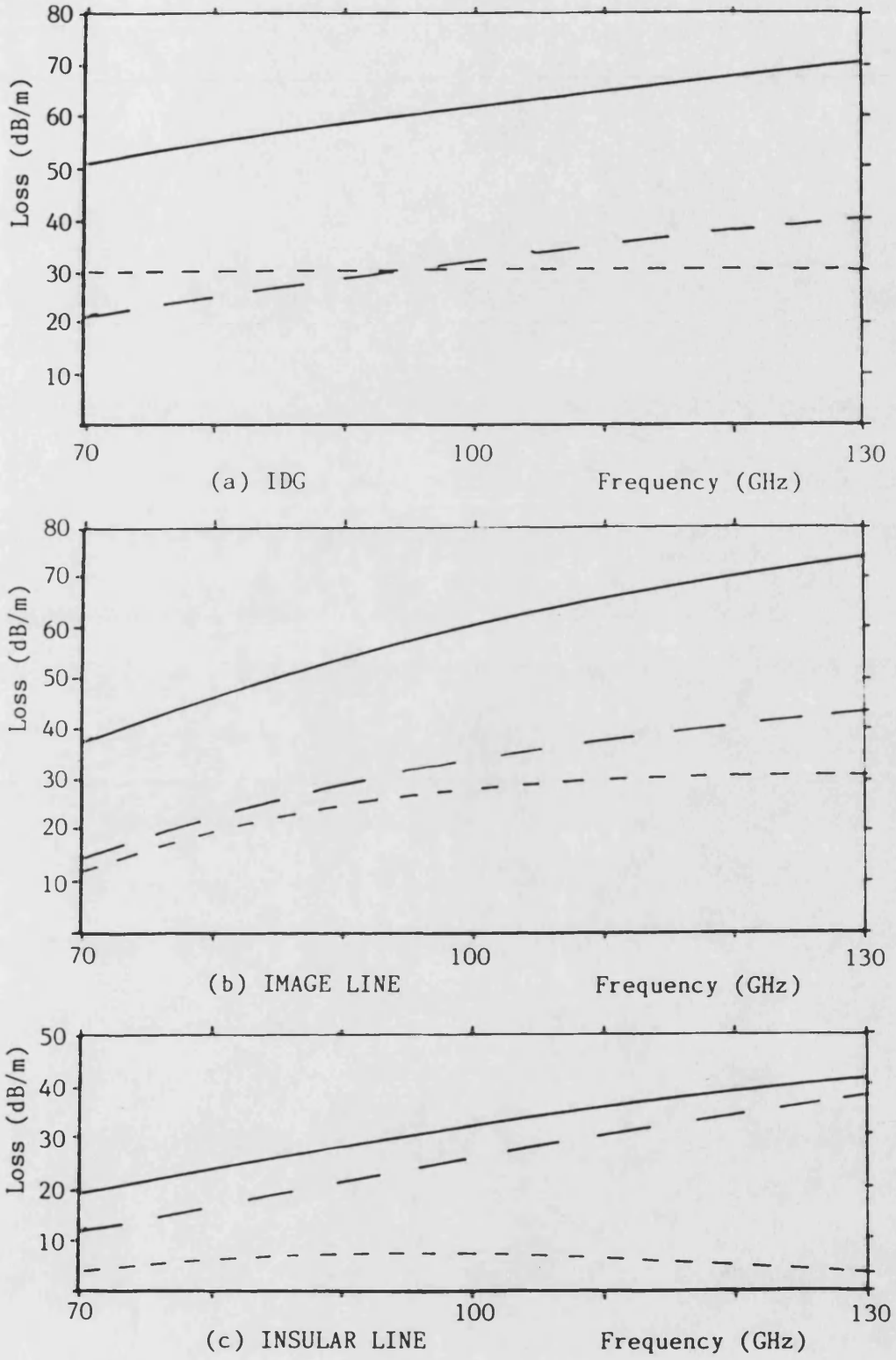

The computed loss curves for the three guides of fig.5-17

(curves (b) and (c) taken from [7])

Figure 5-18

frequency as the field becomes increasingly more confined to the high permittivity dielectric and so reduces the field at the conductor surface. A similiar trend is observed in the IDG conductor loss curve. This is thought to the increased field confinement into the slot, since the field maximum, by moving deeper into the slot, will reduce the magnitude of the surface currents in the vicinity of the 90^{o} metal edges.

The theoretical curves are of course for idealised structures and in practice the loss can be expected to be higher, for two main resons. Firstly, the physical structures will contain rounded corners and other departures from the ideal case, due to material inhomogenities and limitations in the fabrication process. Hence radiation will be excited along with coupling to higher order modes. This can be expected to be especially problematic for image line which is a more open structure than IDG. As an example, in [8] it is reported that a section of image line which had a thick film printed dielectric layer (and hence a rounded profile) had double the loss of an identical guide with an accurately machined dielectric line. It is interesting to note that in this reference the image line to rectangular waveguide transition had an SWR of 1·3 and a bandwidth of 5% at W-band frequencies. This can be compared to fig. 5-3. A second cause of increased loss over theoretical values will be due to the surface roughness of the conductors as discussed in section 5-6.

Since a dominant portion of the loss is due to dissipation in the dielectric, then a significant reduction in loss can be expected by using a dielectric with a lower tanδ value. However, for materials that are readily machined/extruded/sintered the tanδ tends to be lowest

for materials of low permittivity. Use of a low permittivity material also increases the circuit size, reduces the manufacturing tolerances, and reduces the dispersion. However, a high permittivity line is necessary for the image and insular line structures to provide sufficient field confinement to obtain acceptable bending loss. In IDG the confinement is mostly provided by the slot walls and a lower permittivity insert can be used without a degradation in practical performance. To illustrate the increase in performance that can be obtained an IDG structure with a PTFE insert was analysed. The width of the guide was chosen to allow a transition to rectangular waveguide (WG 27). A comparison between the computed loss for this and the alumina filled guide, along with the guide dimensions, is given in fig. 5-19. PTFE has a tanδ value that is an order of magnitude lower than that assumed here for alumina which is reflected by a dielectric loss component that is reduced accordingly. The increased dielectric volume in relation to the surface area of the slot walls also serves to reduce the conductor loss components.

This brief theoretical comparison has indicated that IDG and image line have comparable loss characteristics. However the loss of IDG over image line can be improved by choosing a lower loss, lower permittivity dielectric, which may not be applicable to the image line structure. The use of a lower permittivity material also has constructional advantages.

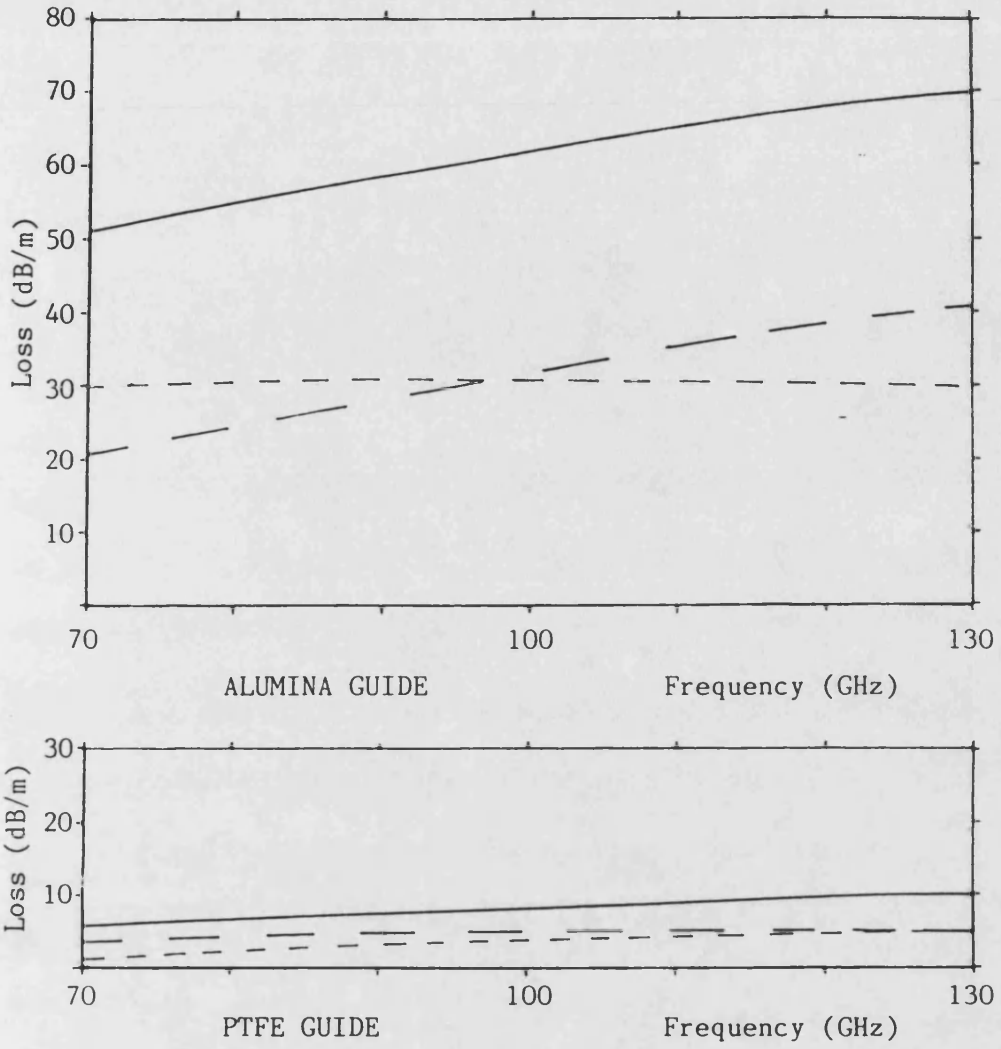

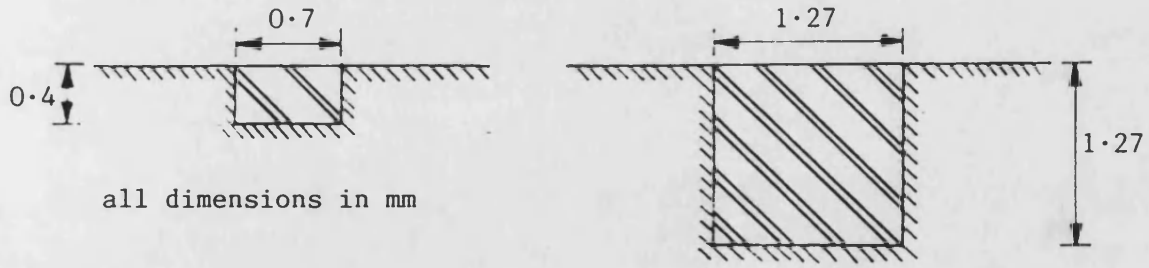

all dimensions in mm

ε_r = 9·8
tanδ = 0·001

ε_r = 2·08
tanδ = 0·0002

The computed loss curves for IDG of different dielectric filling designed to operate over the W-band range.

Figure 5-19

5-14 Concluding Remarks

This chapter has been concerned with the loss characteristics of IDG. Computed results for the loss have been given and reasonable correlation with measured values have been obtained.

The results have shown that the IDG loss can be predicted quite accurately for practical cases of interest, i.e. in the above cut-off, monomode region, and that the loss is comparable with or better than the popular alternatives. This improvement is due to two reasons. Image Line, Insular guide and IDG will all have zero radiation loss for an ideal structure operating in the above cutoff monomode region. However in the practical case the ideal structure will be impossible to achieve due to limitations in manufacturing techniques and material inhomogenities. In general it is easier to machine or stamp a slot in a metal to close tolerances than it is to screen print or machine a dielectric material. Thus it can be expected that at small dimensions especially, IDG could be made to more closely approach the ideal structure. A second reason for expected improvement is the increased shielding provided by the partial enclosure of the dielectric by the metal slot. These metal boundaries produce field confinement in the slot region without the need for a high permittivity dielectric as is required for Image Line. This relaxes the specification for the dielectric material and so one can be chosen with a lower loss tangent. Generally the lowest loss dielectrics have low values of permittivity. The dielectric loss is proportional to the order of the loss tangent and so large improvements can be expected over Image Line.

The computed results have of course been obtained for an ideal structure. Even at X-Band dimensions there will be surface imperfections and material inhomogenities that will excite radiation. Since the irregularities will be electrically larger at larger wavelengths and the guide is closer to exciting a leaky wave at lower frequencies, the correlation with measured results can be expected to be closer at high frequencies. This was illustrated most graphically by the Q-value measurements.

A contribution of practical importance to this work has been the experimental evaluation of the bending loss. This has indicated that bending loss on IDG is acceptable for practical component manufacture.

5-15 References

[1] T. Rozzi and L. Ma,"Mode completeness, Normalisation and Green's Function of the Inset Dielectric Guide", IEEE Trans Microwave Theory Tech.vol MTT-35, Nov 1987.

[2] F.A. Benson,"Waveguide Attenuation and it's Correlation with surface roughness", Proc. IEE.,1953, 100 pt III, p.85.

[3] F.A. Benson,"Attenuation of Rectangular Waveguide", Chapter 14, "Millimetre and Submillimetre Waves",Iliffe, London, 1969.

[4] E.A.J. Marcatili and S.E. Miller,"Improved Relations Describing Directional Control in Electromagnetic Wave Guidance", The Bell Syst. Tech. Journal, Sept 1969, pp.2161-2188.

[5] K. Solbach,"The Measurement of the Radiation Losses in Dielectric Image Line Bends and the Calculation of a Minimum Acceptable Curvature Radius", IEEE Trans Microwave Theory Tech., vol MTT-27, Jan 1979, pp.51-53.

[6] D. Marcuse, "Theory of Dielectric Optical Waveguides, Academic Press, New York, 1974.

[7] R.V. Gelsthorpe, N.Williams, and N.M. Davey,"Dielectric Waveguide; a Low-cost Technology for millimetre wave integrated circuits", The Radio and Electronic Engineer, vol 52, No. 11/12, pp. 522-538, Nov/Dec 1982.

[8] T.H. Oxley, P.L. Lowbridge, "Image Guide and Microstrip Integrated W-Band Receivers", Microwave Journal, vol 26, No.11, Nov 1983, pp 117-136.

CHAPTER SIX

CONCLUSION

6-1 Introduction

It is the objective of this concluding chapter to bring together the work of the preceeding five chapters and to present the major observations that have been made. A discussion of the results and their significance will enable suggestions to be made into further areas of work.

6-2 Discussion of the work presented in this thesis

The work presented in this thesis has been concerned with the analysis of Inset Dielectric Guide (IDG). This guide is intended for use in inter-grated circuit fabrication at frequencies above 100 GHz. In chapter one the practical importance of the millimetre wave portion of the microwave spectrum was discussed, including a brief survey of some of the wave guiding structures applicable over part, or all, of this frequency range. It is apparent that the choice of a particular structure for a certain application is the result of an engineering compromise between several factors, and that there is scope for the development of new structures. The IDG structure was then introduced as a practical evolution of image line with the potential for easier manufacture and improved performance.

A major aim of this work was the development of a rigorous method of analysis for IDG. The method, based upon the Transverse Resonance Diffraction (TRD) approach was introduced in chapter two. To put the TRD method into context, a brief review of some of the other methods of analysis was also given. The detailed explanation of the TRD formulation was given in chapter three. This involved the derivation of the field components from a transverse equivalent circuit model. The resonance of this circuit then gave a set of coupled integral equations in the electric field components transverse to y. These were then solved by Galerkin's method using a basis set that accurately modelled the electric field variation across the

slot.

Results obtained from the dispersion equation were given in chapter four. The method of computation was described, and the accurate choice of basis functions in the formulation of the dispersion equation was demonstrated by the fast convergence of the solution. The accuracy of the computed results for β was verified by excellent agreement with measured results. The fundamental hybrid field was essentially LSE_{01}, with constant electric field variation across the slot. The nature of the field is dependent upon the geometry of the guide. In this work a guide with $h/a > 1$ was generally used since this allowed efficient coupling to the fundamental grounded dielectric slab, the limiting case for IDG as $h/a \to 0$, is TM_{01} and so as the aspect ratio is decreased the hybrid field can be expected to become more LSM in nature.

The solution for β enabled the field components to be computed. These were plotted for several modes. The singularity in the field due to the edge discontinuity was clearly seen, as well as the LSE nature of the fields.

Chapter five was concerned with the loss of IDG. This can be separated into radiation, conduction and dielectric loss components. For an ideal IDG structure, diffraction of the slot field will only take place into the x-y plane. Thus for bound mode propagation, radiation can be neglected. This of course holdsonly for a straight line. When discontinuities such as bends are analysed then the radiation continuum must be considered. The dielectric loss was found by solving the dispersion equation for a complex permittivity, and the conduction loss, by a perturbation method using the expressions for the loss free fields. It was found that the dielectric loss was the dominant contribution to the overall loss. The major part of the conductor loss was due to the current components in

the slot sidewalls.

Comparisons between the computed and measured loss values for two IDG geometries showed good agreement, although there was evidence of some radiation loss at lower frequencies. This was thought to be due to surface abrasions and dielectric inhomogenities in the measured samples that were a departure from the ideal structure assumed in the analysis. Of considerable practical importance is the loss from bends since this is an inherent problem with open structures of this type. Measurements taken on two 90^0 bends gave good results and demonstrated that low loss bends are feasible in IDG.

Theoretical comparisons with image and insular line at W-Band showed that IDG has a comparable loss to image line. The guides were fabricated from alumina, with dimensions chosen to give the same dispersion at 90GHz. However, IDG can be fabricated from a lower loss dielectric, since it does not rely on a high permittivity material for its field confinement. Since the loss of both image line and IDG is due mostly to dielectric loss, the ability to be able to use low loss dielectric material is a considerable practical advantage. The improvement to be gained was demonstrated by computing the loss for a PTFE filled guide at W-Band.

6-3 Further Work arising from this work

The investigation of IDG presented here is by no means complete and the work has highlighted several areas in which further work could be directed. These include:-

i) Investigate Component Design in IDG

This includes the design and experimental verification of such passive devices as couplers and filters which are important system components. The field in IDG with a constant electric field across the slot, and a maximum near the slot surface is ideally suited for the integration of

a diode. This needs to be investigated experimentally. A demonstration of a practical method of diode integration in a dielectic guide would dispell one of the major criticisms of dielectric guides. This work must also address the question of how an impedance parameter can be defined so as to aid the matching of "lumped element" devices such as diodes into IDG circuits.

ii) Investigate Fabrication Techniques

For the experimental work of this thesis the guides were fabricated by machining the dielectric inserts to fit a machined slot. At the small dimensions required for high frequency circuits this would be impractical. Alternative methods such as electroforming need to be evaluated and the tolerances achievable assessed. The research involves a study of the manufacture of the slot, the method of filling the slot with dielectric material, and an investigation of the various materials that could be used.

iii) Extend Analysis to include the Radiation Continuum

The radiation continuum must be included when any disontinuities are analysed. The most important application of this is the analysis of the bend, which is required to enable low loss bends to be designed. The continuum is also required in the formulation of the Green's operator for the guide to enable the field arising from a diode for example, to be calculated.

iv) Extend TRD Formulation to other Guiding Structures

The TRD method has been used to analyse image line, finline, microstrip and IDG. A structure which lends itself to the TRD method is that of ridged waveguide.

6-4 Concluding Remarks

After a surge of interest in the 70's the research into dielectric guides has taken a low key existence. This is mainly due to a lack of systems applications for military use above 100 GHz at present, since a large amount of research funding is provided from military sources. Another problem has been the poor performance that has generally been obtained from dielectric integrated circuits. Practical problems such as the integration of active devices, and radiation losses, has tended to limit practical applications. However, undoubtedly there will be a time when applications will be required at frequencies where the popular structures like microstrip and finline can no longer be used, and dielectric guides will come into their own. Then IDG, as a more practical variant of image line could become accepted.

This thesis, as the initial work into IDG, has demonstrated a practical structure that is well characterised, has low loss, and can be fabricated cost-effectively. The need to continue work in this area is evident.

APPENDIX I

The determination of the y-dependance for the potential functions in the slot.

The scalar functions $\Psi e(x,y)$ and $\Psi h(x,y)$ describe the field variations for the y-directed TM and TE fields respectively. By analogy with transmission theory, the variations along the axis of propagation will be that of the current and voltage components respectively.

Consider the general case of a uniform transmission line, terminated with a load at y = -h. At any point along the line, measured from the line input at y = 0, the voltage and current components will be:

$$Vy = V^+ e^{j\beta(y+h)} + \rho V^+ e^{-j\beta(y+h)} \qquad \text{(I-1a)}$$

$$Iy = \frac{V^+}{Zo} e^{j\beta(y+h)} + \rho \frac{V^+}{Zo} e^{-j\beta(y+h)} \qquad \text{(I-1b)}$$

where the reflection coefficient ρ, is given by:

$$\rho = \frac{Z1 - Zo}{Z1 + Zo} = \frac{Yo - Y1}{Y1 + Yo}$$

Equations (I-1) can thus be rewritten as:

$$Vy = \frac{V^+}{Y1+Yo}\left[Yo\left[e^{j\beta(y+h)} + e^{-j\beta(y+h)}\right] + Y1\left[e^{j\beta(y+h)} - e^{-j\beta(y+h)}\right]\right]$$

$$= \frac{V^+}{Y1+Yo}\left(Yo\cos\beta(y+h) + jY1\sin\beta(y+h)\right) \qquad \text{(I-2a)}$$

$$Iy = \frac{YoV^+}{Y1+Yo}\left[Yo\left[e^{j\beta(y+h)} - e^{-j\beta(y+h)}\right] + Y1\left[e^{j\beta(y+h)} + e^{-j\beta(y+h)}\right]\right]$$

$$= \frac{YoV^+}{Y1+Yo}\left(jYo\sin\beta(y+h) + Y1\cos\beta(y+h)\right) \qquad \text{(I-2b)}$$

The expressions for the y-dependance must be dimensionless. To ensure the continuity of the fields across the air/dielectric region interface at y=0, it is convenient to normalise (I-2) to their values at y=0. Thus the y-dependance for a TM mode will be given as:

$$f'(y) = \frac{jYo' \sin\beta(y+h) + Y1' \cos\beta(y+h)}{jYo' \sin\beta h + Y1' \cos\beta h} \qquad \text{(I-3)}$$

and for a TE mode:

$$f''(y) = \frac{Yo'' \cos\beta(y+h) + jY1'' \sin\beta(y+h)}{Yo'' \cos\beta h + jY1'' \sin\beta h} \qquad \text{(I-4)}$$

For the case of a line terminated in a short circuit ($Y1 = \infty$), these expressions reduce to:

$$f'(y) = \frac{\cos\beta(y+h)}{\cos\beta h} \qquad \text{(I-5)}$$

$$f''(y) = \frac{\sin\beta(y+h)}{\sin\beta h} \qquad \text{(I-6)}$$

APPENDIX II

The evaluation of the inner products Pnm, Pn(ρ), Qnm, Qn(ρ).

The inner products that are required for the even and odd mode formulations respectively are defined as :

$$Pnm = \langle fm(x), \Phi hn(x) \rangle, \quad Pm(\rho) = \langle fm(x), \Phi h(\rho,x) \rangle \quad n,m = 0,2,4\ldots$$

and

$$Qnm = \langle fm(x), \Phi en(x) \rangle, \quad Qm(\rho) = \langle fm(x), \Phi e(\rho,x) \rangle \quad n,m = 1,3,5,\ldots$$

The expansion set fm(x) are the wieghted Gegenbauer polynomials, normalised under the wieghting function such that :

$$\int_0^{a/2} w(x)\, C_n^{\frac{1}{6}}(2x/a)\, C_m^{\frac{1}{6}}(2x/a)\, dx = \delta mn \qquad (II\text{-}1)$$

The individual terms are thus

$$fm(x) = \frac{1}{Nm}\, w(x)\, C_m^{\frac{1}{6}}(2x/a) \qquad (II\text{-}2)$$

where the normalisation factor Nm satisfies :

$$Nm^2 = \int_0^{a/2} w(x)\, \left(C_m^{\frac{1}{6}}(2x/a)\right)^2 dx \qquad (II\text{-}3)$$

From mathematical tables [1] the result is found :

$$\int_{-1}^{1} (1 - x^2)^{\nu-\frac{1}{2}} \left(C_m^{\nu}(x)\right)^2 dx = \frac{\pi\, 2^{(1-2\nu)}\, \Gamma(2\nu + m)}{m!\, (m + \nu)\, (\Gamma(\nu))^2} \qquad (II\text{-}4)$$

putting $t = (a/2)x$, $\nu = \frac{1}{6}$ in (II-4) gives

$$2\int_0^{a/2} (1 - (2t/a)^2)^{-\frac{1}{3}}\, \left(C_m^{\frac{1}{6}}(2t/a)\right)^2 (2/a)\, dt = \frac{\pi 2^{\frac{2}{3}}\, \Gamma(m + \frac{1}{3})}{m!\, (m + \frac{1}{6})\, (\Gamma(\frac{1}{6}))^2} \qquad (II\text{-}5)$$

so that

$$Nm^2 = \frac{a\pi 2^{-\frac{4}{3}} \Gamma(m + \frac{1}{3})}{m!\,(m + \frac{1}{6})\,[\Gamma(\frac{1}{6})]^2} \qquad \text{(II-6)}$$

The inner products Pmn and Pm(ρ)

Writing Pmn out fully gives :

$$Pmn = \langle w(x) \frac{1}{Nm} C_m^{\frac{1}{6}}(2x/a)\ \Phi hn(x) \rangle \qquad \text{(II-7a)}$$

$$= \frac{1}{Nm} \frac{2\,\delta n}{\sqrt{a}} \int_0^{a/2} (1 - (2x/a)^2)^{-\frac{1}{3}}\ C_m^{\frac{1}{6}}(2x/a) \cos(n\pi/a)x\ dx \qquad \text{(II-7b)}$$

From tables [1] :

$$\int_0^1 (1 - t)^{\nu-\frac{1}{2}} C_{2n}^{\nu}(t) \cos bt\ dt = \frac{(-1)^n \pi \Gamma(2n + 2\nu) J_{\nu+2n}(b)}{(2n)!\,\Gamma(\nu)\,(2b)^{\nu}} \qquad \text{(II-8)}$$

setting $x = (a/2)t, \nu = \frac{1}{6}$, $m = 2n$

$$\int_0^{a/2} (1 - (2x/a)^2)^{-\frac{1}{3}} C_m^{\frac{1}{6}}(2x/a) \cos(2b/a)x\ (2/a)\ dx$$

$$= \frac{(-1)^{\frac{m}{2}} \pi \Gamma(m + \frac{1}{3})\, J_{m+\frac{1}{6}}(b)}{m!\,\Gamma(\frac{1}{6})\,(2b)^{\frac{1}{6}}} \qquad \text{(II-9)}$$

by comparing (II-7b) with (II-9), b is found to equal (nπ/2) and so :

$$Pnm = \frac{1}{Nm}\ \delta n\ \sqrt{a}\ \frac{(-1)^{\frac{m}{2}}\ \pi\ \Gamma(m + \frac{1}{3})\ J_{m+\frac{1}{6}}(n\pi/2)}{m!\ \Gamma(\frac{1}{6})\ (n\pi)^{\frac{1}{6}}} \quad (m = 0,2,4,..) \qquad \text{(II-10)}$$

Taking the limit of Pnm as n tends to zero gives

$$Pmo = \frac{1}{No} \frac{\sqrt{a}\ \pi\ \Gamma(\frac{1}{3})}{\Gamma(\frac{1}{6})\ 2^{\frac{5}{6}}\ \Gamma(1 + \frac{1}{6})} \qquad m = 0 \qquad \text{(II-11a)}$$

$$= 0 \qquad m = 2,4,... \qquad \text{(II-11b)}$$

The inner products $Pm(\rho)$ can be determined from (II-10) by using

$$Pm(\rho) = \frac{a}{\sqrt{2\pi}} Pm\bar{\rho} \qquad \bar{\rho} = \frac{a}{\pi}\rho \tag{II-12}$$

It is convenient to normalise Pnm to Poo so that :

$$Pmn = \frac{No}{Nm} \frac{2^{\frac{5}{6}} (-1)^{\frac{m}{2}} \Gamma(1 + \frac{1}{6}) \Gamma(m + \frac{1}{3})}{m!\ \Gamma(\frac{1}{3})} \frac{J_{m+\frac{1}{6}}(n\pi/a)}{(n\pi)^{\frac{1}{6}}} \tag{II-13}$$

The normalised values of Pmn are then given as , for $n > 0$:

$$Po n = 1{\cdot}6530102 \frac{J_{\frac{1}{6}}(n\pi/2)}{(n\pi)^{\frac{1}{6}}}$$

$$P2n = -2{\cdot}809577 \frac{J_{2+\frac{1}{6}}(n\pi/2)}{(n\pi)^{\frac{1}{6}}}$$

$$P4n = 3{\cdot}1367249 \frac{J_{4+\frac{1}{6}}(n\pi/2)}{(n\pi)^{\frac{1}{6}}}$$

$$P6n = -3{\cdot}3493233 \frac{J_{6+\frac{1}{6}}(n\pi/2)}{(n\pi)^{\frac{1}{6}}}$$

$$P8n = 3{\cdot}5101615 \frac{J_{8+\frac{1}{6}}(n\pi/2)}{(n\pi)^{\frac{1}{6}}} \qquad \text{and so on.}$$

The inner products Qmn and Qm(ρ)

Qmn is defined as :

$$Qmn = \frac{1}{Nm} \frac{2}{\sqrt{a}} \int_0^{a/2} (1 - (2x/a)^2)^{-\frac{1}{3}} C_m^{\frac{1}{6}}(2x/a) \sin(n\pi/a)x \, dx \tag{II-14}$$

$$n,m = 1,3,5,....$$

Again from tables [1], the result is found :

$$\int_0^1 (1 - t^2)^{\nu - \frac{1}{2}} C_m^{\nu}(t) \sin bx \, dx = \frac{(-1)^{\frac{m-1}{2}} \pi \Gamma(m + 2\nu) J_{m+\nu}(b)}{m!\ \Gamma(\nu) (2b)^{\nu}} \tag{II-15}$$

and so

$$Qmn = \frac{1}{Nm} \frac{\sqrt{a}\,(-1)^{\frac{m-1}{2}}\,\pi\,\Gamma(m+\frac{1}{3})\,J_{m+\frac{1}{6}}(n\pi/a)}{m!\;\Gamma(\frac{1}{6})\;(n\pi)^{\frac{1}{6}}} \qquad \text{(II-16)}$$

Again it is convenient to normalise the Qmn's to Poo so that :

$$Q_{1}n = 2{\cdot}5250135\;\frac{J_{1+\frac{1}{6}}(n\pi/2)}{(n\pi)^{\frac{1}{6}}}$$

$$Q_{3}n = -2{\cdot}9955311\;\frac{J_{3+\frac{1}{6}}(n\pi/2)}{(n\pi)^{\frac{1}{6}}}$$

$$Q_{5}n = 3{\cdot}2517213\;\frac{J_{5+\frac{1}{6}}(n\pi/2)}{(n\pi)^{\frac{1}{6}}}$$

$$Q_{7}n = -3{\cdot}4344529\;\frac{J_{7+\frac{1}{6}}(n\pi/2)}{(n\pi)^{\frac{1}{6}}}$$

$$Q_{9}n = 3{\cdot}5784795\;\frac{J_{9+\frac{1}{6}}(n\pi/2)}{(n\pi)^{\frac{1}{6}}} \qquad \text{and so on.}$$

Reference

[1] I.S. Gradshteyn and I.M. Ryshik, " Table of Integrals, series and products", New York: Academic Press, 1965, p.827.

APPENDIX III

The derivation of the field amplitude components

The slot region

Having solved the dispersion equation (3-59) for β, the amplitude coefficients Xm, Zm can be found from (3-55) as

$$\begin{bmatrix} \underline{X} \\ \underline{Z} \end{bmatrix} = \underline{\underline{Y}}^{-1} \begin{bmatrix} -Hzo\ \underline{Po} \\ \underline{0} \end{bmatrix} \qquad \text{(III-1)}$$

From equations (3-11a) and (3-49):

$$Ex(x,o) = \sum_{n=0,2,}^{\infty} Exn\ \Phi hn(x) = \sum_{m=0,2,}^{\infty} Xm\ fm(x) \qquad \text{(III-2)}$$

and so by taking the inner product of both sides with $\Phi hn(x)$:

$$Exn = \sum_{m=0,2,}^{\infty} Xm\ Pmn = \underline{X}^T \cdot \underline{Pn} \qquad \text{(III-3)}$$

The amplitude coefficients for Ez(x,o) are found in a similiar manner by differentiating (3-11c) wrt. x and equating with (3-49) so that:

$$(a/\pi)\ dEz(x,o)/dx = (a/\pi) \sum_{n=2,4,}^{\infty} Ezn\ (n\pi/a)\ \Phi hn(x) = \sum_{m=2,4,}^{\infty} Zm\ fm(x) \qquad \text{(III-4)}$$

giving

$$Ezn = (1/n)\ \underline{Z}^T \cdot \underline{Pn} \qquad \text{(III-5)}$$

The amplitude coefficients for the transverse magnetic components are found from equation (3-46a). From equation (3-11d):

$$(\pi/a) \int Hx(x,o)\ dx = - \sum_{n=2,4,}^{\infty} (1/n)\ Hxn\ \Phi hn(x) \qquad \text{(III-6)}$$

and so by placing the series expansions for the field components in (3-46a), and writing the x-independant parts of the admittance operators

as Y(k) the expression is obtained:

$$\begin{bmatrix} \sum_{n=0}^{\infty} Hzn\,\Phi hn(x) \\ \sum_{n=2}^{\infty} (1/n)\,Hxn\,\Phi hn(x) \end{bmatrix} = \begin{bmatrix} \sum_{k=0}^{\infty} Y_{11}^{s}(k)\,\Phi hk(x)\,\Phi hk(x') & \sum_{k=2}^{\infty} Y_{12}^{s}(k)\,\Phi hk(x)\,\Phi hk(x') \\ \sum_{k=2}^{\infty} Y_{21}^{s}(k)\,\Phi hk(x)\,\Phi hk(x') & \sum_{k=2}^{\infty} Y_{22}^{s}(k)\,\Phi hk(x)\,\Phi hk(x') \end{bmatrix} \cdot \begin{bmatrix} \sum_{m=0}^{\infty} Xm\,fm(x) \\ \sum_{m=2}^{\infty} Zm\,fm(x) \end{bmatrix} \quad \text{(III-7)}$$

Multiplying by $\Phi hn(x)$ and integrating wrt. x and x' over the aperture gives:

$$Hzn = Y_{11}^{s}(k)\,\underline{X}^{T}\cdot\underline{Pn} + Y_{12}^{s}(k)\,\underline{Z}^{T}\cdot\underline{Pn}$$

$$= \frac{\cot\sqrt{U^2 - n^2}(\pi h/a)}{\sqrt{U^2 - n^2}} \left(-jU\,\underline{X}^{T}\cdot\underline{Pn} + \frac{(a/\pi)\beta}{U}\,\underline{Z}^{T}\cdot\underline{Pn} \right) \quad \text{(III-8a)}$$

$$Hxn = n(Y_{21}^{s}(k)\,\underline{X}^{T}\cdot\underline{Pn} + Y_{22}^{s}(k)\,\underline{Z}^{T}\cdot\underline{Pn})$$

$$= \frac{n\cot\sqrt{U^2 - n^2}(\pi h/a)}{\sqrt{U^2 - n^2}} \left(\frac{-(a/\pi)\beta}{U}\,\underline{X}^{T}\cdot\underline{Pn} + \frac{1}{jU}\left(\frac{U^2 + \overline{\beta}^2 - n^2}{n^2}\right)\underline{Z}^{T}\cdot\underline{Pn} \right) \quad \text{(III-8b)}$$

From equations (3-11b) and (3-11e) the amplitude coefficients for the y-directed field components can be written in terms of the equivalent circuit voltage and current amplitudes as:

$$\begin{bmatrix} Eyn \\ Hyn \end{bmatrix} = \left((n\pi/a)^2 + \beta^2\right)^{\frac{1}{2}} \begin{bmatrix} (1/j\omega\varepsilon) & 0 \\ 0 & (1/j\omega\mu_0) \end{bmatrix} \begin{bmatrix} In' \\ Vn'' \end{bmatrix} \quad \text{(III-9)}$$

and so from (3-12):

$$\begin{bmatrix} Eyn \\ Hyn \end{bmatrix} = \begin{bmatrix} (1/j\omega\varepsilon) & 0 \\ 0 & (1/j\omega\mu_0) \end{bmatrix} \begin{bmatrix} (\omega\varepsilon/j\,Kyn)\cot Kyn\,h & 0 \\ 0 & 1 \end{bmatrix} \begin{bmatrix} (n\pi/a) & j\beta \\ j\beta & (n\pi/a) \end{bmatrix} \begin{bmatrix} Exn \\ Ezn \end{bmatrix} \quad \text{(III-10)}$$

To be consistent with the expressions for the other magnetic components the expression for Hyn must be normalised to Yoo" so that

$$Eyn = \frac{-\cot\sqrt{U^2 - n^2}(\pi h/a)}{\sqrt{U^2 - n^2}} \left[n\,\underline{X}^T\cdot\underline{Pn} + j(a/n\pi)\beta\,\underline{Z}^T\cdot\underline{Pn} \right] \qquad (III\text{-}11a)$$

$$Hyn = \frac{1}{jU} \left[j\beta(a/\pi)\,\underline{X}^T\cdot\underline{Pn} + \underline{Z}^T\cdot\underline{Pn} \right] \qquad (III\text{-}11b)$$

The air region

From equations (3-26a) and (3-49):

$$Ex(x,o) = \int_0^\infty ex(\rho)\,\Phi h(x,\rho)\,d\rho = \sum_{m=0,2,}^{\infty} Xm\,fm(x) \qquad (III\text{-}12)$$

Multiply both sides by $h(x,\rho')$ and integrate wrt. x from 0 to infinity (remembering that $fm(x)=0$ for $|x|>a/2$) to obtain:

$$\int_0^\infty ex(\rho)\,\delta(\rho - \rho')\,d\rho = \sum_{m=0,2,}^{\infty} Xm\,Pm(\rho) \qquad (III\text{-}13)$$

$$\Rightarrow ex(\rho) = \underline{X}^T\cdot\underline{P}(\rho) \qquad (III\text{-}14)$$

In a similiar fashion:

$$(a/\pi)\,dEz(x,o)/dx = (a/\pi)\int_0^\infty ez(\rho)\,\rho\,\Phi h(x,\rho)\,d\rho = \sum_{m=2,4,}^{\infty} Zm\,fm(x) \qquad (III\text{-}15)$$

which leads to the result:

$$ez(\rho) = (\pi/a\rho)\,\underline{Z}^T\cdot\underline{P}(\rho) \qquad (III\text{-}16)$$

From (3-26e)

$$(\pi/a)\int Hx(x,o)\,dx = -(\pi/a)\int_0^\infty hx(\rho)\,(1/\rho)\,\Phi h(x,\rho)\,d\rho \qquad (III\text{-}17)$$

and so by an analogous procedure to that used in the slot region the

expressions are obtained:

$$hz(\rho) = -\frac{1}{U\,Ky(\rho)}\left[(a/\pi)(Ko^2-\beta^2)\,\underline{X}^T\cdot\underline{P}(\rho) + j\beta\,\underline{Z}^T\cdot\underline{P}(\rho)\right] \qquad \text{(III-18a)}$$

$$hx(\rho) = \frac{\rho}{U\,Ky(\rho)}\left[-j(a/\pi)\beta\,\underline{X}^T\cdot\underline{P}(\rho) + \left(\frac{Ko^2-\rho^2}{\rho^2}\right)\underline{Z}^T\cdot\underline{P}(\rho)\right] \qquad \text{(III-18b)}$$

The fourier amplitude coefficients for the y-directed components can be written as:

$$\begin{bmatrix} ey(\rho) \\ hy(\rho) \end{bmatrix} = (\beta^2+\rho^2)^{\frac{1}{2}}\begin{bmatrix} (1/j\omega\varepsilon_0) & 0 \\ 0 & (1/j\omega\mu_0) \end{bmatrix}\begin{bmatrix} I(\rho)' \\ V(\rho)'' \end{bmatrix} \qquad \text{(III-19)}$$

and so from (3-27a)

$$\begin{bmatrix} ey(\rho) \\ hy(\rho) \end{bmatrix} = \begin{bmatrix} (1/j\omega\varepsilon_0) & 0 \\ 0 & (1/j\omega\mu_0) \end{bmatrix}\begin{bmatrix} (-\omega\varepsilon_0/Ky(\rho) & 0 \\ 0 & 1 \end{bmatrix}\begin{bmatrix} \rho & j\beta \\ j\beta & \rho \end{bmatrix}\begin{bmatrix} \underline{X}^T\cdot\underline{P}(\rho) \\ (\pi/a\rho)\underline{Z}^T\cdot\underline{P}(\rho) \end{bmatrix} \qquad \text{(III-20)}$$

Remembering that hy(ρ) must be normalised to Yoo", the results are obtained:

$$ey(\rho) = -\frac{1}{j\,Ky(\rho)}\left[\rho\,\underline{X}^T\cdot\underline{P}(\rho) + j\beta(\pi/a\rho)\,\underline{Z}^T\cdot\underline{P}(\rho)\right] \qquad \text{(III-21a)}$$

$$hy(\rho) = \frac{1}{jU}\left[j(a/\pi)\beta\,\underline{X}^T\cdot\underline{P}(\rho) + \underline{Z}^T\cdot\underline{P}(\rho)\right] \qquad \text{(III-21b)}$$